2019

ILLUMINATING DNA PACKAGING IN SPERM CHROMATIN: HOW POLYCATION LENGTHS, UNDERPROTAMINATION AND DISULFIDE LINKAGES ALTERS DNA CONDENSATION AND STABILITY

Daniel Kirchhoff
University of Kentucky, dcki223@uky.edu
Digital Object Identifier: https://doi.org/10.13023/etd.2019.233

STUDENT AGREEMENT:

I represent that my thesis or dissertation and abstract are my original work. Proper attribution has been given to all outside sources. I understand that I am solely responsible for obtaining any needed copyright permissions. I have obtained needed written permission statement(s) from the owner(s) of each third-party copyrighted matter to be included in my work, allowing electronic distribution (if such use is not permitted by the fair use doctrine) which will be submitted to UKnowledge as Additional File.

I hereby grant to The University of Kentucky and its agents the irrevocable, non-exclusive, and royalty-free license to archive and make accessible my work in whole or in part in all forms of media, now or hereafter known. I agree that the document mentioned above may be made available immediately for worldwide access unless an embargo applies.

I retain all other ownership rights to the copyright of my work. I also retain the right to use in future works (such as articles or books) all or part of my work. I understand that I am free to register the copyright to my work.

REVIEW, APPROVAL AND ACCEPTANCE

The document mentioned above has been reviewed and accepted by the student's advisor, on behalf of the advisory committee, and by the Director of Graduate Studies (DGS), on behalf of the program; we verify that this is the final, approved version of the student's thesis including all changes required by the advisory committee. The undersigned agree to abide by the statements above.

Daniel Kirchhoff, Student

Dr. Jason DeRouchey, Major Professor

Dr. Mark Lovell, Director of Graduate Studies

ILLUMINATING DNA PACKAGING IN SPERM CHROMATIN: HOW POLYCATION LENGTHS, UNDERPROTAMINATION AND DISULFIDE LINKAGES ALTERS DNA CONDENSATION AND STABILITY

DISSERTATION

A dissertation submitted in partial fulfillment of the
requirements for the degree of Doctor of Philosophy in the
College of Arts and Sciences
at the University of Kentucky

By
Daniel Kirchhoff
Lexington, Kentucky
Director: Dr. Jason DeRouchey, Professor of Chemistry
Lexington, Kentucky
2019

ABSTRACT OF DISSERTATION

ILLUMINATING DNA PACKAGING IN SPERM CHROMATIN: HOW POLYCATION LENGTHS, UNDERPROTAMINATION AND DISULFIDE LINKAGES ALTERS DNA CONDENSATION AND STABILITY

During spermiogenesis, somatic chromatin is remodeled and a vast majority (>90%) of DNA histones are replaced by short arginine-rich peptides called protamines. This compaction is immense, with protamine-DNA self-assembly in sperm chromatin resulting in a final volume roughly 1/6th of a somatic nucleus. This near crystalline organization of the DNA in sperm is thought crucial both for the transport of the paternal genes as well as for the protection of genetic information as sperm chromatin is transcriptionally inactive and all DNA repair mechanisms are shut down.

Chapter 1 will include an overview of the topics discussed in this document, including: sperm chromatin, Sperm chromatin remodeling, DNA damage, and the effect of DNA damage to sperm DNA.

Chapter 2 will contain a brief overview of the techniques used within this study. This includes: Small-angle X-ray Scattering, gel electrophoresis, DNA precipitation assays, and ethidium bromide dissociation assays.

In chapter 3, we will discuss the effect of DNA packaging on the accessibility of free radicals to damage condensed DNA. A variety of polycations were used to condense plasmid DNA in reconstituted samples. After condensation, the DNA-polycation condensates were exposed to 2,2'-Azobis(2-amidinopropane) dihydrochloride (AAPH) for 1 hour, decondensed, and the plasmid DNA examined by gel electrophoresis. By comparing the intensities of the supercoiled, open coiled and linear bands, we were able to identify the presence of single-strand nicks and double-strand breaks in DNA. DNA packaging densities for all polycation-DNA systems were determined by small-angle X-Ray scattering (SAXS). Our results show that for similar length polycations, the amount of oxidative damage scales directly with the DNA packaging with more tightly condensed DNA being damaged less. However, our results also show that DNA damage is also dependent on polycation length, with DNA condensed by shorter polycations being damaged more than DNA condensed with longer polycations even at similar packaging densities.

Protamine has long been thought to play a role in protecting spermatic DNA from damaging agents in vivo. However, the relationship between the hypercondensation of sperm chromatin, the DNA integrity, and the transfer of epigenetic information from sperm to oocyte and potential to alter gene expression in the early embryo are poorly understood. In Chapter 4, we examine how underprotamination affects free radical accessibility and DNA stability in reconstituted sperm chromatin. Specifically, reconstituted salmon protamine- plasmid DNA condensates (polyplexes) were formed at precise protamine/DNA ratios and subsequently

subjected to exposure to AAPH free radicals. Agarose gel electrophoresis was then used to assess DNA damage by observing topology alternations in the decondensed polyplexes. FPG-DNA glycosylase has also been used to more accurately determine oxidative damage beyond just nicks and double-strand breaks in the various condensed states. We show that higher levels of protamination correlate to greater levels of protection to the DNA from oxidative damage up until full charge compensation. Furthermore, we also demonstrate that poorly compacted chromatin could be recovered by the introduction of small cationic peptides in underprotaminated condensates as well as actual sperm nuclei. SAXS studies were performed to show that the introduction of cationic peptides resulted in tighter DNA packaging densities in the underprotaminated sperm chromatin.

In Chapter 5, we examine the role of disulfide bonds on DNA packaging in mammalian sperm chromatin. Mammalian protamine, unlike fish, are known to have cysteine residues capable of forming inter- and intra-protamine disulfide bonds. In bull, prior work had shown evidence for the formation of a unique hairpin secondary structure due to the folding of the ends of the protamine molecule by intramolecular disulfide linkages. Between folds is an arginine-rich region known as the DNA binding region. The DNA binding region has a local arginine fraction (~60-75%) that is much higher than the arginine fraction within the full bull protamine sequence (~50%). Previous work by the DeRouchey lab has shown that the percent arginine was crucial for DNA condensation in small arginine-rich peptides. We hypothesize that the fraction of arginine is also critical to DNA remodeling in sperm chromatin. SAXS studies showed that disulfide bond reduction resulted in complete decondensation of bull sperm nuclei. Here, we have used cysteine alkylation chemistry to add neutral or charged functional groups to the protamine cysteine, thereby inhibiting the formation of these disulfide bonds. This chemistry both prevents the formation of the hairpin as well as modifies the overall charge of the protamine. Through ethidium bromide exclusion assays, we measured binding of these altered protamines to calf thymus DNA and determined that a percent cationic charge of above 50% is necessary for the protamine to effectively condense DNA. In addition, we show that DNA condensation of bull protamine with the hairpin is nearly identical to piscine protamines which have no disulfide linkages but a net arginine fraction of 60-75%. Upon disruption of the hairpin, however, complete condensation does not occur despite a net charge on the protamine of +26.

KEYWORDS: Sperm Chromatin, Protamine, Disulfide Linkages, Underprotamination, DNA condensation, DNA Damage

Daniel Kirchhoff

5-24-2019

ILLUMINATING DNA PACKAGING IN SPERM CHROMATIN: HOW POLYCATION LENGTHS, UNDERPROTAMINATION AND DISULFIDE LINKAGES ALTERS DNA CONDENSATION AND STABILITY

By
Daniel Kirchhoff

Jason DeRouchey
Director of Dissertation

Mark Lovell
Director of Graduate Studies

05/24/2019
Date

Acknowledgments

First and foremost, I would like to thank my advisor, Dr. Jason DeRouchey, for his support and mentorship throughout my Ph.D. studies. I would like to thank the members of the DeRouchey research group, both past and present, for their help throughout my time at the University of Kentucky: Ehigbai Oikeh, Kanthi Nuti, Iris Begum, Nasir Uddin, Richard Mitchell, Md. Abu Dinar, Joseph Duke, Cody Gay Dr. Min An, Dr. Xiaolu Zhang. I would like to acknowledge my undergraduate research assistants: Jacquelyn Rhinehart, Matthew Brady Ekman, and Danielle Berkowitz for helping me perform numerous experiments. I would like to thank Dr. Hunter Mosely and Christian Powell for their help in performing sequence alignments and biochemical informatics. I would like to thank Dr. Sean Parkin for his help in setting up and performing the X-Ray scattering experiments used in this study. I would like to thank my committee members: Dr. Stephen Testa, Dr. Folami Ladipo, Dr. Barry Ball, and Dr. Trevor Creamer for their help in my Ph.D. studies. Finally, I would like to thank my friends and family for their help and support during my Ph.D. journey.

Table of Contents

List of Tables

List of Figures

Chapter 1: Section 1: Introduction

Section 1.1: Introduction to DNA Condensation.

In somatic cells, the entire genetic code is contained within deoxyribonucleic acid, or DNA. DNA is immense, both in terms of the physical size of the molecule and in terms of the information contained within it. In a typical human cell, the total DNA stretched out end to end would be approximately 2 meters, or 6 feet, long. [1] The genetic information contained within DNA is encoded within the four canonical DNA bases in the form of base pairs. These base pairs consist of adenine, thymine, guanine and cytosine. A typical somatic cell, containing 23 pairs of chromosomes, contains approximately 6 billion base pairs of DNA per cell. This massive length of DNA is sequestered in its entirety within the nucleus of the eukaryotic cell. For eukaryotes, the nucleus is approximately 10 μm in diameter and contained within the cell body which is approximately 20 – 50 μm in diameter. [1, 2] The size constraints of the somatic nucleus results in the DNA needing to be compacted some 20,000x. [3] As discussed below, the compaction of DNA in sperm nuclei is even more immense. In somatic and sperm cells, the compaction of the DNA occurs through the association of DNA with basic proteins to form a complex called chromatin.

Section 1.2: Somatic and Sperm Chromatin Packaging

Section 1.2.1 Somatic Chromatin Packaging

DNA in somatic chromatin is compacted in a complex, multi-level fashion as depicted in Figure 1.1. [4] DNA packaging within eukaryotic cells is accomplished by the interaction of basic proteins known as histones on the DNA. Histones consist of a core of 8 different proteins. At the primary level, DNA interacts with this histone core by wrapping 1.65 times around the core to form the nucleosome. Approximately 146 base pairs of DNA are involved in each wrapped

nucleosome. Nucleosomes are joined together by short, 20 base pair sections of linker DNA, and give histone-DNA structure a 'beads on a string' appearance (Fig 1.1). [5] Nucleosomes further condense and arrange themselves into a larger solenoid-shaped structure known as the 30 nm fiber. [6] This fiber further compacts and wraps around itself, forming larger and larger fibers, ultimately resulting in fully condensed chromatin with the appearance of the well-described X-shaped chromosome. [5]

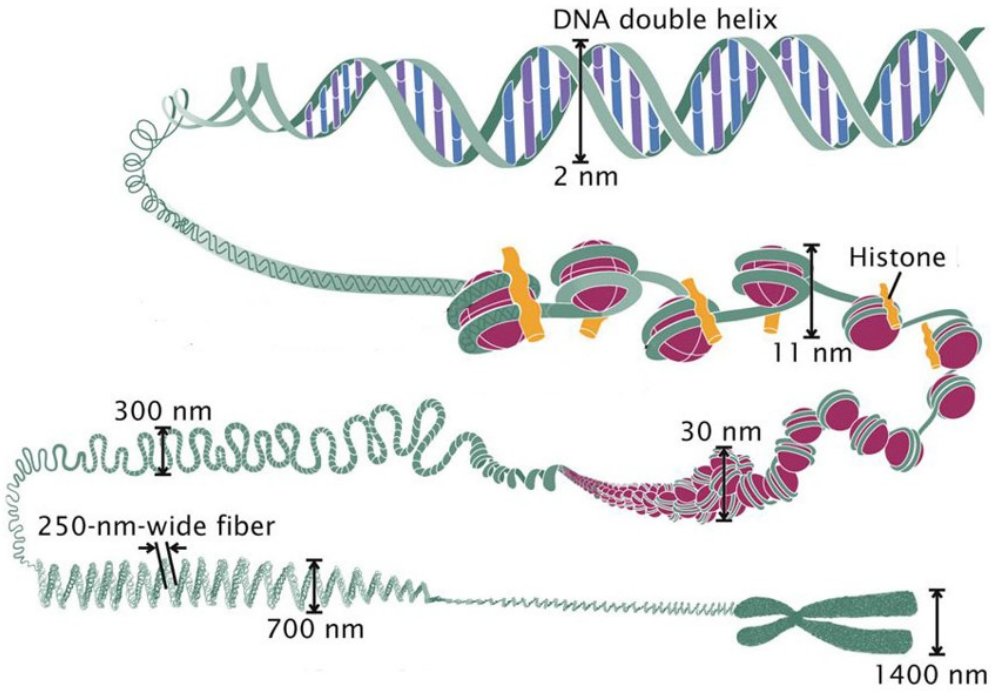

Figure 1.1: Somatic chromatin packaging is a multistep process in which DNA is wrapped around somatic histones, ultimately resulting in the chromatin existing in a highly compacted state. Adapted from [4]

Section 1.2.2: Sperm Chromatin Packaging

In contrast to somatic cells, DNA in sperm cells is packaged to a much higher degree. A typical sperm cell consists of three distinct sections, the head, the midpiece, and the tail, as illustrated in Figure 1.2. [7] The sperm tail consists of a flagellum, which the sperm uses for

movement, and the midsection contains numerous mitochondrion, which functions in energy production. [7] The sperm head consists primarily of the nucleus, which contains the highly condensed haploid paternal genome, encapsulated by the acrosome cap, which assists in breaking down the outer membrane of the ovum. [7] In contrast to the ~10 μm diameter somatic nucleus size, the typical human sperm nucleus measures approximately 4.4 μm long and 2.8 μm across.[8] This immense compaction of DNA in the sperm is necessary to facilitate the safe transport of the paternal gene to the egg; the primary function of the sperm cell.

DNA compaction within sperm nuclei is accomplished by the use of short basic peptides known as protamines which replace somatic histones during the late stages of spermatogenesis. Protamines are typically 30-50 amino acids long and contain a high fraction of arginine residues.[9] The exact length and sequence are species dependent.[10] Salmon protamine, for example, is 32 amino acids long with 21 arginines (Figure 1.3). [11] At physiological pH, arginine contains a +1 charge, therefore protamines are highly cationic. As discussed in more detail in the next section, mammalian protamines are typically longer, around 50 amino acids long, but still have a high fraction of arginine residues. [12] Because of this large cationic charge, protamine forms no traditional protein secondary structures, such as β-sheets or α-helices, due to the cationic repulsions between arginine residues. Protamine, with its lack of formal structure, is typically referred to as an intrinsically disordered protein. [13]

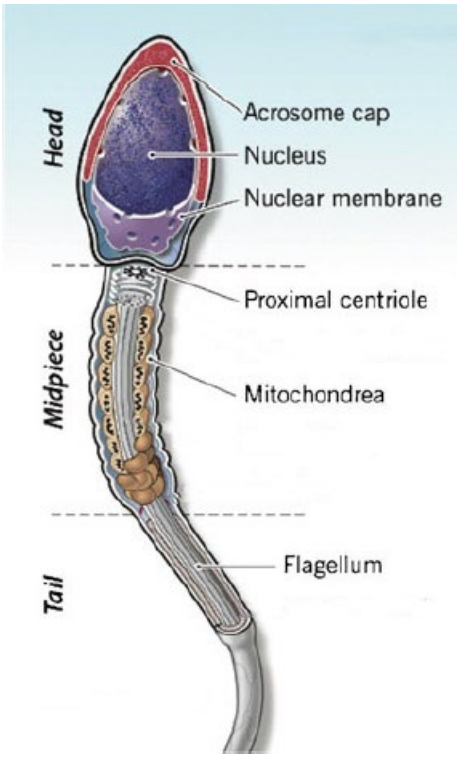

Figure 1.2: A sperm cell contains three main sections, A head, where the sperm chromatin is contained, a mitochondrion rich midsection, and a tail which functions in movement. Adapted from [7]

PRRRRSSSRPVRRRRRPRVSRRRRRRGGRRRR

Figure 1.3. The amino acid sequence for salmon protamine P1. Each of the 21 arginine residues are highlighted in red, resulting in a net cationic charge of +21.

Both in vivo and in vitro, protamines are known to interact electrostatically with the negatively charged phosphate backbone of the DNA and condenses it into toroidal structures. [10, 14] Shown in Figure 1.4, are reconstituted toroidal protamine-DNA condensates as visualized by atomic force microscopy (AFM). [15] These toroids are ~50-75 nm in diameter and are typically around 25 nm thick. [16] Each toroid contains approximately 50,000 base pairs of DNA. [16] DNA helices within these toroids are condensed into a highly ordered hexagonal lattice. [15, 17] In

sperm, the protamine-DNA toroids reside exclusively within the nucleus of the sperm head, although the exact arrangement and orientation of the toroids within the nucleus has yet to be

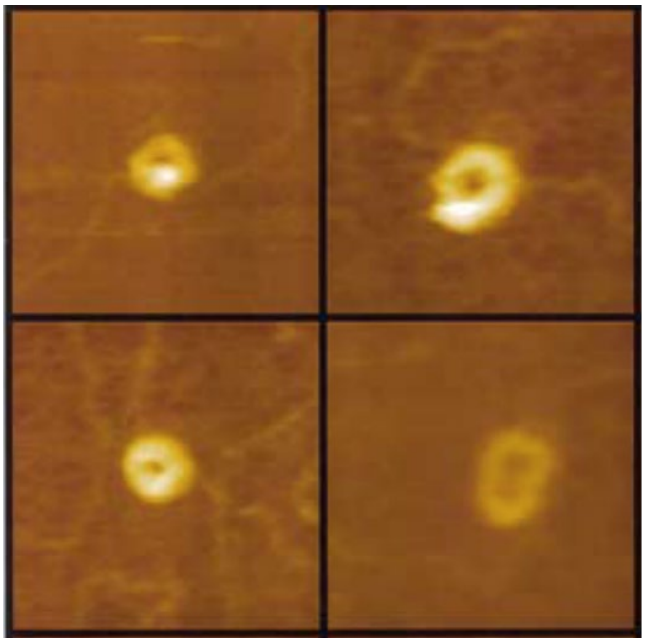

Figure 1.4: Images from Allen et al. showing treatment of plasmid DNA with bull protamine P1 results in the formation of reconstituted protamine toroids, which are observable by AFM imaging. Adapted from Allen, M.J., E.M. Bradbury, and R. Balhorn, AFM analysis of DNA-protamine complexes bound to mica. Nucleic Acids Research, 1997. **25**(11): p. 2221-2226. [15]

ascertained. [18] To compact the haploid DNA genome within the small sperm head, DNA compaction is at a near-crystalline packing density. Although a majority DNA within sperm nuclei is packaged by protamines, a small fraction of the DNA remains packaged by histones. For example, around 90% of DNA in human sperm is packaged by protamines while other species, such as bull, has more than 99% of the DNA packaged by protamine. [19] The ratio of protamines to histone in the fully mature sperm head varies from species to species.

The extreme DNA packaging found within sperm nuclei is thought to be crucial for several reasons. First, sperm are extremely small in size to allow for the efficient delivery of the paternal genome. Such a small delivery apparatus necessitates tight condensation of the haploid genome within the sperm head. [20] Second, the tight packaging within sperm nuclei is believed to instill

a protective effect to the DNA. DNA within the sperm nuclei are transcriptionally inactive due to the inaccessibility of the DNA helices to repair enzymes.[21] As repair is not present, and sperm cells are produced in a highly oxidative environment, it is thought that proper chromatin remodeling in the sperm is crucial for protecting the DNA from oxidative damaging agents in vivo. [22, 23]

Section 1.2.3: DNA Packaging Within Eutherian Sperm Nuclei

Mammalian protamines, like piscine protamines, are short peptides with a large number of arginine residues. For example, bull protamine is 50 amino acids long with 26 arginines. [24] The full bull protamine sequence is given in Figure 1.5. Here, the arginine residues are highlighted in red and the cysteines are highlighted in blue. Comparing mammalian protamines to simpler species, it is a common trait that the overall length of the mammalian protamine is slightly higher (50 AA vs 30 AA) and the overall percent charge is lower e.g. 52% charge in bull protamine vs 66% arginine in salmon protamine. Another significant difference between piscine and most

Figure 1.5: Bull protamine P1 amino acid sequence contains 7 cysteine residues highlighted in blue and 26 arginine residues highlighted in red, resulting in a +26 cationic charge.

mammalian sperm chromatin packaging is the presence of a disulfide bridge network. Mammalian protamines, like that of most eutherian mammals, has multiple cysteine residues and is known to form inter- and intramolecular disulfide bonds. These cysteines are lacking in fish protamine. [25]

Bull is an interesting model animal to study as it possesses only one form of protamine, termed P1. [26] Looking at the sequence of bull protamine P1, it is clear that a large percentage

of the arginine residues reside towards the center of the sequence while the amino and carboxyl ends of the sequence are mostly uncharged. This central region has thus been called the 'DNA binding domain' due to the dominance of basic arginine residues and its importance to driving DNA condensation. While the exact nature of the disulfide network is not well understood, in bull P1 a previous study focused on identifying the inter- and intramolecular disulfide linkages within the bull sperm chromatin. [27] Intramolecular disulfide bonding was shown to occur between Cys-6 and Cys-14 and Cys-39 and Cys-47. [26] These intramolecular disulfide bonds force the ends of the protamine sequence to fold over on itself, resulting in the formation of a staple shape, commonly referred to as a hairpin (Figure 1.6). [27] We note that upon forming the hairpin, the local cationic charge density of the binding region is nearly identical to the salmon protamine charge density at ~70% arginine.

Cys-5, Cys-22, and Cys-38 have been shown to be involved in the formation of intermolecular disulfide bonds connecting neighboring protamine chains. [27] Due to the inability to crystallize protamine-DNA, the exact positioning of the protamines along the DNA helix in the sperm chromatin is not known. A proposed model was given by Vilfan et al. for how protamine molecules might be linked in vivo. Figure 1.6 shows a protamine dimer based on this model with a proposed 'tail to tail' arrangement. [26] Notice that the protamine sequence on the upper protamine hairpin is reversed in relation to the sequence of the bottom protamine hairpin. Prior work showed that in native bull sperm chromatin, one protamine molecule is bound per ~11 bp of DNA or approximately 1 helical turn of DNA. Each protamine dimer would be expected to bind two helical turns of DNA or 22 base pairs. [26] Once formed, the S-S bond network confers substantial stability to the mammalian sperm chromatin. For example, a nearly complete reduction of the protamine disulfide bridges to free sulfhydryls is required in vitro and in vivo decondensation of mammalian sperm nuclei.

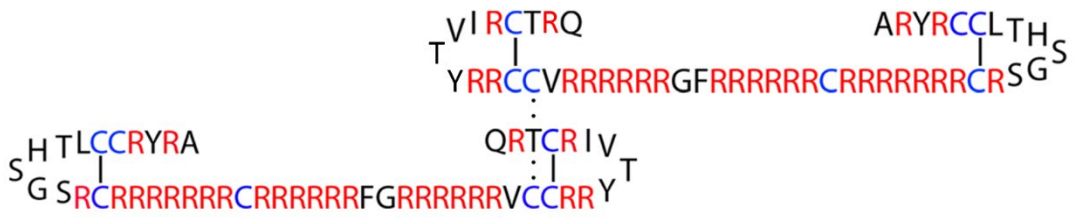

Figure 1.6: The intermolecular disulfide bond between Cys-38 and Cys-38 results in the formation of a protamine dimer. The protamine sequences of the dimer are reversed in relation to each other, this is termed the 'Tail to Tail' arrangement

Less is known about protamine P2. While protamine P1 is present in all mammalian sperm, protamine P2 has been observed in primates, most rodents and a few other placental mammals.[10] Most of the work in this dissertation will focus on P1 protamine, but it is important to note the similarity for P1 and P2. P2 has been shown to have high (>60%) sequence identity among P2 molecules for different species and 50-70% sequence identity between P2 and P1. [10] One example, the sequence for horse protamine P2 is given in Figure 1.7. [10, 28] In animals with both P1 and P2, the exact P1/P2 ratio is highly species specific. But it has been shown that when the P1/P2 ratio is abnormal, more DNA fragmentation and poor fertilization outcomes are observed.

ARTTAGSYRRYRRRCCSPRRLYRLRRRRYRSSRRRRRRPCRRRRHRRVCRRVRRRRRCCRRR

Figure 1.7: Horse protamine P2 amino acid Sequence. P2 protamines are typically longer than protamine P1 protamines, horse protamine P2 is 62 residues long and contains 36 arginine residues (red) and 6 cysteine residues (blue).

The spacing between the DNA helices within completely condensed sperm chromatin is referred to as the interaxial spacing. Through small-angle X-ray scattering (SAXS) techniques, discussed in greater detail in section 2.1, the spacings between the DNA helices within DNA

condensates can be determined in a straight forward manner. The DeRouchey lab has recently shown that in isolated bull sperm nuclei, the interaxial spacing is 30.1 Å. [29] Since the diameter of DNA is 20 Å, this equates to 10.1 Å of water separating the DNA helices. Furthermore, by subjecting the bull sperm chromatin to a reducing agent, Hutchinson et al. showed that the disulfide bonds within the bull sperm chromatin can be broken. [29] Once the intermolecular disulfides break, the sperm chromatin complex relaxes and the interaxial spacing decreased to 29.0 Å, suggesting that bull sperm chromatin in its native state exists in a strained environment.[29] Upon a complete reduction of the intraprotamine disulfide bonds, it was shown that this ultimately leads to decondensation. This is especially surprising as the bull protamine still has a net +26 charge. Typically, a polycation of net charge of +3 or higher is sufficient to enable DNA condensation. This work suggested that the disulfide-mediated secondary structure, the formation of this hairpin, was also critical for proper protamine function. It is a major focus of this dissertation, especially chapter 5, to more fully investigate the importance of the hairpin to DNA remodeling in the sperm chromatin.

Section 1.3: Sperm Chromatin Remodeling

The development of mature sperm cells from stem cells is called spermatogenesis, shown in figure 1.8. [7] During spermatogenesis, diploid spermatogonium mature into haploid spermatozoa. As part of this maturation process, the sperm chromatin changes from histone-based packaging to a protamine-based packaging. [30] This is accomplished first by removal of the DNA histones from the chromatin by sperm-specific transition proteins. [31] These transition proteins are then ultimately replaced with arginine-rich protamines. [31] The exact processes behind chromatin remodeling is still poorly understood, however, it is presumed that both the transition proteins and sperm protamines are initially phosphorylated, to help neutralize the high

cationic charge of the protamines, then subsequently dephosphorylated during the chromatin remodeling process. [31] This maturation process begins in the testis and concludes in the epididymis (Figure 1.9). [32-34] In mammalian species, as sperm travel from the head of the epididymis to the epidydimal tail, free thiols on the protamine cysteine are oxidized and disulfide linkages form within the protamines. [35] The enzyme responsible for this thiol oxidation within sperm cells is phospholipid hydroperoxide glutathione peroxidase (PHGPx). [36] Some evidence indicates the intraprotamine disulfide bonds form early in the maturation process, while interprotamine linkages form later after the protamines are bound to the DNA surface.

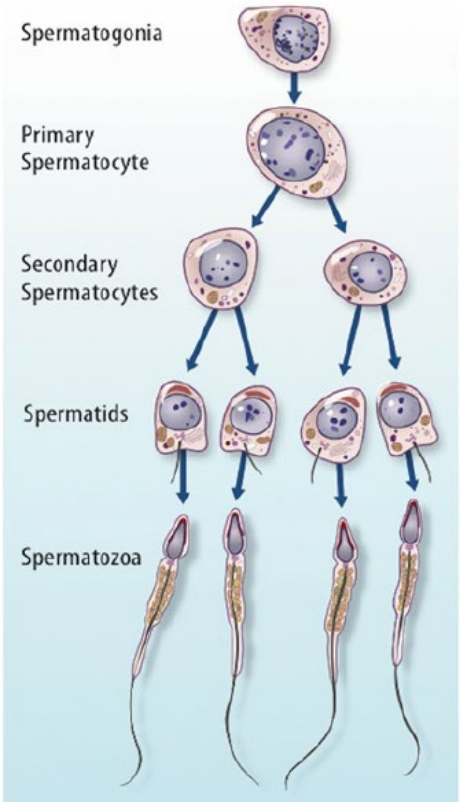

Figure 1.8: Sperm maturation is a lengthy multistage process, taking 74 days in total in humans. During this process diploid spermatic stem cells are maturing into haploid sperm cells. Adapted from [7]

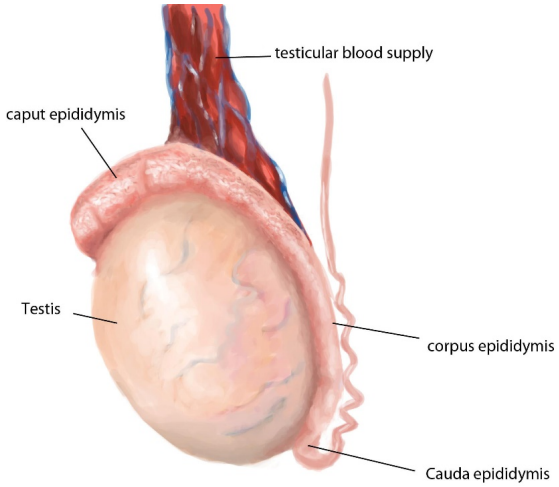

Figure 1.9: Anatomy of a human testicle, disulfide bond formation occurs as the sperm transit from the caput epididymis to the cauda epididymis. Adapted from [34]

Once chromatin remodeling concludes, the sperm DNA is transcriptionally inactive, and all DNA repair mechanisms are shut off. [23] Spermatogenesis in its entirety is a surprisingly long cycle, taking upwards of 74 days in humans. [30]

Section 1.4: DNA Condensation In Vitro

In our study, the majority of the data on DNA packaging was acquired by the use of DNA condensates created *in vitro*. Reconstituted DNA condensates have been well studied and typically occurs when a cation of +3 charge or higher is combined with DNA in an aqueous solution. Once this occurs, DNA will spontaneously condense and fall out of solution.[37] Condensation of DNA can depend on a number of factors, such as the nature and charge of the polycation. Due to the interplay of ion binding and attractions within the DNA condensates, small polycation chains (e.g. trivalent spermidine) are observed to have a critical concentration in bulk solution. [38] DNA condensation only occurs above this critical concentration. For very large polycations, (e.g. protamine or polylysine), the critical concentration is essentially too small to observe and DNA condensation occurs in a more discontinuous fashion with the addition of even small concentrations of the large polycations. DNA condensation and the resulting packaging density is not particularly sensitive to DNA length for DNA longer than a persistence length (~50 nm or 150 base pairs). Once DNA condensation occurs, the helices order themselves into a tightly packed hexagonal lattice with regular interaxial spacing, which can easily be determined using SAXS. Short DNA strands, less than 400 base pairs, tend to form small, poorly ordered particles. [39] Condensation will not occur for very short DNA chains, below ~25 bp, or less than a single persistence length of the DNA. DNA packaging densities, and thus interaxial spacings, are cation dependent. Relevant for this work, protamine-DNA packaging in salmon and bull sperm nuclei has

been previously reported by the DeRouchey lab with an observed interaxial spacing of 29.2 Å and 30.1 Å respectively. [29, 40]

Section 1.5: Introduction to DNA Damage and ROS Damaging Agents

Section 1.5.1: Sources of DNA Damage

As discussed above, DNA in nature exists primarily in a highly compacted form. Wwhether through histone mediated packaging or protamine mediated packaging, this compacted DNA is still susceptible to damage from a variety of damaging agents. This damage can result from a variety of sources, both environmental and endogenous. Environmental sources include UV radiation, chemical agents, smoking and various other environmental factors. [41] Endogenous damage typically occurs through reactive oxygen species (ROS), often generated as the result of cellular processes. [41, 42] Biologically, we are most interested in describing the effect of DNA damage from ROS sources, therefore we will limit our discussion to reactive oxygen damaging agents. The most common ROS in sperm cells is superoxide. [43]Two common sources of superoxide within sperm cells is oxidative phosphorylation and the NADH dependent oxidoreductase. [43]

Common reactive oxygen species include superoxide, hydrogen peroxide, the hydroxyl radical and the peroxyl radical, these are shown in Figure 1.10. [44] ROS exists at low levels within

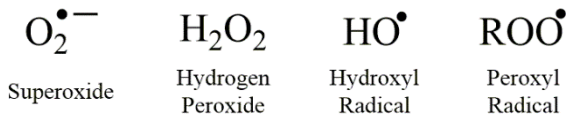

Figure 1.10: Several different ROS species are important in biological systems

cells and are part of normal cellular function. [45] Within sperm, ROS are often the product of mitochondrial metabolism and, amongst other functions, are critical to the immune response

within white blood cells. [46] Reactive oxygen species such as H_2O_2 are important during capacitation, a critical part of sperm physiology in which the sperm undergoes membrane changes in the female genital tract prior to fertilization. [47, 48] These cellular radical species are kept in balance by the antioxidant capabilities of the cell. [49] Cellular antioxidants include superoxide dismutase, catalase, vitamin A, vitamin E, and glutathione. [50] These antioxidants are present in sperm cells as well and function to absorb excess radical species and prevent them from damaging sperm cellular components. [50] When the production of radical species is excessive, the antioxidant capabilities of the cell are overwhelmed and excess oxidative species can cause damage to cellular components such as membranes and DNA. [44]

Section 1.5.2: ROS effect on DNA

Regardless of the source, damaging agents, including ROS, can result in many different lesions or aberrations to DNA. These include DNA base pair damage, inter and intrastrand crosslinks, single and double-strand breaks, and base pair mismatches (Figure 1.11). [51] DNA damage can have a profound effect on cellular health and function. [52] Excessive DNA damage within cells, if not repaired, can lead to cellular dysfunction and apoptosis, as well as impart genetic variation into the organism. This can lead to a greater incidence of cancers and immunological disorders, among other cellular abnormalities. [53, 54] The scope of ROS damage

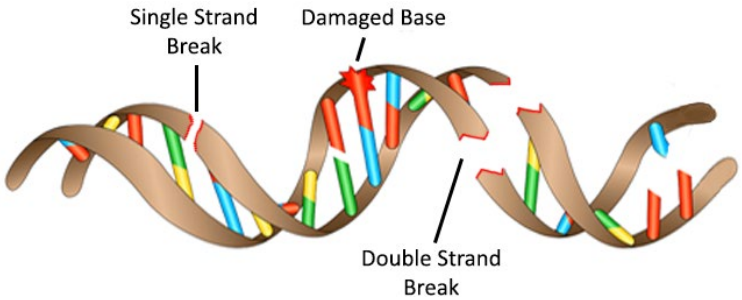

Figure 1.11: Through ROS action on DNA, several DNA lesions are possible, including base damage, single and double strand breaks. Adapted from [51]

on DNA is quite large. In this study, we have limited the types of DNA damage we will discuss and quantify to DNA base pair damage and DNA single and double-strand breaks.

All 4 DNA bases are susceptible to ROS damage. Guanine, however, is particularly prone to oxidative stressors chiefly due to its low oxidation potential of -1.3V, the lowest of all 4 DNA bases. [55] Guanine, which normally pairs with cytosine can be reacted with ROS species to form 8-Oxo-2'-deoxyguanosine (8-oxo-dG), one of the most well-described DNA base lesions. [56] Multiple pathways for this oxidation exist but typically occurs through a one-electron oxidation at

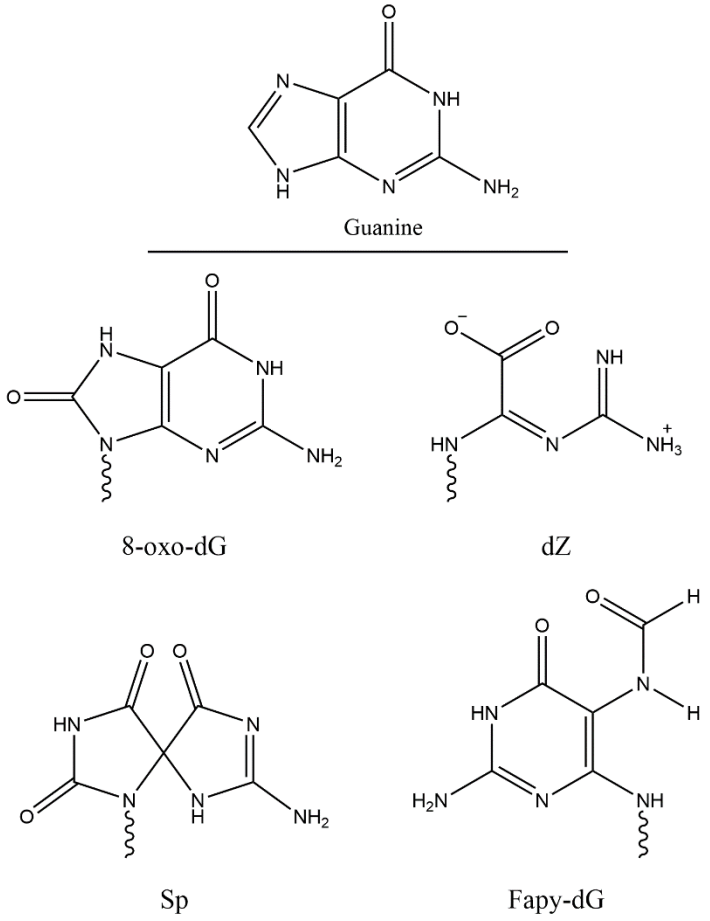

Figure 1.12: The DNA base Guanine is particularly susceptible to damage and results in the formation of several different exotic products

either the C8/N7 double bond or the C4/C5 double bond. [44] 8-oxo-dG can base pair with adenine as opposed to cytosine which causes a base pair transversion, a mutation in which a purine base is substituted for a pyrimidine base within the DNA. [57] 8-oxo-dG can be further oxidized to form more exotic DNA base lesions, a selection of which include: spiroiminodihydantoin (Sp), 2,2,4-triamino-5(2H)-oxazolone (dZ) and 2,6-diamino-4-hydroxy-5-formamidopyrimidine (Fapy-dG). The chemical structures of these lesions are provided in Figure 1.12. [42, 44, 55] These base pair lesions, and others, can result in aberrant base pairing and lead to cellular mutations or apoptosis if not repaired.

ROS sources can also cause DNA single-strand nicks and double-strand breaks to the DNA helix. [58] Single-strand nicks are typically caused by the extraction of a hydrogen from the sugar-phosphate backbone of DNA by a reactive oxygen species. [59] This extraction results in both the formation of water and of a radical on the backbone of the DNA, which propagates the reaction. [60] The end result of this hydrogen extraction is the cleaving of the DNA backbone which leads to a single strand break. This is shown in figure 1.13 . Double breaks occur when two single-strand breaks are within one helical turn of each other on the complementary DNA strand. [61]

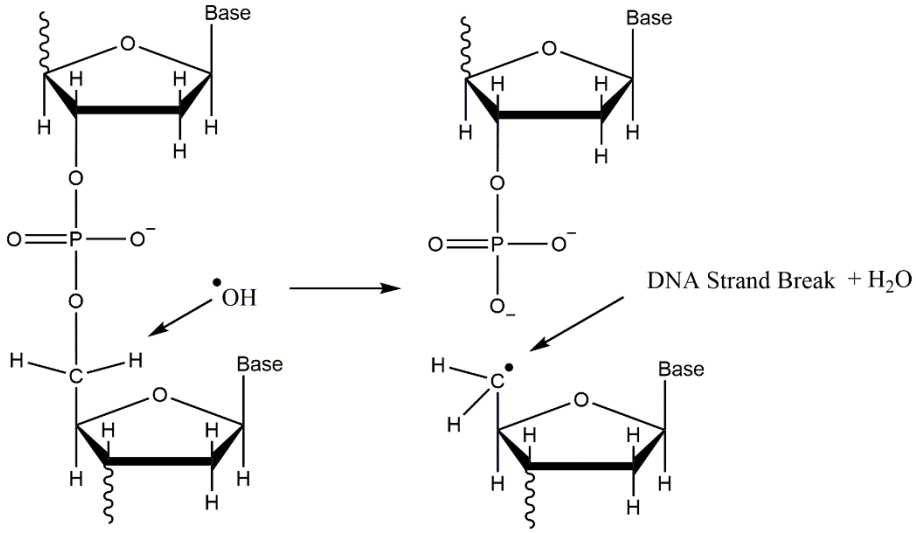

Figure 1.13: Extraction of a hydrogen from the DNA backbone by the hydroxyl radical results in the formation of water and a radical on the DNA backbone, this ultimately results in a DNA strand break.

Section 1.5.3: The AAPH DNA Damaging Agent

In our damage studies, we have used 2,2'-Azobis(2-amidinopropane) dihydrochloride, AAPH, as a damaging agent. AAPH, although not a ROS, is a commonly used radical generator due to its widespread availability and ease of use. [62] AAPH is both readily soluble in aqueous solutions, common in biological systems, and exhibits well described first-order degradation mechanics. [62, 63] AAPH generates both carbon-centered radicals as well as alkoxyl and peroxyl radicals, which are relevant in biological applications. [64] AAPH has been shown experimentally to generate radicals at a constant rate, which allows for greater precision between experiments.

[65] An abbreviated AAPH degradation reaction scheme is listed in Figure 1.14, showing the generation of the carbon-centered, alkoxyl, and peroxyl radicals. [35, 64].

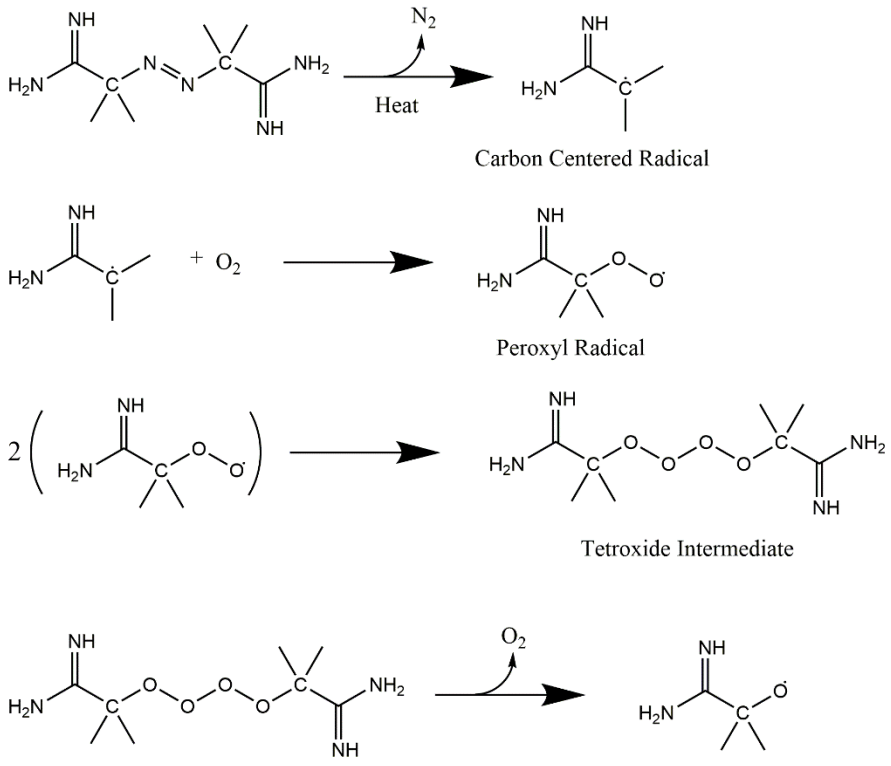

Figure 1.14: AAPH degredation products result in the formation of several radical species including the peroxyl radical. Adapted from [62]

Prior research has shown that AAPH readily forms strand breaks in plasmid DNA. [66, 67] Treatment of guanine with AAPH has resulted in the formation of several guanine oxidative damage products, showing that AAPH can cause relevant base damage. [68] As discussed in Chapter 3 and 4, we also observe that AAPH allows us to form multiple types of DNA lesions, including DNA base damage and single and double-strand breaks.

Section 1.6: DNA Damage and Detection Within Sperm Chromatin

Sperm exist in an extremely oxidatively damaging environment, with numerous endogenous radical sources being in close proximity to the DNA within the sperm nuclei, such as the abundant mitochondria within the sperm midsection. [69] Since DNA repair mechanisms do not function in mature sperm nuclei, any damage subjected to the spermatic DNA will remain on the DNA until after fertilization occurs, when sperm chromatin is 'unpacked' from the protamines. [23] Since spermatogenesis and spermiogenesis are upwards of 74 days long, and DNA repair mechanisms do not function after spermatogenesis, we hypothesize that there is much time for DNA damage to accrue in the spermatic DNA with even slight errors in the chromatin remodeling. [30]

Sperm containing greater levels of DNA damage can lead to many different effects to both the sperm itself and to the offspring after fertilization occurs. Sperm containing large amounts of DNA damage is indicated in reduced male fertility levels (discussed in detail in section 1.7 below). [70] High levels of DNA damage is associated with increased prevalence of childhood cancers, and can introduce genetic aberrations into the embryo, possibly increasing the predisposition of the offspring to genetic abnormalities. [71, 72]

DNA damage within sperm nuclei is typically assessed by one of several different testing methods. The acridine orange (AO) test and the sperm chromatin structure assay (SCSA) are two

of the most common methods for assessing damaged sperm. [73] The AO test is performed through the intercalation of acridine orange into the sperm DNA. [74] The intercalated nuclei are then excited for fluorescence and the resulting emissions are observed. Acridine orange fluoresces green when intercalated into double-stranded DNA and red when intercalated into single-stranded DNA. [74] By observing the resulting colors, an assessment of the prevalence of DNA damage within the sperm nuclei can be determined, with green corresponding to nuclei with good chromatin integrity, and red corresponding to nuclei with poor chromatin integrity. Nuclei that fluoresce yellow are indicative of nuclei with moderate levels of DNA damage. [75]

Coupling of the acridine orange test to a flow cytometer allows for large numbers of labeled sperm nuclei to be measured quickly. This analysis is referred to as the Sperm Chromatin Structure Assay, or SCSA. [76] By comparing the absolute number of sperm cells showing red or yellow fluorescence to the total number of sperm cells counted, a DNA fragmentation index, or DFI, can be obtained. [76] This value allows for the absolute quantification of the extent the DNA damage within sperm nuclei and is quite useful therapeutically. Patients with a DFI of greater than

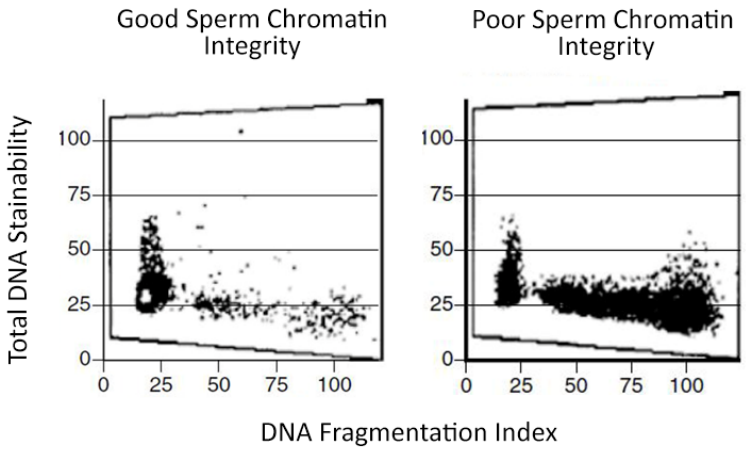

Figure 1.15: Images from Everson et al showing a sample Sperm Chromatin Structure Assay readout. Each data point is one sperm cell. Sperm with poor chromatin integrity are on the right side of the plots, while sperm with good chromatin integrity are on the left side of the plots. Adapted from [76]

20% are often at risk for infertility. [77] A sample SCSA readout is shown in Figure 1.15, where each dot represents one measured sperm.

Section 1.7: Assessment and Prevalence of Male Infertility.

Infertility is a complicated condition with both males and females playing a major role in the inability for a couple to conceive. When attributing incidences of infertility to men, the term 'male factor' is typically used. [78] Fertility rates in men are currently decreasing in Western nations, and as a result, the mechanisms and causes behind male factor infertility are beginning to be more appreciated than they were in the past. [79] Worldwide, 10-15% of couples will experience incidences of infertility at some point; of this, 40-50% can be attributed to the male factor. [70, 80] Typically, male factor infertility is diagnosed through the analysis of several different parameters in the patient's semen. [81] These semen parameters include: overall sperm count, assessment of sperm mobility, description of sperm morphology, percentage of living vs. dead sperm, pH of the ejaculate, and overall semen volume. [81] 15% of men diagnosed with infertility, however, have completely normal semen parameters. [82, 83] In patients such as this, DNA damage in sperm chromatin may play a critical role in their infertility. [70] Normal semen parameters do not typically assess for the integrity of the sperm chromatin, apart from obvious issues with the morphology of the sperm head. [84] Because of this, testing into to the absolute integrity of the DNA within the sperm nuclei, whether through the assessment of DNA damage or the determination of levels of protamine, have become more important. [85] With the increase in the use of assisted reproductive technologies, particularly with Intra Cytoplasmic Sperm Injection (ICSI), in which a singular sperm is directly injected into an egg cell, sperm selection is critical. Therefore, the direct assessment of an individual sperms' chromatin integrity is becoming more important as well. [76, 82, 84]

Section 1.8: Research Goals and Scope of This Study

In this study, our overall goal was to better understand how protamine dysfunctions alter the DNA packaging in sperm chromatin and how such mispackaging may relate to the accessibility of ROS and ultimately to DNA protection within the sperm nucleus. Although focused on sperm chromatin and protamine-DNA condensation, many of these results will have broad implications for supramolecular self-assembly of DNA and polycations with potential applications in materials, chemical, and biomedical engineering technologies. Chapter 2 gives an overview of the methods used throughout this dissertation. In chapter 3, we focus on understanding how DNA protection is related to the DNA packaging density in the DNA condensate. DNA condensed with a variety of different polycation condensing agents were studied. We show how the protection in the condensed state is not only dependent on how tightly packaged the DNA molecules are but also on the length of the polycation. This likely suggests the polycations are dynamic within the condensates, and resulted in short polycations, despite having tightly packaged DNAs, being more susceptible to damage than longer polycation chains. Chapter 4 focuses on the effect of underprotamination within DNA condensates. It is known in vivo that protamine synthesis can be disrupted, resulting in more damaged sperm chromatin. We examined in reconstituted protamine-DNA how condensates lacking sufficient levels of protamine relates to the susceptibility of the DNA bases to damage by free radical species. We will also show how small cationic peptides can be used to recover the DNA protection even in isolated sperm nuclei. Lastly, Chapter 5 focuses on the role of disulfide bond formation within bull protamine. We will show how disulfide bond formation effectively increases the local cationic charge density of the bull protamine binding domain, allowing it to effectively condense DNA. By altering the local cationic charge density through the cleavage of the disulfide linkages and destruction of the bull protamine hairpin, we will show through a variety of microscopy and biochemical methods that

DNA condensation is greatly altered. The formation of chromatin inclusion bodies resembling sperm nuclear vacuoles and the effect of sperm maturation on chromatin interaxial spacing will also be discussed.

Chapter 2: Methods

Section 2.1: Introduction Into Small Angle X-Ray Scattering

Section 2.1.1: Arrangement of DNA Helices in Condensed DNA Systems

DNA condensed by polycations typically arrange themselves into an ordered hexagonal lattice. [86] The interaxial spacing between the DNA helices within this lattice are typically on the order or ~28 - 33 Å, with 7 - 15 Å of water existing in between the DNA helices. [86] This arrangement, and the resulting interaxial spacings make DNA condensates well-suited characterization by X-Ray scattering techniques. [87] A schematic of the arrangement of a DNA-cation condensate is shown in Figure 2.1. The distance between the parallel planes of DNA is referred to as the Bragg spacing, while the distance between the helices is termed the interhelical, or interaxial spacing. The Bragg spacing is determined through X-Ray scattering techniques, while the interhelical spacing can be determined through simple geometry.

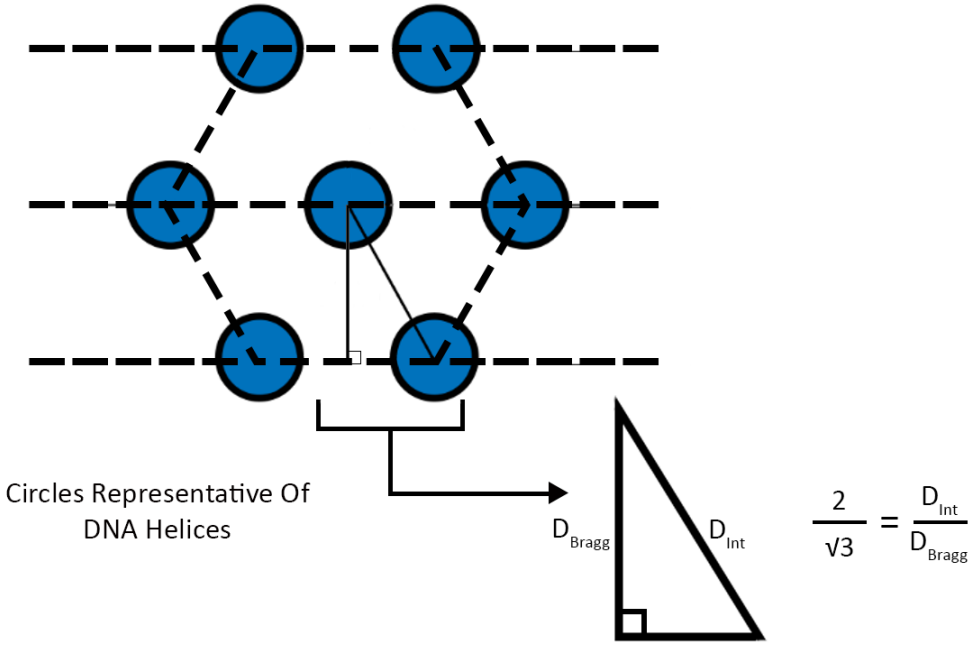

Figure 2.1: Typical arrangement of DNA helixes within a DNA-cation condensate. Through SAXS techniques and simple geometry, the Bragg spacing (D_{Bragg}) and Interhelical spacing (D_{Int}) can be determined.

Section 2.1.2: SAXS Theory and Principle

Since the structures and distances involved in DNA condensates typically range in size on the order of angstroms, X-Rays, which range in magnitude from 0.1 – 100 Å, are well suited to elucidate information about the structural arrangement of DNA within these condensates. [88, 89] When incident X-Ray radiation encounters a sample, in our case condensed DNA, the X-Rays are scattered by the electron cloud of the atoms within the sample. [89] A majority of this scattering is very diffuse and not particularly useful, however, a portion of the X-Rays will be scattered in a specular fashion, where the orientation of the incident radiation is the same as the outgoing radiation. [89]

When X-Rays scatter in a specular fashion, they can interfere with each other either constructively or destructively. [90] Constructive interference occurs when overlapping waves are in phase with each other, and destructive interference occurs when overlapping waves are out of phase with each other. [89, 90] When X-Rays strike a sample, a portion of the incident beam is scattered, and another portion of the beam penetrates the sample and can be scattered by another atom on a plane within the sample. [89] This interaction can be described through Braggs law, shown in Equation 2.1:

$$2dsin\theta = n\lambda \quad (Equation\ 2.1)$$

Where n is an integer, λ is wavelength, θ is the scattering angle and d is the interplanar distance, also called the Bragg spacing. [90] Constructive interference resulting from the interaction of X-Rays with atoms on different planes within a sample results in the creation of a strong signal known as the Bragg peak. This can be used to determine details on the diffracting structure. [89]

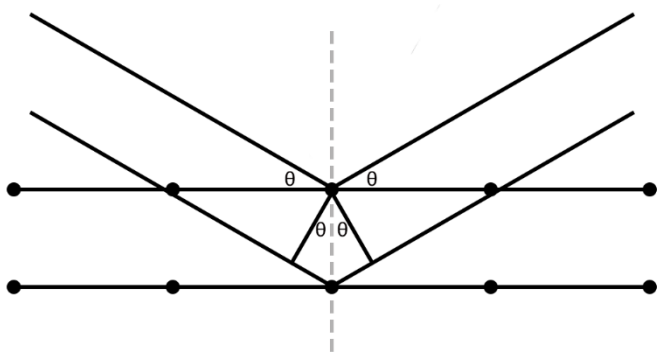

Figure 2.2: Schematic illustrating Braggs law. Adapted from [90]

By observing Braggs law, we see that interplanar distance (d) is inversely proportional to the scattering angle (Figure 2.2). [89] Therefore, different scattering angles can be used for the determination of structural characteristics of different magnitudes. [89] The scattering angles used in X-Ray structural determination are typically grouped into the 3 main categories, Ultralow Small Angle X-Ray Scattering (USAX), which encompasses scattering angles in the range of 0.001 - 0.3°, Small Angle X-Ray Scattering (SAXS), which includes angles of 0.1 - 10° and Wide Angle X-Ray Scattering (WAXS), which encompasses angles of >10 °. [89] Through these scattering angles, structures on the order of the following magnitudes can be accurately described: USAXS: <10 nm, SAXS: 1-100 nm, WAXS: >100 nm. [89]

Section 2.1.3: SAXS Experimental Setup

The experimental setup for the SAXS experiments used in this study is shown in Figure 2.3. Here, the X-Ray beam passes through the beam guide into the sample which is held in the sample holder. From there, the X-Rays are scattered by the sample and travel towards the detector, passing through a helium-filled box which is present to minimize aberrant scattering. Once hitting the detector, the scattering pattern is recorded.

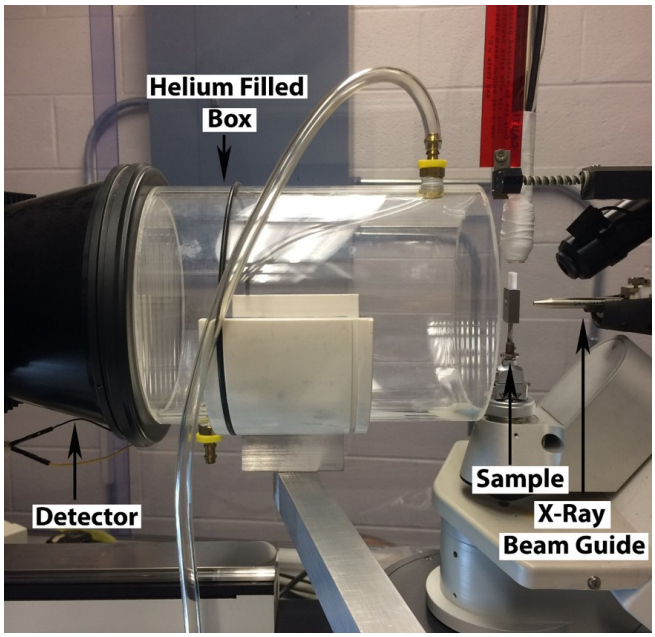

Figure 2.3: SAXS experimental setup at UK X-Ray Crystallography Lab.

The sample holder used in this SAXS setup is shown in Figure 2.4. There are two types of sample holders, each with their own distinct use. Sample Holder A is used for measuring DNA condensates. In this sample holder, the DNA condensate is first placed in the holding device shown part C, which consists of three plastic chips with small cutouts. The DNA condensate (often a hard DNA pellet) is placed in the small circle on the apex of the triangular cutout along with some sample buffer. Two mylar windows are then placed on either side of the triangle cutout to prevent the sample and buffer from falling out. The mylar windows are affixed to the plastic chips by the application of a small amount of silicone vacuum grease. The two plastic spacers with the large circular cutouts are then placed on either side of the Teflon chip containing the DNA condensate and mylar windows. This assembly is then placed in sample holder A and placed on the SAXS instrument via a small magnet on the X-Ray unit proper. Sample holder B is for use with X-Ray capillary tubes. The X-Ray capillary tubes are made of glass and are 80 mm long and 0.7 mm

in diameter. The X-Ray capillary tubes are for measuring sperm nuclei, which are centrifuged into the capillary tube, which is then placed into sample holder B.

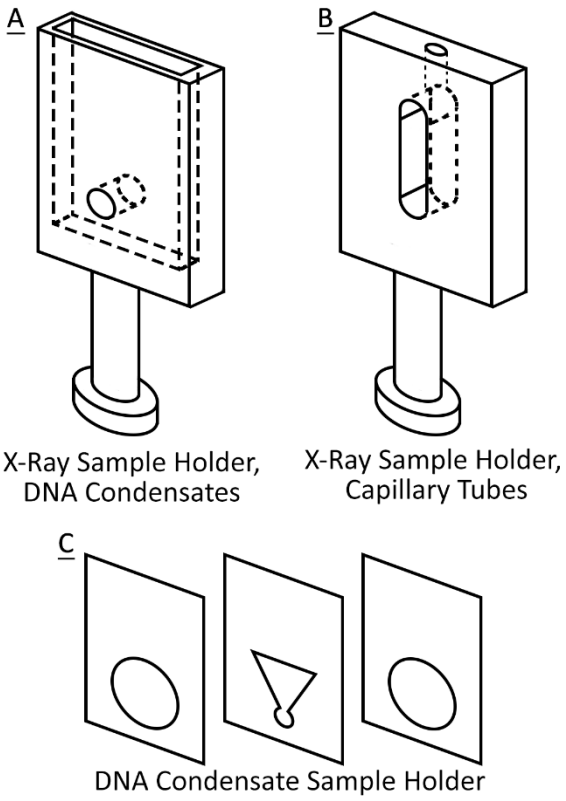

Figure 2.4: SAXS sample holders used in UK X-Ray crystallography lab. Sample holder A can be used for DNA condensates, while sample holder B is used for sperm nuclei

Section 2.1.4: SAXS Data Analysis

The resulting data generated from the SAXS analysis of DNA condensates is a scattering ring shown in Figure 2.5. To analyze the data and determine the Bragg spacing, the center of the X-Ray beam is determined, and the scattering pattern is radially integrated. This generates a plot of q vs. intensity. q is the scattering vector; this vector is inversely proportional to the distances between the DNA helices within the DNA condensate. By fitting a Gaussian curve to the scattering vector, we are able to obtain an exact q value and calculate the Bragg spacing through the relationships in Equation 2.2 and 2.3:

$$q = \frac{4\pi}{\lambda}\sin\theta \quad (Equation\ 2.2)$$

and

$$D_{Bragg} = \frac{2\pi}{q_{Bragg}} \quad (Equation\ 2.3)$$

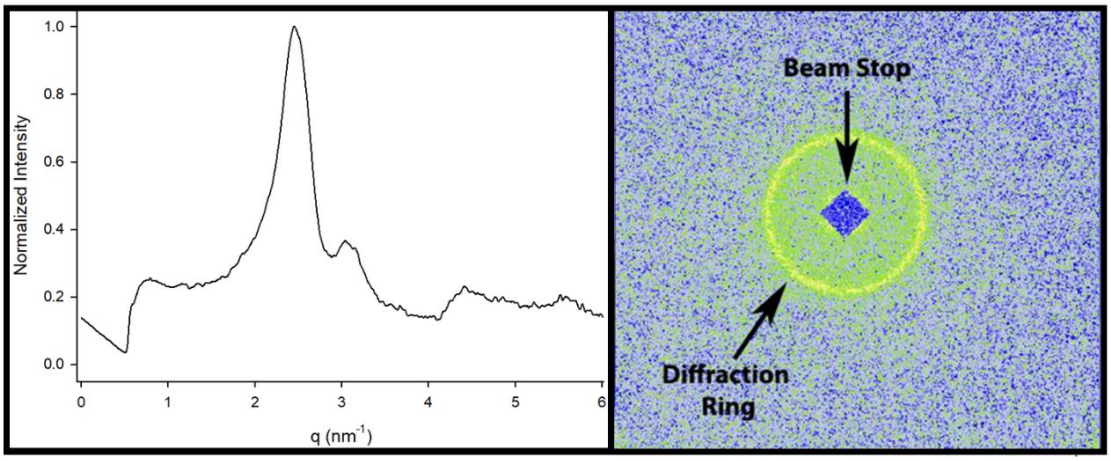

Figure 2.5: A typical SAX experiment results in the formation of a distinct ring (right). Integration of this ring allows determination of the scattering vector Q (left).

With the determination of the Bragg spacing, the interhelical, or interaxial spacing, can be determined through the relationship shown in Equation 2.4, where D-Int is the interhelical spacing:

$$\frac{2}{\sqrt{3}} = \frac{D_{int}}{D_{Bragg}} \quad (Equation\ 2.4)$$

Section 2.2: Gel Electrophoresis

Section 2.2.1: Principle of Gel Electrophoresis:

Gel electrophoresis is one of the most prominent analytical techniques used in both nucleic acid and protein chemistry. The principle behind gel electrophoresis involves the separation of proteins or DNA fragments by differences in size, conformation, and charge density. [91] This separation is accomplished by introducing the analyte into a gel which is then suspended within an ionic buffer and introduced into an electric field. As a result of this field, the analyte will migrate towards either the anodic or cathodic end of the electric field, depending on the net charge of the analyte. This migration will separate analytes based on not only on their net charge but their molecular weight and overall conformation. [92] Highly charged, low molecular weight analytes are able to migrate faster through a gel than lesser charged, high molecular weight analytes.

Section 2.2.2 Composition of Electrophoresis Gels

Gels used in gel electrophoresis typically fall into two main classes, agarose gels, and polyacrylamide gels. Agarose gels are polymers of the disaccharide agarose, which consists of D-galactose and 3,6-anhydro-L-galactopyranose. [93] Acrylamide gels are polymers of the acrylamide monomer, with N,N' methylenebisacrylamide functioning as a crosslinker. [93] Chemical structures of these two common gel mediums, acrylamide, and agarose are given in Figure 2.6.

By inducing polymerization of these materials, a gel can be formed with a gel matrix consisting of a regular pore size. By controlling the concentration either the agarose or acrylamide, the pore size of the gel can be readily controlled. Controlling the gel pore size allows for the resolution of analytes of many different sizes. Larger pore sizes are most appropriate for

resolving larger analytes, such as large DNA fragments, while smaller pore sizes are best suited for smaller analytes, such as low molecular weight proteins, or small DNA fragments. [94] Agarose

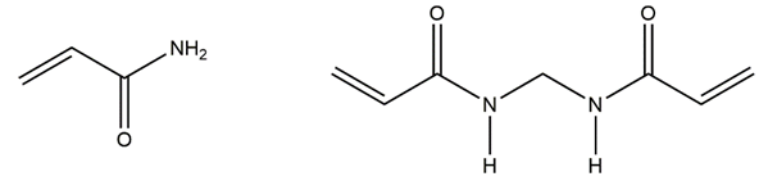

Acrylamide Monomer N,N'-Methylenebisacrylamide

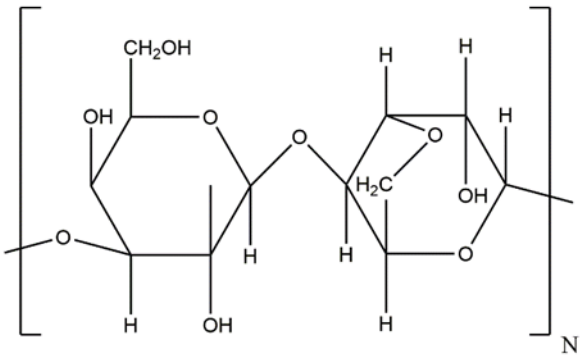

Agarose

Figure 2.6: Acrylamide monomer and Agarose are two common gel mediums. Bis-acrylamide functions as a crosslinker in acrylamide gels.

gels typically have a larger pore size than polyacrylamide gels, and therefore are typically used for electrophoresis of nucleic acid. [94] Polyacrylamide gels typically have a smaller pore size and are used for protein electrophoresis or resolution of small DNA fragments. The relationship between either agarose or acrylamide gel percentage and the effective DNA resolution range can be seen in Table 2.1 and Table 2.2. Notice that agarose gels can typically resolve larger DNA fragments than acrylamide gels. [95]

Table 2.1: Relationship between agarose gel percentage and DNA resolution range [95]

Agarose Gel Percentage	DNA Base Pair Resolution Range:
0.2%	5,000-40,000 Base Pairs
0.8%	1,000-7,000 Base Pairs
1.0%	500-5,000 Base Pairs
1.5%	300-3,000 Base Pairs

Table 2.2: Acrylamide gels are used to resolve small DNA fragments as well in protein electrophoresis [95]

Acrylamide Gel Percentage	DNA Base Pair Resolution Range:
8%	60-400 Base Pairs
10%	50-300 Base Pairs
12%	40-200 Base Pairs
20%	<40 Base Pairs

Section 2.2.3: Gel Electrophoresis Apparatus Setup

A schematic for a typical agarose gel setup is shown in Figure 2.7. Here we see the gel is immersed in its entirety in an ionic buffer. The anodic and cathodic ends of the power supply are present on opposite sides of the gel. Application of a voltage across the gel results in the generation of an electric field. Cationic species will be attracted towards the anode, while anionic species will be attracted to the cathode.

Analytes are introduced into the sample well, and once the electric field is applied across the gel, analytes will travel into the gel, with the direction of migration depending on the net charge of the analyte. In the case of DNA, the net negative charge attributed to the sugar-phosphate backbone of the DNA will result in the DNA migrating towards the anode. The velocity of an analyte migrating through a gel is defined by Equation 2.5: [96]

$$V = (E)(q)/f \quad (Equation\ 2.5)$$

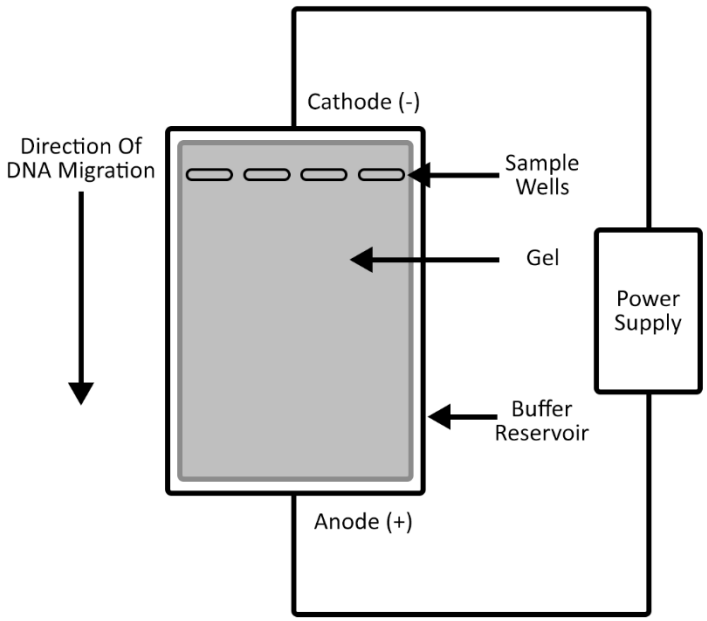

Figure 2.7: Typical setup for a gel electrophoresis experiment

where *E* is the strength of the electric field, *q* is the net charge of the analyte, and *f* is the frictional coefficient. [96] The net charge of the analyte is dependent on the number of charged moieties within an analyte, in the case of a protein, this is the number cationic and anionic amino acid residues, while DNA has a large net negative charge. The frictional coefficient is dependent on several different factors, including the pore size of the gel, the molecular mass of the analyte and overall conformation of the molecule. [96] We see that highly charged proteins will have a large

q value and thus migrate through a gel much faster than a lesser charged protein in a gel with a constant electric field strength. Bulky proteins will have a larger frictional coefficient and migrate slower than smaller proteins with lesser frictional coefficients. [93]

Section 2.2.4: Acid-Urea Gel Electrophoresis

Separation of small basic proteins typically requires different gel conditions than is afforded by conventional agarose or polyacrylamide gel electrophoresis. [97] Small cationic proteins include protamines, one of the principle analytes in this study. To sufficiently resolve protamines by gel electrophoresis, an "Acid-Urea Gel" is employed. [98] Acid urea gels are polyacrylamide gels with the addition of both acetic acid, to reduce the pH of the gel, and urea, a strong denaturant. [97] A high percentage of polyacrylamide is typically used, around 15%, to ensure adequate resolution of the small peptides. [99]

Section 2.2.5: Staining and Visualization of Electrophoresis Gels

Once an analyte has adequately migrated through a gel, it must be stained in order to view the resolved analyte, which is typically in the form of a gel band. There are many different stains used in gel electrophoresis, two of the most common stains are ethidium bromide and Coomassie Blue, shown in Figure 2.8 These stains were used for the majority of this study.

Ethidium bromide is a planar molecule which is used to stain nucleic acids. This staining occurs through the intercalation of the ethidium bromide between the base pairs of the nucleic acid. Within DNA, one ethidium bromide intercalates every 2.5 base pairs. [100] Ethidium bromide can be excited with UV light with an excitation maxima of 300 nm and results in an emission at 600 nm. [94] DNA concentrations as low as 10 ng can be observed.

Coomassie blue is a commonly used stain in protein electrophoresis. Coomassie blue is a nonspecific dye which binds all proteins regardless of their sequence. [101] Coomassie blue staining typically requires proteins within the gel matrix to first be 'fixed' prior to staining. Fixing a gel is performed by immersing the gel in a solution of methanol and acetic acid, which causes the proteins to crosslink and precipitate out within the gel. This prevents the proteins from diffusing out of the gel during the staining process. Samples stained in Coomassie blue can be easily observed in natural light, as the blue stain is visible to the naked eye. Coomassie blue staining is typically quite sensitive, with protein concentrations as low as 10 ng being able to be adequately observed. [101] In our study, we used a Coomassie stain called Acquastain (Bulldog Bio) which requires no lengthy fixation step and still affords protein detection as low as 10 ng protein.

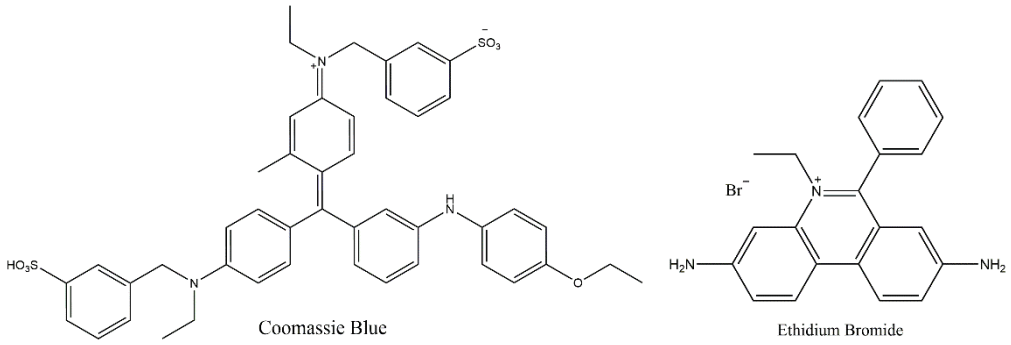

Figure 2.8: Chemical structures of Coomassie Blue and Ethidium Bromide, two commonly used gel electrophoresis stains. Coomassie Blue is used for protein staining, while ethidium bromide is used in DNA staining.

Section 2.3: Description of Cation and DNA proportions (N/P Ratio)

In order to accurately describe the interactions between positively charged protamines and the negatively charged DNA phosphates in the DNA condensates, we will discuss the formation of protamine-DNA complexes in terms of the N/P charge ratio, where N is the number

of moles of positively charged guanidinium moiety on the arginine side chain and P is the number of moles of negatively charged phosphates from DNA as given in Equation 2.6.

$$\frac{N}{P}\ Ratio = \frac{(+)\ Charge\ From\ Arginine\ Guanadinium}{(-)Charge\ From\ DNA\ Phosphate} \quad (Equation\ 2.6)$$

At physiological pH, each arginine residue contributes 1 cationic charge, while each DNA base pair contributes 2 anionic charges. At a N/P charge ratio of 1, then there are just enough positive charges to compensate for the negative charges from the DNA. In a typical condensation experiment, we will keep the concentration of DNA constant and alter the amount of cation present within the condensate, thereby allowing for different N/P ratios. Through this nomenclature, the amount of cation and DNA present within a condensate can be easily described.

Section 2.4: DNA – Cation Binding Assays

Section 2.4.1: Ethidium Bromide Displacement Assay

Ethidium bromide displacement assays are a commonly used method used to observe the binding of a cation to DNA. Ethidium bromide is a planar molecule which can easily intercalate into the hydrophobic environment in between the base pairs of DNA. [102] Once intercalated, the fluorescence intensity of ethidium bromide increases by upwards of 20 fold [103]. This massive increase in fluorescence can be exploited to observe the binding of a cation to the DNA. Cationic species can interact with the negatively charged phosphate backbone of the DNA, condensing the DNA and displacing the intercalated ethidium bromide. Once this displacement occurs, the effective fluorescence of the ethidium bromide will decrease. This reduction in fluorescence can be used to measure the condensation of DNA by a cation. In this study, the excitation and emission

wavelengths for the ethidium bromide displacement assays were set at 520 nm and 595 nm, respectively. [103] We have represented the reduction in fluorescence in terms of 'relative fluorescence, which is defined through the relationship in Equation 2.7 [104]

$$Relative\ Fluorescence: \frac{F - F_o}{F_{Max} - F_o} \quad (Equation\ 2.7)$$

where F is the sample emission intensity, F_0 is the emission intensity of ethidium bromide without DNA, F_{Max} is the emission intensity of only DNA and ethidium bromide. The results are normalized, so that DNA with no cation present has an absorbance of 1, by observing the reduction in fluorescence, the amount of DNA bound by a cation can be easily observed. The ethidium bromide displacement assay has several advantages, the most advantageous being that it can be performed using only a small amount of DNA, as low as several micrograms.

A sample ethidium bromide displacement assay is shown in Figure 2.9. Here, ethidium bromide is intercalated into calf thymus DNA (ctDNA) and then condensed with polyarginine. We

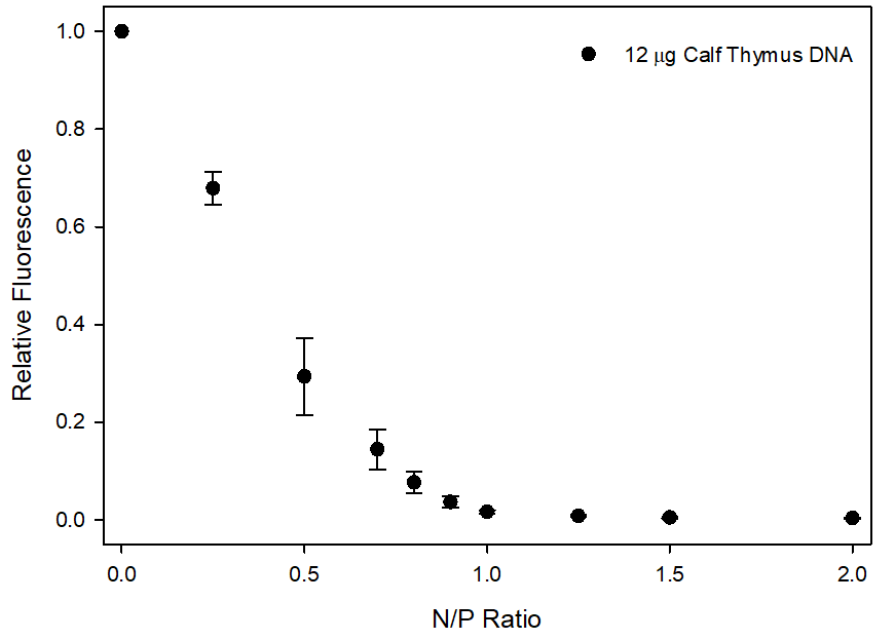

Figure 2.9: DNA Condensation ability of ctDNA measured by ethidium bromide exclusion assay in 10 mM Tris buffer. Values are given as mean ± standard error (n = 3).

see a progressive decrease in fluorescence as the protamine binds the DNA. At high protamine/DNA ratios, we see the nearly all the fluorescence has dissipated.

Section 2.4.2: UV-Vis DNA Precipitation Assay

A UV-Vis DNA precipitation assay is an assay used to both measure and observe the progress of a cation binding DNA in solution. [105] In DNA precipitation assays, aqueous DNA and cation are combined and allowed to condense for several minutes. As the cation binds the DNA, the DNA precipitates and falls out of solution. After centrifugation, the amount of DNA left in the supernatant can be measured. DNA has a strong UV-Vis absorbance at 260 nm due to the π to π^* transitions in the purine and pyrimidine rings of the DNA bases. [106] By monitoring the absorbance at 260 nm, the amount of DNA bound by a cation can be determined. By normalizing the absorbance at 260 nm, so that DNA with no cation present has an absorbance of 1.0, the percentage of DNA bound by a cation can be easily determined. DNA precipitation assays are a much more direct measurement of DNA binding than the ethidium bromide displacement assays. However, they require a much greater minimum DNA concentration, on our instruments, a minimum of 50 μg.

An example of a DNA precipitation assay is shown in Figure 2.10. Here we see the progressive binding of the aqueous DNA protamine. Naked DNA without the presence of any cation shows an absorbance of 1.0, addition of the cation to the DNA progressively decreases the absorbance. At N/P 1.10, all the DNA is bound by the cation and results in an absorbance of 0.

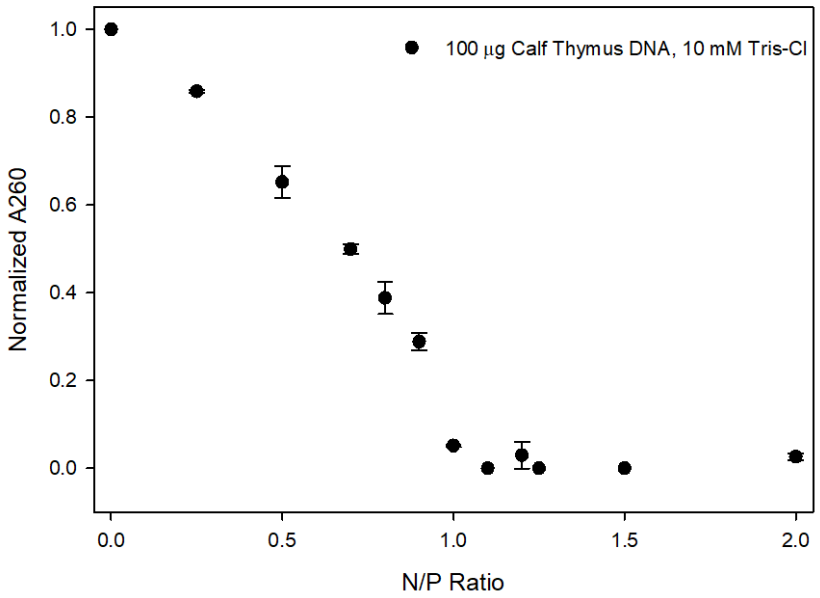

Figure 2.10: DNA precipitation assay using protamine. By condensing aqueous DNA with a cation and monitoring the residual DNA concentration at A260, the extent of cation binding can be determined. Values are given as mean ± standard error (n = 3).

Section 2.5: The FPG Enzyme

In order to accurately describe the types of damage sustained to DNA by our damaging agent, AAPH, we have employed the use of an enzyme that allows for the direct detection of damage to the DNA base that does not result in a single or double-strand break. This enzyme, formamidopyrimidine DNA glycosylase (FPG) recognizes purine bases that have sustained base damage and excises them from the DNA. [107] This allows for the introduction of a DNA strand break wherever a damaged purine is present along a DNA strand.

Chapter 3: Effect of DNA - Cation Architecture on Polyplex Stability and Damage Susceptibility

Section 3.1: Introduction

The packaging of DNA into cellular nuclei is a compaction of massive proportions. In somatic nuclei, the entire genome, a DNA molecule ~2 meters in length, is packaged by association with basic proteins called histones to fit into a nucleus with approximately 10 μm diameter. This packaging of the genome represents a near 10,000-20,000x compaction of the DNA in somatic cells.[2, 3] The complex of DNA and cellular proteins (histones) in eukaryotic chromosomes is called chromatin. Chromatin is composed of an elementary repeating unit called the nucleosome where DNA wraps around a core of histone proteins.[6] These chromatin fibers undergo further levels of packaging into higher order structures, ultimately giving rise to the classic X-shape structure called the metaphase chromosome. [108, 109] In contrast to somatic cells, sperm spells package their DNA with small arginine-rich peptides known as protamines. [10] During spermiogenesis, first transition proteins and subsequently protamines replace the vast majority of histones in the sperm chromatin and package the DNA sufficiently to fit in the sperm nuclei. In sperm, the nuclei composes the majority of the sperm cell head. Both in vivo and in vitro, protamine-DNA condensates give rise to toroidal structures (Figure 3.1, left). Within these toroids, the DNA is condensed into a near-crystalline packaging state with DNA helices arranged in a hexagonal lattice (Figure 3.1, right). [110] Due to the extreme packaging of the genome, the DNA within mature sperm chromatin is rendered nearly transcriptionally inactive. Small amounts of mRNA have been detected in sperm; however the exact source of the mRNA is still debated. [111] It is thought that the chromatin remodeling that occurs during spermiogenesis serves at least two major purposes. First, protamine condensation enables the reduction of the genome in size, allowing for easy storage and transfer of the DNA to the ovum, but also second, protects the DNA from damage. [20] Chromatin, and in particular sperm chromatin, exist in a highly oxidative

environment. [112, 113] Protecting the genome from damage is critical, as DNA damage is implicated in both cancers and various disease states. [114]

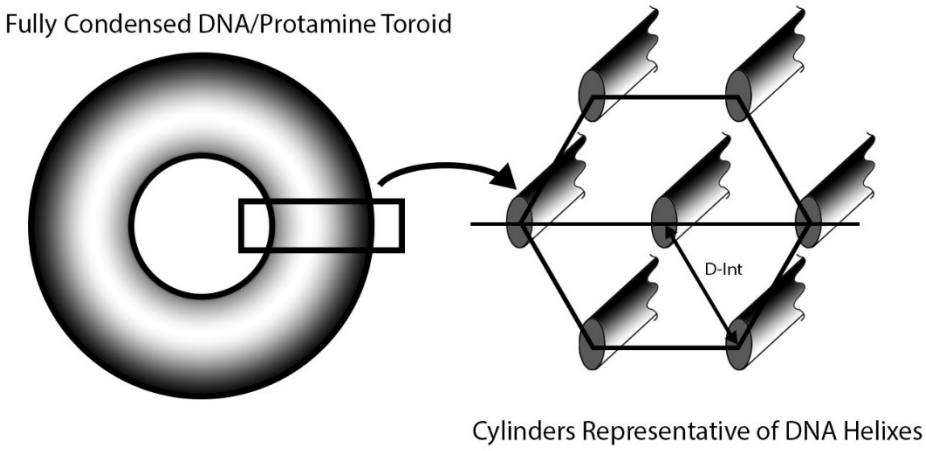

Figure 3.1, DNA condensed by polycations typical organize themselves into a hexagonal array with a regular interaxial spacing between the DNA helices. The exact interaxial spacing is cation dependent.

Takata et al. showed recently that histone compaction protects genomic DNA from radiation damage and attack by chemical agents. [115] Naked, uncondensed DNA, subjected to ROS damage by way of a Fenton reagent had a 100x greater incidence of strand breaks than histone condensed DNA under the same conditions. [116] Studies into the effect of iron-catalyzed damage on nucleosome assemblies showed that DNA was preferentially cleaved in the linker portions of the nucleosome, suggesting that the histones protected the DNA from the oxidative damage. [117] Although DNA repair mechanisms function in somatic chromatin, double-strand breaks can result in repair by non-homologous end joining, which can impart genetic variation into the DNA, and is implicated in the formation of tumor cells, thus DNA damage should be avoided. [118]

In sperm chromatin, it is thought the protamine condensation of the genome serves a similar protective role as the histones, although little is known regarding the extent of protection

in these highly condensed states. [116] In sperm nuclei, where the majority of DNA is condensed with protamines, low levels of protamine (or underprotamination) has been shown to correlate to increased levels of DNA damage. [119] Analysis of sperm chromatin through the comet assay has shown that greater incidences of strand breaks are present within sperm nuclei which test positive for Chromomycin A_3, an indicator of poorly condensed DNA. [120, 121] Protection of DNA is thought to be particularly critical in sperm chromatin, as all DNA repair mechanisms are nonfunctioning. [122]

We hypothesize that the accessibility of free radicals will be directly related to the packaging density within the condensed polycation-DNA complex, or polyplex. In this chapter, we have formed polyplexes using different polycations which condense the DNA to different packaging densities. We are interested in understanding how different packaging states affect the susceptibility of the condensed DNA to oxidative damage from free radicals. More specifically, we examine the role of cation length, and packaging density and the resulting prevalence of DNA strand breaks caused by ROS.

When DNA is condensed by a cationic polymer, it typically self-assembles resulting in a tightly packaged hexagonal array of DNA helices separated by water. [123, 124] Through small-angle X-ray scattering (SAXS) techniques, the DNA interaxial spacing can be determined, where a smaller interaxial spacing results in a greater packaging density. [86] In this chapter, reconstituted samples were prepared by condensing DNA with a selection of polycations of differing lengths and chemical identity including lysine and arginine, and both short peptides and high molecular weight polymers. In our cation selection, we have selected R_3-pSer-R_3, a cation containing a phosphorylated serine, as well as a similar non-phosphorylated cation, R_6. This will serve as a model for protein phosphorylation and dephosphorylation, an important process in sperm chromatin remodeling as well as other biological systems. [125] DNA packaging density was

determined using SAXS. Condensates, using plasmid DNA, were subsequently exposed to free radicals to quantify the relationship between DNA packaging density and resistance to damage. We have chosen to use 2,2'-Azobis(2-amidinopropane) dihydrochloride (AAPH) as our damaging agent, due to its ease of use and consistency in radical generation, as well as its well-characterized effect on plasmid DNA. [62, 63, 66] We anticipated that condensates of greater packaging density should be more resistant to oxidative damage as space constraints will hinder access of the radical species to the condensed DNA. However, as we will show, our results show that DNA damage in the condensed state is not only related to packaging density but also the nature of the condensing agent.

Section 3.2: Materials And Methods

Section 3.2.1: Materials

Calf thymus DNA, protamine-Cl from salmon, poly-L-lysine hydrochloride (P2658, 15-30 kDa, average M_w of ~20900), poly-L-arginine hydrochloride (P4663, 5-15 kDa, average M_w of ~13300), ethidium bromide, sodium azide and dextran sulfate from *leuconostoc spp*. (avg molecular weight 9,000-20,000) was purchased from Sigma-Aldrich. pBR322 plasmid was purchased from New England BioLabs. 50x TAE was purchased from Omega Bio-Tek. 1M Tris-Cl was purchased form MediaTech. Hexaarginine (R6) and a phosphorylated serine hexaarginine peptide (R3-pSer-R3) were custom synthesized and purified (>98%) by GenScript Corp. (Piscataway, NJ). 10x PBS was purchased from Fisher BioReagents. All reagents used without modification unless noted.

Section 3.2.2: Ethidium Bromide Exclusion Assay

Stock solution of DNA was prepared by dissolving calf-thymus DNA in 10 mM Tris–HCl buffer (pH 7.5) overnight to a final concentration of 1030 mg/mL. The DNA concentration was determined by UV absorption at 260 nm where A_{260} = 1 corresponds to a DNA concentration of 50 μg/mL. For the EB exclusion assay, 12 μg calf thymus DNA was placed in 10 mM Tris buffer and ethidium bromide was added at a 1/10 molar ratio of ethidium bromide to DNA base pair. The sample volume of ethidium bromide-DNA was adjusted to a final volume of 500 μL using 10 mM Tris buffer. [104] Stock polycation solutions were prepared by taking the polycations as received and dissolving it in 10 mM Tris-HCl buffer to the desired concentration. Polycation solution was added to the ethidium bromide/DNA sequentially at the desired N/P charge ratios. Samples were allowed to equilibrate for a minimum of 5 minutes between cation additions before measurement by fluorescence spectroscopy. Measurements were performed with samples in a quartz cuvette and polycation solution addition was never more than 2% of the total solution volume. Fluorescence was read at λ_{ex}=520 and λ_{em}=595. Data was reported as relative fluorescence: $(F-F_0)/(F_{Max}-F_0)$, where F is the sample emission intensity, F_0 is the emission intensity of ethidium bromide without DNA, F_{Max} is the emission intensity of only DNA and ethidium bromide. [104] Ethidium bromide exclusion assay was performed using the following polycations: R_6, R_3-pSer-R_3, poly-Arg, poly-Lys, and salmon protamine chloride. All measurements were performed on a Thermo Lumina Spectrophotometer. All plotted exclusion assay results are an average of at least 3 measurements for a given polyplex sample; standard error was calculated.

Section 3.2.3: UV-Vis Monitored Precipitation Assay

Stock solutions of calf thymus DNA (ctDNA) and polycation were prepared as previously described. Precipitation of the ctDNA was studied by UV absorption monitored assay using a

Thermo Evolution 201 UV-Vis Spectrophotometer. 100 μg ctDNA was placed in a microcentrifuge tube, and polycation solution was added to achieve the desired N/P charge ratio. Polycation-DNA, or polyplexes, were then incubated at room temperature for a minimum of 10 minutes. Samples were subsequently centrifuged at 11,000g for 15 minutes, and the resulting supernatant was removed. Values of A_{260} were measured in the supernatant by placing 200 μl in a cuvette for measurement in the UV/Vis spectrophotometer. Results of the precipitation assay were normalized and plotted as normalized optical absorbance (A_{260}) versus N/P charge ratio. [126] A minimum of 3 samples were created for each data point and the results were averaged and plotted, standard error was calculated.

Section 3.2.4: DNA-Polycation Protection Assays

AAPH was activated by dissolving solid AAPH in DI water and incubating for 60 minutes at 60 °C. While AAPH was being activated, the desired amount of polycation stock solution was added to 200 ng of pBR322 plasmid DNA (pDNA) and mixed in a microcentrifuge tube. To ensure complete condensation of the pDNA, protection assays were performed at final cation N/P ratios: R_6: N/P 6.0, poly-Lys: N/P 6.0, poly-Arg: N/P 1.5, protamine: N/P 4.0, R_3-pSer-R_3: N/P 16. These Polyplexes were incubated for a minimum of 10 minutes at room temperature. Sufficient stock solutions of AAPH and 10X phosphate buffered saline (PBS) and distilled water were added to the microcentrifuge tube to achieve a final volume of 10 μL and a final concentration of 200 μM AAPH and 1X PBS. The diluted polyplex/AAPH solutions were then incubated at 60 °C for 60 minutes to damage the condensed DNA. After damaging, polyplexes were decondensed through competition with an added polyanion. Here we used 100 μg of dextran sulfate (DS) as our competitor and incubated the polyplex/DS mixture for a minimum of 10 minutes at room temperature to facilitate DNA release. This amount of DS was sufficient for full release of all the

polyplexes studied. Samples were subsequently mixed with 2 μL of DNA gel loading dye (6X) and loaded into 1% agarose gels in 1 x TAE buffer. Gels were allowed to run at 95 V and 70 mA for 90 minutes in 1X TAE buffer. The gels were then stained in ethidium bromide (EtBr, 2.5 μg/mL in 1X TAE buffer) for 45 minutes. Gels were visualized using a Bio-Rad ImageDoc gel imaging system. Gel lane integration was performed using ImageLab software. The polycation damage gel and resulting lane integrations were repeated 3 times. Lane integrations were averaged, and standard error was calculated. Protamine protection gel acquired with Ehigbai Oikeh (UK Department of Chemistry)

Section 3.2.5: DLS analysis of Polycation Condensates

DNA polyplexes for dynamic light scattering (DLS) analysis were created by combining 2 μg pBR322 plasmid and salmon protamine chloride at N/P 2.0. Particles were created in a plastic DLS cuvette in 2 mL deionized water. Particles were allowed to incubate at room temperature for 5 minutes, then measured. Particle size was determined by a Brookhaven ZetaPALS Zeta Potential Analyzer using the Multi-Angle Particle Size Option. The procedure was repeated the with the following cation N/P ratios: R_6 - N/P: 3.0, poly-Lys - N/P: 2.0, poly-Arg - N/P: 2.0, R_3-pSer-R_3 - N/P: 3.0. Each sample was measured 5 times, the results were averaged, and standard error was calculated.

Section 3.2.6: SAXS Analysis of Polycation Condensates

DNA polycation condensates were measured by SAX as described in section 2.3 and 2.4. Briefly, DNA condensates were placed in the sample holder described in section 2.4. Samples were measured by SAXS on an X8 Proteum diffractometer with Cu*Kα* radiation. Data was collected on a PT-135 CCD detector, fitted with a helium-filled box between the sample and the detector to

minimize aberrant scattering. Data analysis was performed on FIT2D and Origin data analysis software. Results are reproducible to ± 0.15 Å.

Section 3.3: Results

Section 3.3.1: DNA-Polycation Interaxial Spacings

Through the addition of DNA to polycations of differing length and composition, we are able to create polyplexes of differing DNA packaging densities. These are shown in table 3.1. Interaxial spacing was determined by SAXS analysis by assuming a hexagonal lattice for all polyplexes. Bragg spacings, which corresponds to the maximum in the scattering, are calculated as $D_{Bragg} = 2\pi/q_{Br}$, where q_{Br} is the maximum of the scattering vector, q. For a hexagonal lattice, the relationship between the Bragg spacing and the actual interaxial distance between DNA helices (D_{int}) is calculated as $D_{int} = (2/\sqrt{3})D_{Bragg}$. The resulting D_{int} values are given in Table 3.1. Here we see that DNA condensed with arginine containing polycations result in a higher packaging density than poly-Lys. The addition of the phosphorylated serine into the R_6 cation adds a large anionic charge into peptide and results in a much looser interhelical spacing. [86]

Table 3.1: Data from DeRouchey et al. showing interhelical spacings (D_{int}) of DNA condensates condensed by different cations. [86, 127]

Cation Type	D_{Int} (Å) (± 0.15 Å)
R_6	28.6
Poly-Arg	27.3
Poly-Lys	30.4
Protamine	29.3
R_3-pSer-R_3	33.3

Section 3.3.2: Effect of Polycation on Ethidium Bromide Exclusion from Polyplexes

Through the intercalation of ethidium bromide into calf thymus DNA, then subsequent condensation with a polycation, cation binding is able to be observed by the reduction of ethidium bromide fluorescence as ethidium bromide is excluded from the DNA. We performed EtBr exclusion assays for five different polycation-ctDNA complexes. Results are shown in Figure 3.2.

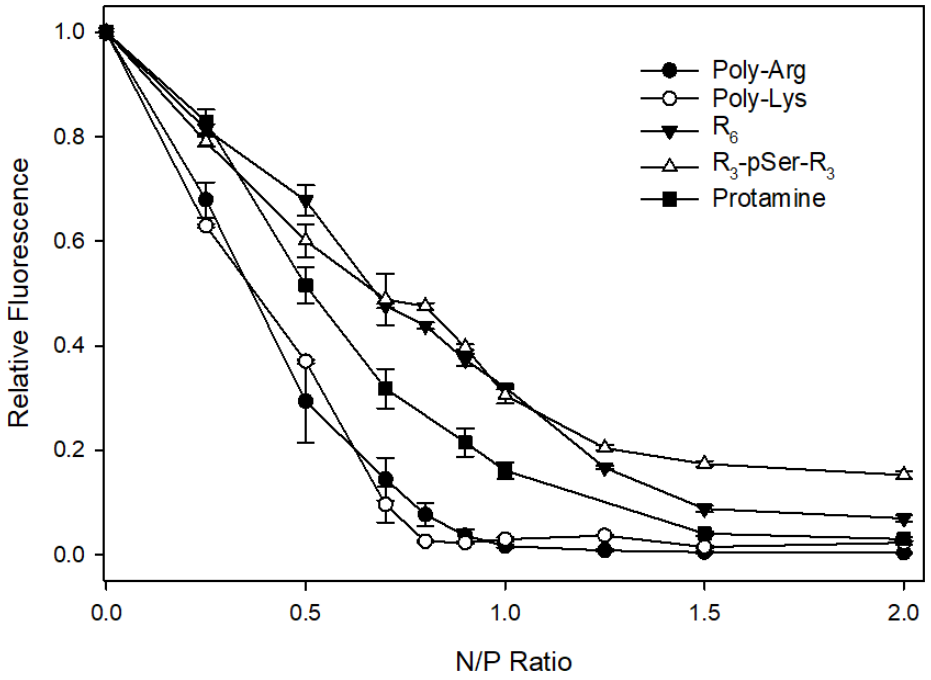

Figure 3.2: Ethidium bromide displacement assays of polycations of differing length and composition. Long cations (Poly-Arg and Poly-Lys) show complete DNA condensation by N/P: 1.0. Short cations (R_6, R_3-pSer-R_3) show complete DNA condensation by N/P: 2.0. Protamine, a mid-length cation, shows complete binding by N/P: 1.5. Values are given as mean ± standard error (n = 3).

Long polycations, such as the high molecular weight poly-Arg, and poly-Lys, both show a similar binding curve, with complete DNA condensation occurring by N/P: 1.0. Short cations, such as R_6 and R_3-pSer-R_3 require greater amounts of cation to fully condense the DNA, with complete binding occurring by N/P: 2.0. Protamine, an intermediate length polycation, shows complete binding by N/P: 1.5. R_3-pSer-R_3, that was observed by SAXS to result in the lowest packaging

density, show considerable levels of ethidium bromide relative fluorescence (~20%) even at high N/P ratios.

Similar binding curves are obtained by UV-Vis spectroscopy, shown in Figure 3.3. Long and mid-length polycations (poly-Arg, poly-Lys, and protamine), show complete binding by N/P: 1.0 and N/P: 1.20 respectively. Short cations, such as R_6 an R_3-pSer-R_3, result in complete DNA condensation by N/P: 2.0.

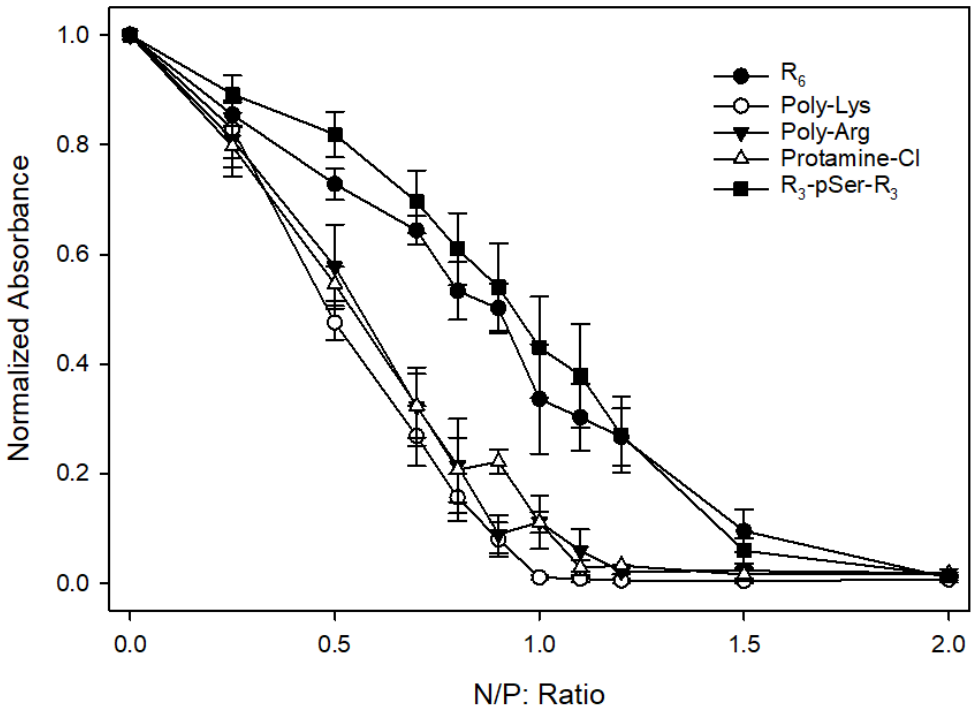

Figure 3.3: UV-Vis precipitation assay shows complete DNA binding by short cations (R_6, R_3-pSer-R_3) by N/P: 2.0. Mid-length and long cations (Protamine, Poly-Arg, Poly-Lys) show complete DNA binding by approximately N/P: 1.20 . Values are given as mean ± standard error (n = 3).

Section 3.3.3: PolyCation DLS Studies

DLS studies show that all polyplexes create similar sized colloidal particles that range in size from 239 to 369 nm, shown in Table 3.2. Polyplex particle sizes in these nanoparticles do scale approximately with the DNA packaging densities observed in our fibrous polycation-DNA

samples used for SAXS measurements. R_3-pSer-R_3/DNA, which resulted in the loosest DNA packaging density also gives rise to significantly larger nanoparticles. This shows the substantial effect that the phosphorylated serine and resulting in large DNA interaxial spacing has on the architecture of the polyplex. Protamine particle size is consistent with prior published results. [128]

Table 3.2: Particle size for DNA – PolyCation Condensates

Cation	**Diameter (nm)**
R_6	239 ± 10
Poly-Arg	246 ± 6
Poly-Lys	269 ± 6
Protamine	255 ± 7
R_3-pSer-R_3	369 ± 8

Section 3.3.4: Effect of AAPH on Plasmid DNA

Before examining the effects of exposure of free radicals in condensed DNA, we first examined the effects of AAPH concentration on uncondensed plasmid DNA (Figure 3.4). Here we see the effect that plasmid conformation has on the ability of the plasmid to travel through an agarose gel. Plasmid DNA can form three distinct conformations depending on the type of DNA damage sustained to the plasmid. Native, undamaged plasmid forms a fast-moving supercoil, a single-strand break (or nick) forms a slow-moving open coil, and double-strand breaks result in linear DNA, which migrates faster than an open coiled plasmid, but slower than a supercoil [66, 129]. All three conformations are observed in Figure 3.4. The uppermost band present in the control and 10 μM AAPH lanes is a population of catenated plasmid. High amounts of AAPH damage results in fragmented DNA, which is viewed as a smear on the gel.

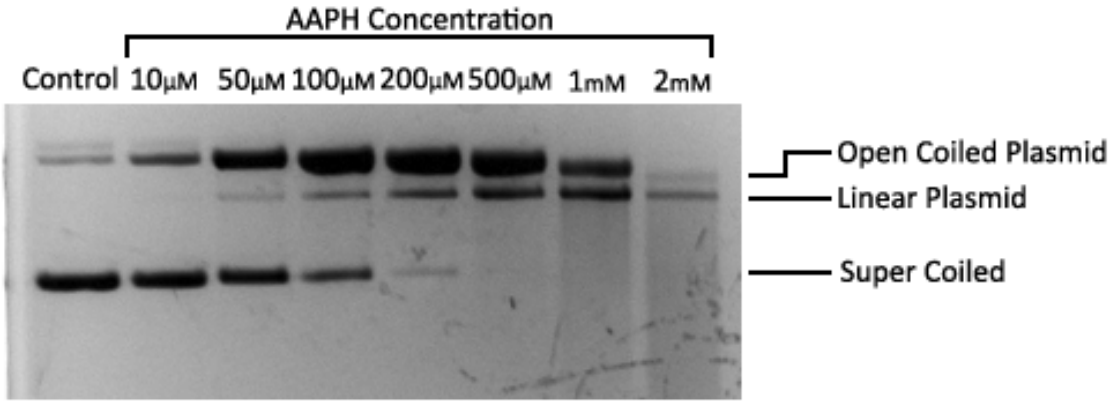

Figure 3.4: By observing migration differences of AAPH damaged plasmid across an agrose, the presences of DNA strand breaks can be observed. Undamaged plasmid is seen as a fast moving supercoil, single strand nicks result in a slow moving open coil, double strand breaks result in linear DNA which migrates faster than open coil DNA, but slower than a supercoil.

Section 3.3.5: DNA Polycation Protection Assays

The effect that DNA condensation by salmon protamine has on protecting the DNA from radical damage is shown in Figure 3.5. By observing changes in plasmid migration, the prevalence

and extent of the damage subjected to the plasmid DNA by AAPH generated radicals can be quantified. Condensation with protamine clearly has a large effect in limiting how much damage is sustained to the plasmid DNA. Condensation with protamine nearly eliminates the presence of double-strand breaks, and the proportion of the DNA single-strand nicks is substantially reduced.

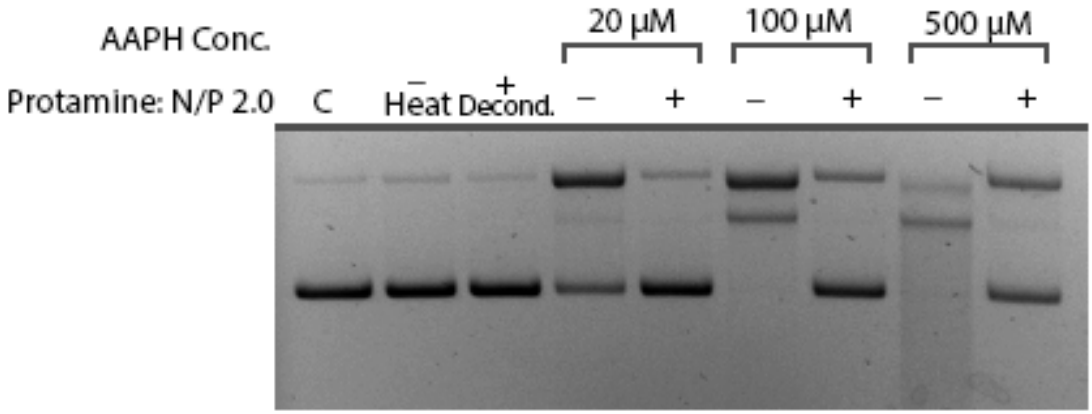

Figure 3.5: By condensing with protamine, substantial protection can be confered to the plasmid. When compared to naked DNA subjected to the same AAPH concentration, a significant population of undamaged supercoiled DNA is evident. Gel aquired with Ehigbai Oikeh (UK Department of Chemistry)

The effect of changing the condensing agent has on DNA protection is shown in Figure 3.6. While we expected the protection to reflect the packaging density of the condensate, what we observed was different. Longest polycations studied (high molecular weight poly-Lys and poly-Arg) were the most effective in protecting the condensed DNA from radical damage. The shortest polycations studied (R_6 and R_3-pSer-R_3) offered the least amount of protection from radicals. The protamine, intermediate in length and charge, showed intermediate protection. Comparing similar length/charge polycations, however, we do see that the relative damage does scale with the packaging density. For example, poly-Arg is more protective than poly-Lys and R_6 is more protective than R_3-pSer-R_3. Lane integration allows to quantify the protection for each polyplex system and is shown in Figure 3.7, gel was performed 3 times

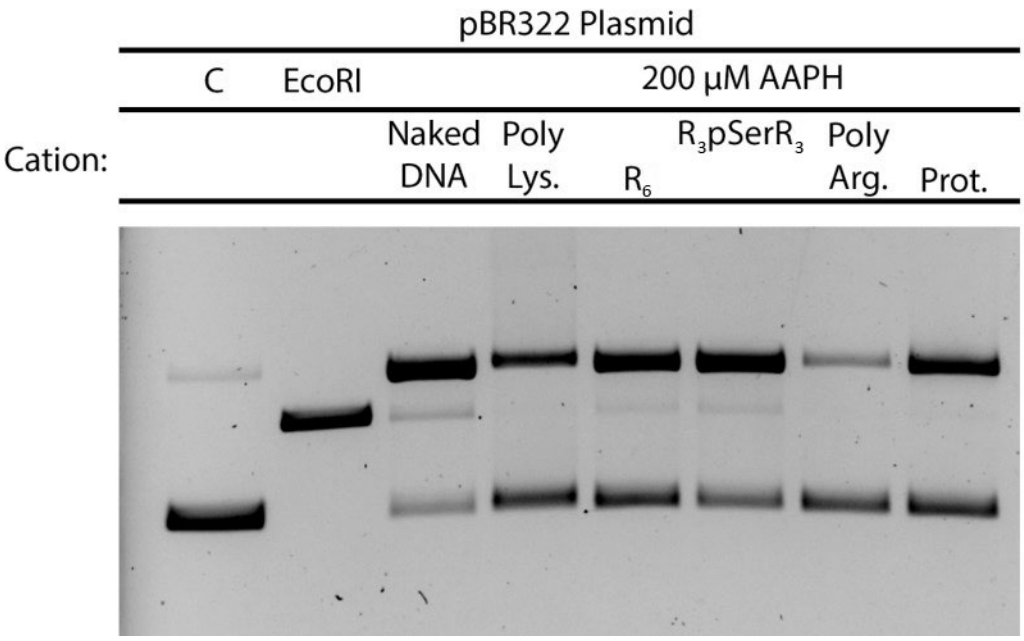

Figure 3.6: By condensing plasmid DNA with cations of differing types, differing amounts of protection is afforded to the plasmid DNA. Longer cations (poly-Arg, Poly-Lys) protects better than mid-length and short cations (Protamine, R_6 and R_3pSerR_3)

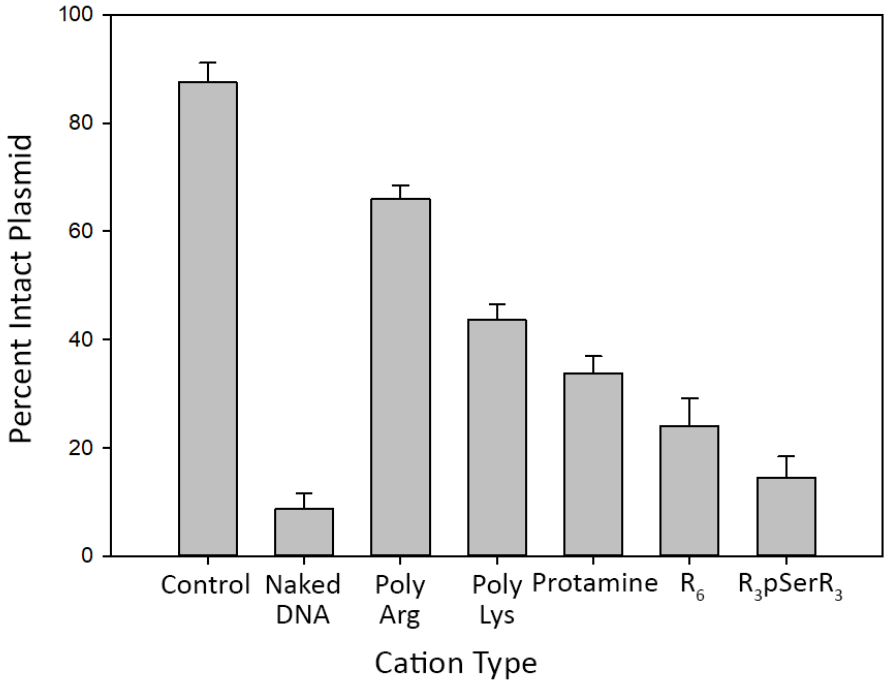

Figure 3.7: Lane integrations of AAPH damage gel showing the relationship between exact cation type and damage susceptablility. Values are given as mean ± standard error (n = 3).

Section 3.4 Discussion

DNA - polycation condensates order themselves into tight hexagonal arrays for maximum packaging efficiency. SAXS analysis allows for the determination of the interaxial spacing between the packaged DNA helixes. Arginine-based peptides, such as protamine and poly-Arg prove to be the most effective in packaging DNA as shown through the tight DNA interhelical spacing, whereas lysine-based packaging yields a much looser packaging as seen by the larger interhelical spacing measured by SAXS.

This difference in packing density is reflected in biological systems. Arginine-based packaging, through the use of protamines, is found predominantly in sperm chromatin resulting in transcriptionally inactive DNA that is incapable of being repaired in the sperm. Lysine-based packaging is mainly found in somatic chromatin, where the DNA is packaged by histones with lysine-rich tails. Somatic chromatin is transcriptionally active and therefore needs to be easily accessed by many cellular components, thus requiring a looser packaging density to ensure efficient cellular operation.

Insight into the condensation of the DNA polyplexes can be determined by examining the differing binding curves in the ethidium bromide displacement assay. Poly-Arg and poly-Lys are extremely efficient at condensing DNA, as small amounts of these polycations result in the binding of a large percentage of the DNA. Condensation occurs therefore in a continuous fashion with significant portions of DNA being condensed well before complete charge compensation (i.e. N/P 1.0). Short and midsized polycations require a greater cation concentration to completely condense the DNA. Complete condensation was observed only at N/P charge ratios of 2.0 or higher (i.e. twice the amount of polycation required to charge compensate for the DNA). Possible reasons for the need of greater concentrations of small cations to completely bind DNA, is that the smaller polycations have a weaker binding strength due to the reduced electrostatic

attractions. This results in the cations being more likely to dissociate from the DNA. Therefore, in order to have a sufficient population of cation present and bound to the DNA at any given time, a net greater concentration of cation is needed. The large interaxial spacing afforded by the R_3-pSer-R_3 is reflected in the assay, even at high N/P ratios, ethidium bromide is always able to intercalate into the DNA due to its low packaging density. This is showing that the overall cation-DNA polyplex is much looser than condensation afforded by longer cations. Because of this excess ethidium bromide intercalation, we see residual ethidium bromide fluorescence even when the DNA is completely charge compensated at N/P ratios greater than 2.0.

A better approximation of the concentration of polycation needed to sufficiently condense DNA can be determined by observing the binding curves created by UV-Vis. Here, the interactions between the ethidium bromide and the DNA and cation are removed and only unbound, uncondensed DNA is measured. This allows for a much more direct measurement of cation binding. Long cations and mid-length cations show complete DNA condensation by N/P: 1.0 - 1.10, either exactly or slightly over the amount of cation needed to completely charge compensate the DNA. R_6 and R_3-pSer-R_3 show complete condensation by N/P: 2.0. Both the ethidium bromide displacement assays, as well as the UV-Vis binding curves, confirm that longer cations more efficiently condense DNA than their shorter counterparts. Taking into consideration the final interaxial spacing of the packaged DNA, we can see that condensation efficiency is independent of the final packaging density. R_6 requires a greater net amount of cation than poly-Lys to completely condense DNA, where poly-Lys has comparatively a much looser packaging density than the R_6 cation.

Condensing the DNA has a profound effect on the susceptibility of the DNA to radical damage regardless of the condensing agent. Comparison between the condensed DNA and the naked DNA, shown in Figure 3.5, we see that double-strand breaks are nearly completely

eliminated in all samples and that greater proportion of the condensed DNA remains in the undamaged state for all the polyplexes. Essentially DNA which is bound by a cation is not able to be reached and damaged by reactive oxidative species. Presumably, a majority of the damage sustained would be on the DNA helices present on the outside of the condensate, while the inner DNA remain less affected. Future experiments will need to be conducted to confirm this.

The effect of AAPH damage on condensates of differing cation types can be seen in Figure 3.6, by observing the lane integrations we can discern that neither cation length nor packaging density alone is the determining factor on how effective a cation is in protecting DNA. Cation length is the primary factor in determining protection effectiveness, where long cations protect better than short cations. Secondary to cation length is cation packaging density, where closer spacing protects better than wider spacings. The dependence on the polycation length was not anticipated from our original hypothesis, that damage susceptibility is solely based on radical accessibility to the DNA as determined by DNA interaxial spacing. One possible explanation for this observation is that shorter cations are continually associating and dissociating from the DNA as it binds, because of this there is a greater likelihood of there being an unbound fraction of DNA present within the condensate. Studies into the dynamics of polyplexes consisting of dendrimers and DNA showed that the dendrimers were quite mobile within the polyplex. [130] In our system, small peptides are more likely to be much more mobile than the long polycations. Therefore, the small peptides are more likely to dissociate from the DNA polyplex. This unbound fraction is more susceptible to AAPH mediated damage. Shorter cations are less efficient in condensing DNA, as observed in the ethidium bromide displacement assays. Longer cations, however, condense DNA very efficiently and have a lesser likelihood of dissociation from DNA, reducing the chance of there being an unbound fraction in DNA which is more susceptible to damage susceptible.

Section 3.5: Conclusions and Future Work

We have shown how polycations of differing length and packaging density bind and condense DNA. We have described the relationship between cation concentration and the condensed fraction of DNA by both UV-Vis and ethidium bromide displacement assays. Through these assays, we can observe how effective, or conversely, ineffective a cation is in condensing DNA. We have related this efficacy of a condensing agent to the protection afforded to a DNA polyplex from radical species. Longer cations are the most efficient in condensing DNA and provide the most protection from damaging agents, shorter cations do not bind DNA as effectively and show lesser levels of protection in a polyplex. Protection based on packing density is secondary to cation length where tighter packing protects better than looser packing. Future work in this study will include more accurate descriptions of differences in binding strength of the selected polycations, and more precise quantification and description of the damage products resulting from subjecting the condensed DNA to damaging agents.

Chapter 4: Effect of Aberrant Protamine Ratios On DNA Condensates

Section 4.1 Introduction

During spermatogenesis, somatic chromatin is remodeled, and DNA histones are replaced with small arginine-rich peptides known as protamines. [10] These protamines both condense and package the DNA and result in some of the tightest DNA packaging in nature, with the entire haploid genome existing in a space $1/20^{th}$ of the volume of the somatic nucleus. [131] This tight packaging results in the spermatic DNA existing in both a near-crystalline and transcriptionally inactive state.[7, 23] This tight DNA packaging is thought necessary not only to facilitate easy transport of the male genome by the spermatozoa to the ovum, but also for the protection of DNA from damage, whether through ROS, chemical, or other means. [20, 132, 133] DNA repair mechanisms function during spermatogenesis, however, they are turned off once somatic histones are replaced with protamines, making protecting the spermatic DNA from damage particularly critical. [10, 84] Increased DNA damage to spermatic DNA is thought to impact male fertility potential and have numerous downstream effects such as an increased likelihood of miscarriage during embryogenesis and a greater incidence of genetic disease in the infant. [134, 135]

Protamine levels have been shown to have a profound effect on chromatin integrity in mature spermatozoa.[119] Low levels of protamine, henceforth termed underprotamination, correlates with poorly condensed DNA. [119] Underprotaminated spermatozoa have either an absence of sufficient protamine needed to completely condense spermatic DNA or have an increase in the ratio of residual DNA histones, present in low percentages in sperm cells. [20, 136, 137] Low levels of protamine have been shown to correlate with low fertility levels as well as increased amounts of DNA damage and fragmentation within bull sperm chromatin. [138]

Numerous studies have been undertaken to describe and quantify various levels of protamination and its relationship to sperm chromatin integrity. [139] Protamination levels are most often described through fluorescence methods. Chromomycin A_3 (CMA3) staining is a commonly used method used to indicate the extent of underprotamination within sperm nuclei, where higher levels of CMA3 fluorescence indicates low levels of protamination. [140] Increased CMA3 fluorescence has been shown to positively correlate to increased amounts of DNA strand breaks as shown by nick translation and the terminal transferase assay (TUNEL). [141]. These studies suggest that underprotamination of spermatic DNA leads to greater levels of DNA damage and fragmentation.

While protamine has long been thought to play a role in protecting spermatic DNA from damaging agents in vivo. The relationship between the hypercondensation of sperm chromatin, the DNA integrity, and the transfer of epigenetic information from sperm to oocyte and potential to alter gene expression in the early embryo are poorly understood. In this chapter, we focus on how underprotamination affects free radical accessibility and DNA stability in reconstituted sperm chromatin. Specifically, reconstituted salmon protamine- plasmid DNA condensates (polyplexes) were formed at precise protamine/DNA ratios and subsequently subjected to exposure to AAPH free radicals. Agarose gel electrophoresis was then used to assess DNA damage by observing topology alternations in the decondensed polyplexes. FPG-DNA glycosylase has also been used to more accurately determine oxidative damage beyond just nicks and double-strand breaks in the various condensed states. We show that higher levels of protamination correlate to greater levels of protection to the DNA from oxidative damage up until the condensate is fully charge compensated. Furthermore, we also demonstrate that poorly compacted chromatin could be recovered by the introduction of a short hexa-arginine peptide into underprotaminated condensates as well as actual sperm nuclei. SAXS studies were performed to confirm the peptide

crossed the nuclear membrane, resulting ultimately in tighter DNA packaging densities in poorly packaged salmon sperm nuclei.

Section 4.2 Materials and Methods

Section 4.2.1: Materials

Calf thymus DNA, salmon protamine-chloride, salmon sperm nuclei, ethidium bromide, dextran sulfate from *leuconostoc spp*. (avg molecular weight 9,000-20,000), sodium azide and GeneElute PCR Clean-Up Kit were purchased from Sigma-Aldrich. pBR322 plasmid DNA (4361 bp), Lambda DNA (48502 bp), and formamidopyrimidine [fapy]-DNA glycosylase (Fpg) enzyme were purchased from New England BioLabs. 10x phosphate buffered saline and 0.5M EDTA stock was purchased from Fisher BioReagents. 1M Tris-Cl stock was purchased from Mediatech. 2,2'-Azobis(2-amidinopropane) dihydrochloride and CHAPS detergent was purchased from Acros Organics. Hexaarginine (R_6) was custom synthesized and purified (>98%) by GenScript Corp. (Piscataway, NJ). pUC18 plasmid DNA (2686 bp) was purchased from Thermo. 50x TAE was purchased from Omega Bio-Tek. Glycerol was purchased from Fisher Scientific. 5M sodium chloride stock was purchased from Promega Corp. Chromomycin A3 (CMA3) was purchased from Enzo Life Sciences. All reagents used without modification unless noted.

Section 4.2.2: DNA Precipitation Assays of Underprotaminated Samples

DNA stock was prepared by hydrating calf thymus DNA in Tris buffer, 10 mM Tris-Cl, 400 μM NaN_3, overnight. The DNA concentration was determined UV-Vis measurement, where A_{260}=1, [DNA] = 50 μg/mL. All UV-Vis measurements were performed on a Thermo Evolution 201 spectrophotometer. Protamine-Cl was weighed out and dissolved in Tris buffer to a final concentration of 1 mM.

1 mM protamine-Cl was combined with 100 µg calf thymus DNA at the desired N/P ratios and incubated at room temperature for a minimum of 15 minutes. Tris buffer was added to the Protamine-DNA to a final volume of 300 µL. Samples were centrifuged at 11,000g for 15 minutes and the resulting supernatant was pipetted into a quartz cuvette and A_{260} was measured by UV-Vis. The procedure was repeated with 75 µg DNA, and then again with 100 µg DNA with the addition of NaCl to all reagents to a final concentration of 150 mM NaCl. [105] Precipitation assay was repeated 3 times, the results were averaged and standard error was calculated.

Lambda DNA binding curve was performed by adding 75 µg lambda DNA into lambda buffer, 10 mM Tris, 1 mM EDTA, to a final volume of 200 µL. Protamine-Cl in lambda buffer was added stepwise to the DNA at increasing N/P ratios. The sample was incubated at room temperature for a minimum of 15 minutes and was then centrifuged and measured as previously described. The assay was repeated 3 times, the results were averaged, and standard error was calculated.

Section 4.2.3: Underprotaminated Gel Studies

All gel studies were performed using a 1.0% agarose gel in 1x TAE. All reagents were dissolved in Tris buffer unless noted. Gels were stained in ethidium bromide in 1x TAE, 2.5 µg/mL for 45 minutes, then de-stained in 1x TAE for 20 minutes. 2 µL 6x loading dye was added to each sample prior to introduction into the gel. Gels were visualized under UV light and photographed in a Fotodyne FOTO/Analyst camera box.

Section 4.2.3.1: Protamine-DNA Gel Shift Assay

1 µM Protamine-Cl in tris buffer was added to 400 ng pUC 19 Plasmid at increasing N/P ratios. Tris buffer was added to each underprotaminated sample for a final volume of 10 µL. The

sample was incubated at room temperature for a minimum of 15 minutes then introduced into an agarose gel. Samples were run on the gel for 60 minutes at 95 V, 70 mAmp. The gel was stained and photographed as discussed above.

Section 4.2.3.2: Underprotaminated AAPH Damage Gel

AAPH was dissolved in deionized water and activated by heating at 60 °C for 1 hour. 1 µM Protamine-Cl was added to 200 ng pBR322 plasmid in tris buffer at appropriate N/P ratios. 10x phosphate buffered saline was added to each sample for a final concentration of 1x. Samples were incubated at room temperature for a minimum of 15 minutes. AAPH solution was then added to the condensed DNA for a final concentration of 350 µM. Samples were vortexed and damaged at 60 °C for 1 hour. After damaging, 30 µg dextran sulfate, a competitor anion, was added to the samples to release the DNA from the protamine, resulting in free DNA. The sample was allowed to decondense for no more than 5 minutes to minimize AAPH damage to the naked plasmid. The samples were then introduced into an agarose gel. The gel was run for 140 minutes at 95 volts, 75 mAmps. The gel was stained then photographed. Unbound protamine itself does not confer any protection against free radical damage. To show this, agarose gel electrophoresis of plasmid DNA (400 ng pUC18) treated with AAPH was performed at various N/P ratios ranging from 0 to 10. We show that protamine/DNA is fully condensed at N/P charge ratios of 1.1. Higher N/P ratios, is synonymous with higher levels of unbound protamine free in solution. The protective abilities of protamine are not observed to improve above N/P 2.0

Section 4.2.3.3: FPG Treatment of AAPH Damage Gels

Exposure of DNA to free radicals can lead to damage bases (e.g. 8-oxoguanine or 8-oxoadenine) that do not induce single-strand nicks or double-strand breaks. Therefore analysis of

pDNA performed directly on 1% agarose gel in TAE buffer, as described in section 3.3.4, is likely underestimating the actual oxidative damage of the DNA. To correct for this, we treated the released DNA after radical exposure with formamidopyrimidine [fapy]-DNA glycosylase (Fpg), also known as 8-oxoguanine DNA glycosylase. FPG acts as both an N-glycosylase and an AP-lysase. As an N-glycosylase, Fpg releases damaged purines from dsDNA to generate an apurinic (AP) site. Then the AP-lysase activity removes the AP site leaving a 1 base gap. Treatment of radical exposed damage to FPG should, therefore, better quantify the oxidative damage on the DNA. FPG treated samples were created by first damaging protamine-DNA as previously described. After the dextran sulfate addition, samples were run through a 'GenElute PCR Clean-up Kit' per manufacturer's instructions to remove excess protamine and dextran sulfate. FPG was next introduced to the samples at a final concentration of 100 Units/mL and incubated at 37 °C for 30 minutes. Samples were resolved on an agarose gel as previously described. Gel acquired by Ehigbai Oikeh (UK Department of Chemistry)

Section 4.2.3.4: Underprotaminated-R_6 Damage Gel

Underprotaminated DNA samples were created as previously described. R_6 was added to each underprotaminated samples to a final N/P ratio of 2.0. Samples were damaged at 100 μM AAPH for 60 minutes. DNA was released using 30 μg dextran sulfate and the samples were resolved on an agarose gel at 95 volts, 120 minutes, 70 mAmps. The gel was stained then photographed. Gel acquired with Ehigbai Oikeh (UK Department of Chemistry)

Section 4.2.4: Ethidium Bromide Exclusion Assay

DNA and protamine stocks were prepared as previously described. 12 µg calf thymus DNA and ethidium bromide in Tris buffer were combined at a 1/10 molar ratio ethidium bromide to DNA base pair. 1 mM Protamine in Tris buffer was added stepwise to the ethidium-DNA. Fluorescence was observed at λ_{ex}=520 nm and λ_{em}=595 nm. Results were reported as relative fluorescence: $(F-F_0)/(F_{Max}-F_0)$, Where F is the sample emission intensity, F_0 is the emission intensity of ethidium bromide without DNA, F_{Max} is the emission intensity of only DNA and ethidium bromide. [104] Samples were allowed to condense for a minimum of 5 minutes between measurements. The volume of solution added was never more than 2% of the total solution volume. The procedure was repeated using 1 mM R_6 in Tris buffer in place of protamine.

R_6 titration was performed by creating underprotaminated Protamine-DNA samples using 12 µg calf thymus DNA, then titrating in 1mM R_6, both in Tris buffer, into the underprotaminated DNA samples, measuring the fluorescence intensity between each addition as previously described. For all EtBr exclusion assays, the assay was repeated 3 times, the resulting values were averaged and standard error was calculated.

Section 4.2.5: SAXS Analysis of Salmon Nuclei

Salmon nuclei were first cleaned using the following procedure: nuclei were suspended in tris buffer, then sonicated twice at 35% amplitude using a Fisher 'Sonic Dismembrator', for 2 minutes on ice, waiting 2 minutes between sonication. Nuclei were centrifuged at 1000g for 5 minutes, and the resulting supernatant was discarded. Nuclei were re-suspended in a solution of 10 mM CHAPS, 100mM Tris-Cl, 20% Glycerol, and incubated at 37°C for 30 minutes. Samples were centrifuged at 1000g for 5 minutes and the supernatant was again discarded, and nuclei were resuspended in 10 mM Tris buffer.

Nuclei in Tris buffer were combined with R_6 to a final concentration of 2.75 mM R_6 and left to rest overnight. Nuclei were placed in an X-Ray capillary tube. Nuclei both with and without R_6 addition were measured by SAXS on an X8 Proteum diffractometer with Cu*Kα* radiation. Data was collected on a PT-135 CCD detector, fitted with a helium-filled box between the sample and the detector to minimize aberrant scattering. Data analysis was performed on FIT2D and Origin data analysis software. Results are reproducible within 0.15 Å

Section 4.2.6: Chromomycin A_3 Fluorescence Study

CMA3 solution was prepared by dissolving pure CMA3 in McIlvaine's buffer (16.5 mM Na_2HPO_4, 17.7 mM Citric Acid, pH 7.0), to a final concentration of 0.25 mg/mL with the addition of 10 mM $MgCl_2$. [121, 142] Salmon sperm nuclei were cleaned as previously discussed, then washed 3 times in 1x PBS. Nuclei were fixed to a microscope coverslip using a 3:1 ratio solution of methanol to glacial acetic acid at -20 °C for 10 minutes. After fixation, nuclei were rinsed 3 times in 1x PBS to remove all residual fixative. CMA3 solution was introduced to the top of the fixed nuclei and incubated in the dark for 20 minutes at room temperature. Nuclei were then again rinsed 3 times 1x PBS and observed. Nuclei were observed on an Olympus IX71 inverted fluorescent microscope at 600x magnification, through an excitation/barrier filter wavelength of 450/515 nm. 10 mM Tris buffer was added to the top of the nuclei directly prior to imaging. Images were taken every 60 seconds for 600 seconds.

2.75 mM R_6 in 10 mM Tris-Cl was added to the CMA3 labeled nuclei and observed as previously discussed, images were taken every 60 seconds for 600 seconds. CMA3 fluorescence was graphed as Corrected Total Cellular Fluorescence: integrated fluorescent density – ((area of selected cell) x (average fluorescent of background)). Fluorescence density was determined using ImageJ across 5 distinct nuclei. Values were averaged and standard error was calculated.

Section 4.3 Results

Section 4.3.1: Description of Underprotamination in Protamine-DNA Condensates.

In order to determine the effect that protamination levels have on DNA, it is critical to describe what exactly underprotamination is and have precise definitions of varying levels of underprotamination. This was accomplished through a combination of UV-Vis, gel-shift and ethidium bromide displacement assays.

We have decided to describe underprotamination in the terms of the N/P charge ratio, the ratio of cationic charge from the protamine arginine to the anionic charge from the phosphate backbone of the DNA. By using this specific nomenclature, how condensed, or conversely, how not condensed, the protamine-DNA is can be easily described at each distinct N/P ratio.

Section 4.3.2: DNA Precipitation and Gel Shift Assays For Determination of Underprotamination

The highly cationic protamine progressively binds DNA as N/P ratio increases, as shown in Figure 4.1. As protamine binds the aqueous calf thymus DNA (ctDNA), the protamine-DNA falls out of solution in the form of an insoluble pellet. The residual, unbound ctDNA, present in the supernatant is then quantified by UV-Vis, producing a characteristic binding curve. This binding occurs sequentially until all the ctDNA has been condensed by the protamine. Approximately 40%

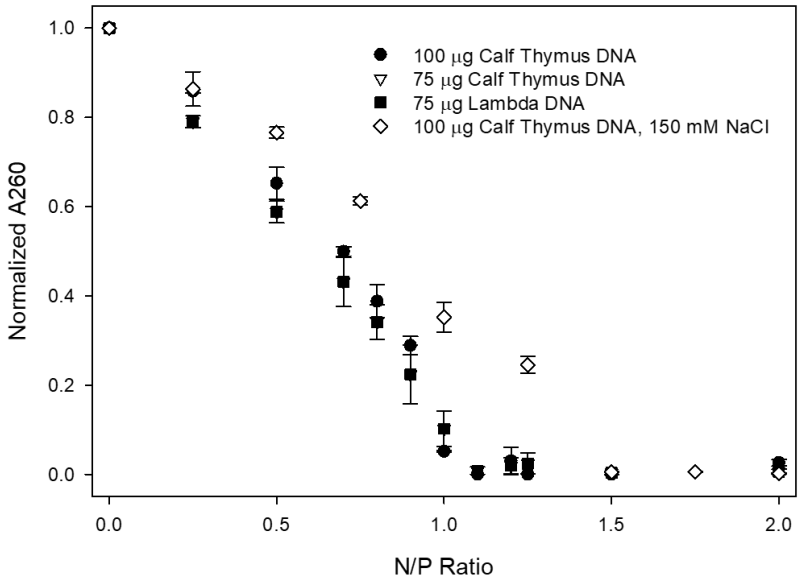

Figure 4.1: DNA precipitation assay of protamine DNA. Treatment of DNA with protamine results in complete binding by N/P: 1.1 regardless of DNA concentration. Physiological salt (150 mM) resulted in complete DNA condensation by N/P: 1.50. (Values are given as mean ± standard error (n = 3).

of the ctDNA is condensed between N/P 0.0 and N/P 0.5, and complete DNA condensation occurs by N/P ~1.1. Here N/P 1.0 represents the point where there is sufficient cationic charge on the protamine to exactly charge compensate the anionic charge of the DNA phosphate backbone. Nearly identical binding curves are observed at lower ctDNA concentrations (0.25 μg DNA/μL and 0.33 μg DNA/μL). Also, the binding curve is relatively insensitive to DNA length. Shown in Figure 4.1 are ctDNA (millions of base pairs long) and lambda DNA (48,500 bp). All three of these binding

curves show a similar slope, with complete DNA condensation occurring at N/P ~ 1.1. reconstituted ctDNA precipitation at physiological salt (150 mM NaCl) did show some significant differences with full condensation requiring approximately N/P 1.5 before the observed absorbance at 260 went to zero.

shows a gel shift assay of protamine-DNA. Plasmid DNA is progressively bound by the protamine as N/P ratio increases. Once bound, the ability for the DNA to migrate through the gel is hindered. At high N/P ratios, the DNA is completely bound by the protamine and is unable to enter the gel and gets stuck in the sample well. The amount of protamine needed for complete DNA binding is increased in a gel-shift assay, as compared to the DNA precipitation assay. One possible explanation for this is that the electrophoresis E-field may have the effect of pulling the protamine-DNA condensate apart. Nearly complete DNA binding occurs at N/P: 1.5.

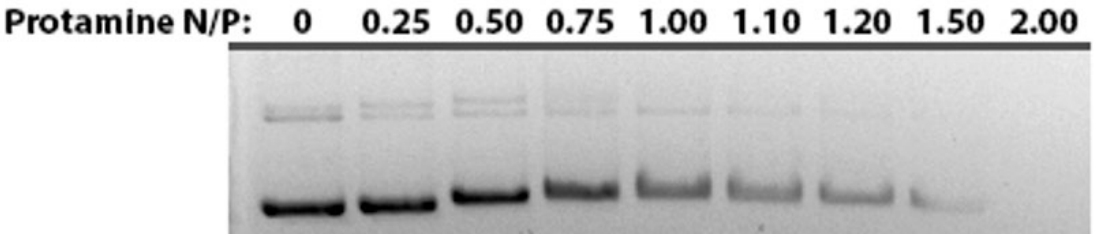

Figure 4.2: Gel shift assay of protamine-DNA condensates. As protamine binds the plasmid DNA, its ablity to migrate into the gel is hindered. At N/P: 2.0 the DNA is completely bound by the protamine resulting in the disapearence of the DNA band.

Section 4.3.3 Effect of AAPH damage on Protamine-DNA and Underprotaminated DNA Condensates

With an experimentally derived description of underprotamination, we can examine the effect of DNA damaging agents on protamine-DNA condensates at differing levels of

underprotamination. In our study, AAPH was used as the damaging agent, the effect of AAPH on plasmid DNA was previously described in Section 3.3.4.

One way to determine damage in plasmid DNA is to use agarose gel electrophoresis, as described in Section 3.3.4, and quantify the ratio of supercoil, open coil, and linear DNA bands observed. One problem with this method is it only quantifies oxidative damage that results in a single strand nick or a double strand break. There are many oxidative products that free radicals can produce in DNA that are not nicks or breaks. Therefore to better quantify the actual oxidative damage resulting from exposure of protamine/pDNA to AAPH, we used a modified nick translation assay. This is done through the treatment of the damaged plasmid with the enzyme '*formamidopyrimidine DNA glycosylase'* (FPG). This assay allows for the excision of damaged purine DNA bases, resulting in the formation of a single or double-strand break in a plasmid where a damaged purine base was present. [143]

To show the effectiveness of FPG to more accurately quantify damaged purine DNA bases, Figure 4.3 shows pDNA either uncondensed or fully condensed by protamine (N/P 2) in the absence or presence of AAPH. Here two different AAPH concentrations were studied representing in either moderate or high levels of damage in the unpackaged DNA. As previously discussed, undamaged plasmid exists almost entirely in the supercoiled form, shown in lane 1. In lane 2, the DNA is subjected to AAPH damage resulting in the majority of the DNA sustaining a single-strand break, this effect is better observed by treatment of damaged condensates with FPG as shown in lane 3, whereas the excision of damaged bases results in a complete disappearance of the supercoiled band. The fraction of open coil and linear DNA increases substantially in the FPG treated lanes as well. The protection effect that protamine has on DNA can be seen in lanes 4 and 5, with both the FPG and non-FPG treated plasmid showing a significant fraction undamaged DNA. These effects are amplified by increasing the AAPH concentration as seen in lanes 6-10.

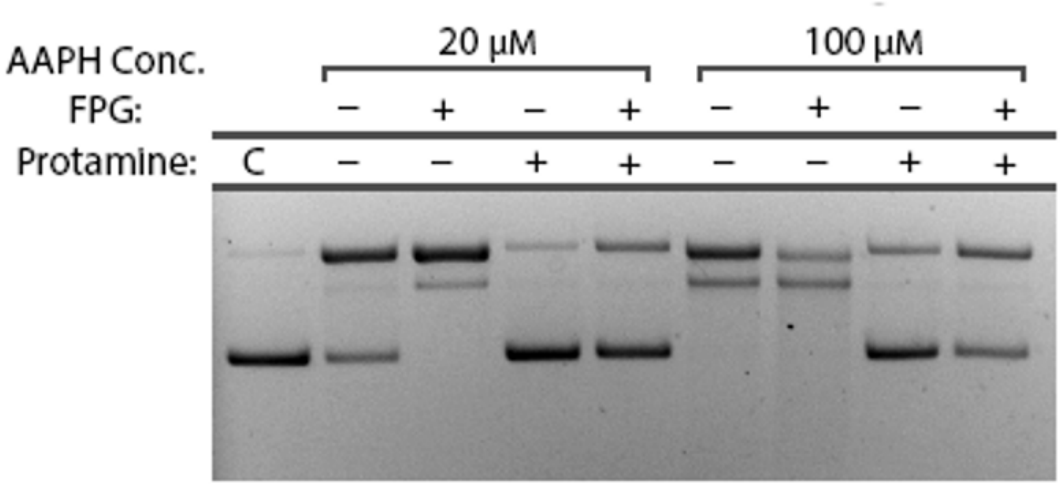

Figure 4.3: FPG treatment allows for better quantification of AAPH damage. FPG excises damaged purine bases, imparting single and double strand breaks into the plasmid DNA. A significant supercoiled band is still present in the lanes containing protamine condensed DNA. FPG gel performed by Ehigbai Oikeh (UK Department of Chemistry)

The effect of underprotamination on DNA damage by AAPH can be seen in Figure 4.4. As levels of protamination increase, the amount of undamaged DNA increases as well. At N/P: 2.0, the linear DNA band disappears, and the DNA exists exclusively as either an open coil or a

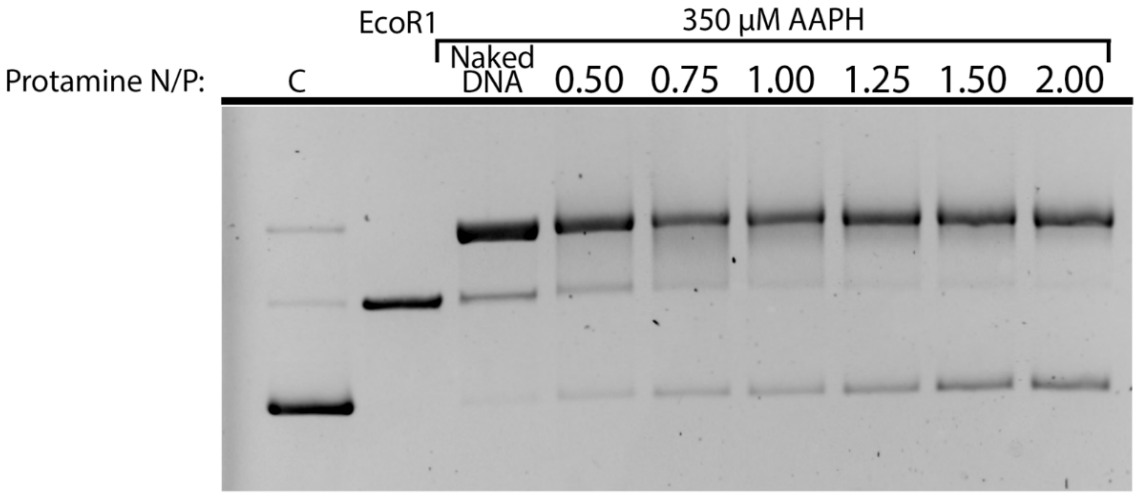

Figure 4.4: Effect of underprotamination on DNA subjected to AAPH Damage. As the protamine N/P ratio increases, greater levels of protection is imparted to the DNA as shown by the growth in the undamaged supercoiled band.

supercoil. The protection effect that protamine has on DNA reaches a maximum at approximately N/P: 2.0. Simply adding more protamine to a DNA condensate does not confer any additional protection to the DNA as shown in figure 4.5.

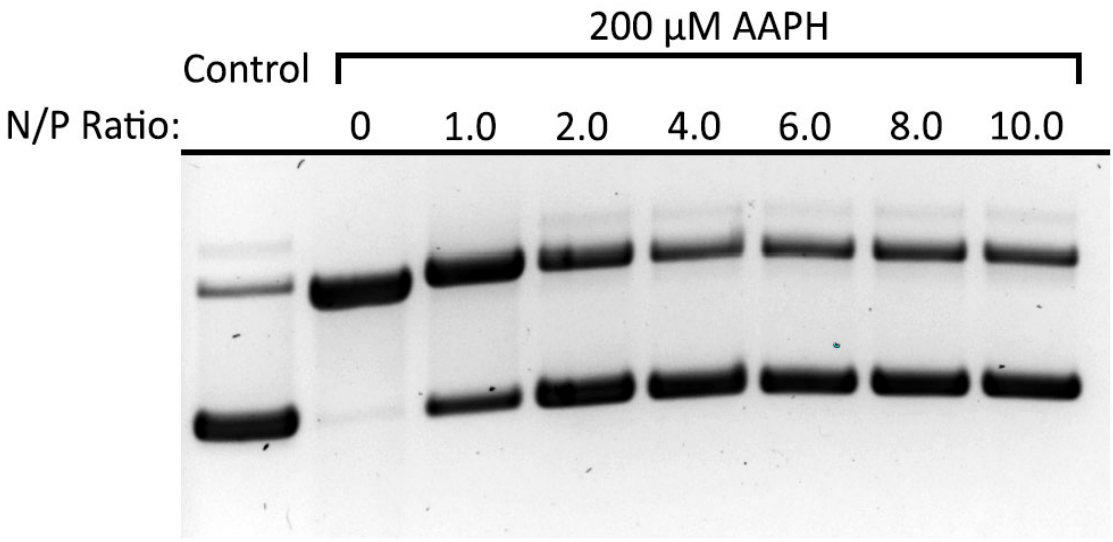

Figure 4.5: High N/P ratios have little effect on the protection afforded to plasmid DNA. No notable protection effect is seen after N/P: 2.0.

Section 4.3.4 The Effect of Oligoarginine Peptides on Underprotaminated DNA Condensates

Our gel electrophoresis studies have thoroughly described the protection afforded to DNA from damaging agents by condensation with protamine. As protamination levels increase, the amount of damage sustained to the condensed DNA decreases, reaching a maximum protection at N/P ~1.5. Next, we sought to observe if a small cationic peptide could further tighten underprotaminated samples and confer additional protection to the condensed DNA. In this study, hexa-arginine (R_6), was chosen as a variety of arginine-rich cell-penetrating peptides are known to be capable of traversing plasma membranes in eukaryotic cells. [144]

Figure 4.6 shows the ethidium bromide exclusion assays of ctDNA for protamine and R_6. Both peptides show complete DNA condensation, meaning the ethidium bromide (EtBr) was completely displaced by the cation, by N/P 1.5. This is higher than N/P: 1.1, the N/P ratio needed

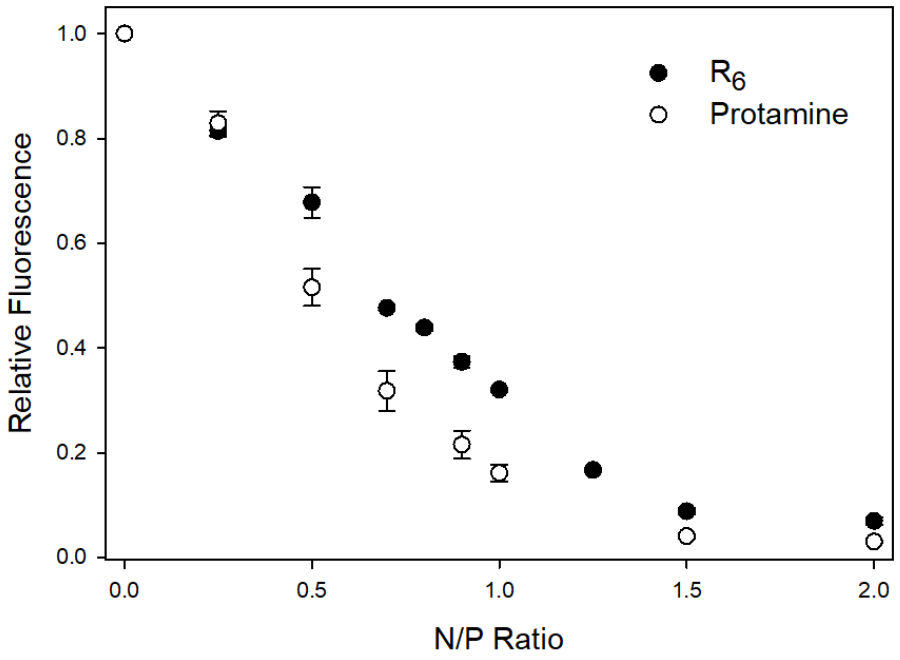

Figure 4.6: Ethidium bromide exclusion assay of ctDNA condensed with protamine and R_6. Complete DNA condensation is observed by N/P: 1.50. Values are given as mean ± standard error (n = 3).

For complete DNA condensation as observed by UV-Vis. This increase in the apparent amount of protamine needed to condense DNA is an effect of the EtBr assay, as the complete exclusion of the EtBr by the condensing agents does not appear to proceed until a sufficient excess of polycation is present. The normalized fluorescence also depends on the polycation with more EtBr being excluded (a lower measured relative fluorescence) by the larger protamine chains when compared to the hexa-arginine peptide.

Next, we wanted to determine if the addition of hexa-arginine to underprotaminated reconstituted samples would result in a more tightly packaged condensate. Figure 4.7 shows an

EtBr exclusion assay for protamine/DNA samples mixed at different starting N/P ratios as a function of added R_6 concentration. For the underprotaminated samples, R_6 clearly is observed to

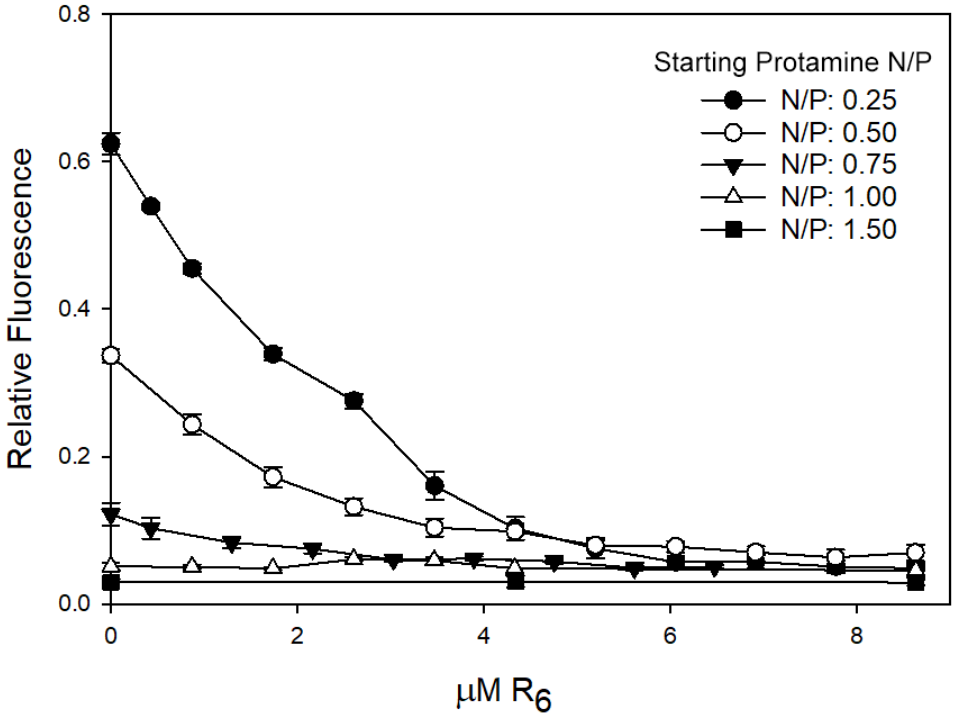

Figure 4.7: Titration of protamine-DNA condensates with R_6. Condensates at low N/P ratios are further tightened by the cationic peptide R_6 as seen by a reduction in EtBr fluorescence. Lines added to guide the eye. Values are given as mean ± standard error (n = 3).

bind the DNA resulting in further exclusion of the EtBr from the DNA helices. This is in essence 'tightening up' the underprotaminated DNA samples. Protamine-DNA at N/P ratios near or above 1.0 shows little effect from the additional R_6 as they are already nearly completely condensed. Complete condensation of the protamine-DNA samples occurred at a final concentration of 8 μM R_6, regardless of the starting N/P ratio.

As shown in figure 4.8, the addition of R_6 to underprotaminated DNA not only further condenses the protamine-DNA, but also confers additional protection of the DNA from AAPH free

radicals. In this gel, protamine/DNA samples of various N/P charge ratios were prepared as described previously. Samples are compared without or with the addition of the R_6 peptide. Here,

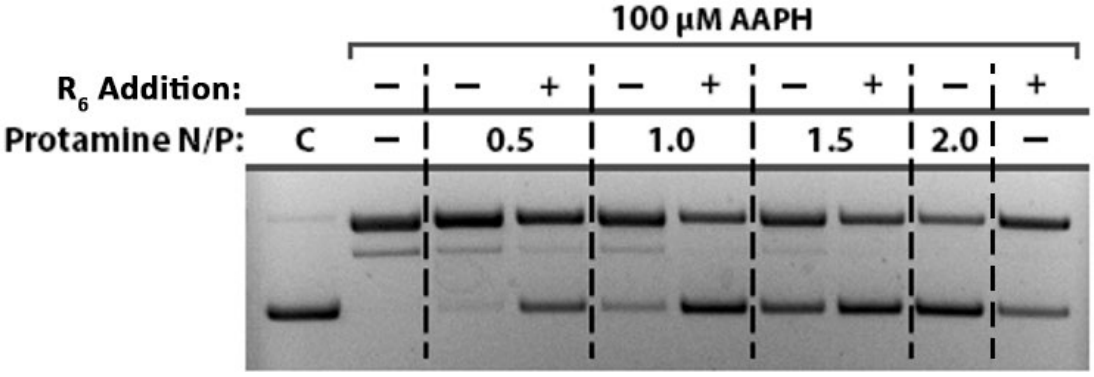

Figure 4.8: Protamine-DNA-R_6 protection gel, R_6 addition 'tightens' the underprotaminated DNA condensates further protecting the DNA from damage, this is seen by a growth in the undamaged supercoiled band. R_6 addition is to yield a net N/P ratio of 2.0. Gel aquired with Ehigbai Oikeh (UK Department of Chemistry)

all samples after the addition of R_6 are equivalent to a final N/P charge density of 2.0. In the final lane, R_6/DNA (N/P 2) with no added protamine is also given for comparison. Underprotaminated DNA at N/P 0.5 shows a large increase in the fraction of supercoiled DNA present when further condensed with R_6. In addition, the presence of the linear band decreases. Protamine-DNA at N/P 1.0 and 1.5 also show an increase in the amount supercoiled DNA present and a loss of any linear DNA with the addition of R_6 to the underprotaminated DNA condensates. Consistent with results in Chapter 3, we also observe less damage on DNA fully condensed (N/P 2) by the more highly charged protamine compared to DNA fully condensed (N/P 2) by the oligomeric hexa-arginine peptide. This likely is a result of intrinsic dynamics within the DNA-polycation complex. Our results may suggest a higher degree of cation mobility in the polyplex for R_6/DNA as compared to protamine/DNA.

Section 4.3.5: CMA3 Analysis of Salmon Nuclei With the Addition of R_6

The effects of R_6 on underprotaminated DNA samples thus far have been shown solely using reconstituted protamine-DNA condensates. As will be described in detail in section 5.5 and 5.6, using both a DNA and a membrane binding dye on isolated nuclei, we have observed through fluorescence imaging that the commercially purchased salmon sperm nuclei, as well as bull and horse nuclei still maintain a nuclear membrane. Next, we sought to determine if the addition of R_6 to isolated nuclei would be able to both cross the nuclear membrane as well as improve the DNA condensation. Through the application of CMA3, a commonly used fluorescent indicator for protamine deficiently in sperm nuclei, we are able to better observe the integration of R_6 into the salmon nuclei. It is known that CMA3 preferentially binds DNA within sperm nuclei, and high levels of CMA3 fluorescence are indicative of poorly condensed sperm DNA, whereas low levels of CMA3 fluorescence correlate with highly condensed, tightly packaged DNA. [140] As shown in Figure 4.9, changes in CMA3 fluorescence was also observed with the addition of R_6 to CMA3 labeled salmon sperm nuclei. In the CMA3 control trial, labeled nuclei were observed over a period of 10 minutes during which the fluorescence intensity of the CMA3 decreased over time. We note that CMA3 intensity in salmon sperm nuclei was significantly higher than we observed in mammalian nuclei perhaps suggesting a higher proportion of underprotamination (or at least poorer DNA packaging) is present in the commercial salmon sperm nuclei. With the addition of R_6 to the labeled nuclei, the level of fluorescence decreased at a much greater rate than the CMA3 labeled nuclei lacking R_6. This is consistent with the R_6 addition to the salmon nuclei did lead to both the peptide crossing the nuclear membrane, as the sperm outer membrane is removed during the nuclei clean-up process, and leading to further tightening of the DNA packaging inside the nuclei.

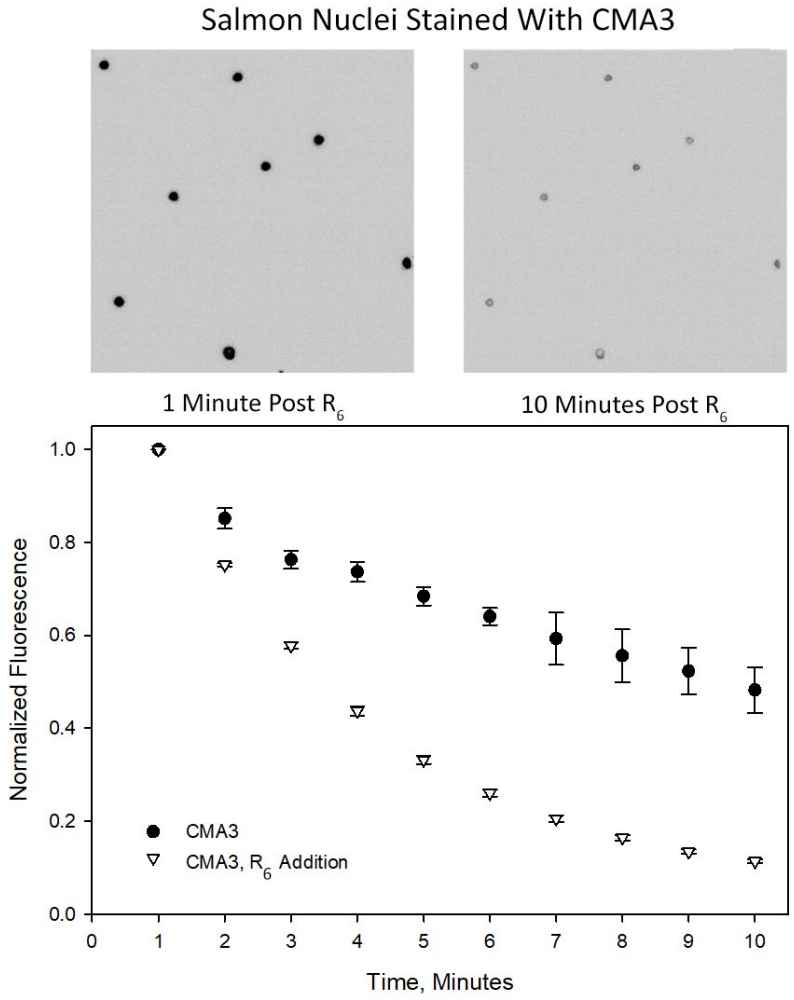

Figure 4.9: CMA3 and R6 integration into salmon sperm nuclei. R6 binds itself to the chromatin within the salmon nuclei, displacing the CMA3, reducing fluorescence. Values are given as mean ± standard error (n = 5).

Section 4.3.6: SAXS Analysis of Salmon Nuclei with the Addition of Cationic Peptides

To further characterize if R_6 was able to cross the nuclear membrane and lead to more highly packaged sperm in the salmon nuclei, we also examined the internal structure of the treated and non-treated sperm nuclei by SAXS (Figure 4.9). Here, Q, the scattering vector, is shown for salmon sperm nuclei with (red, dashed) and without (black, solid line) the addition of

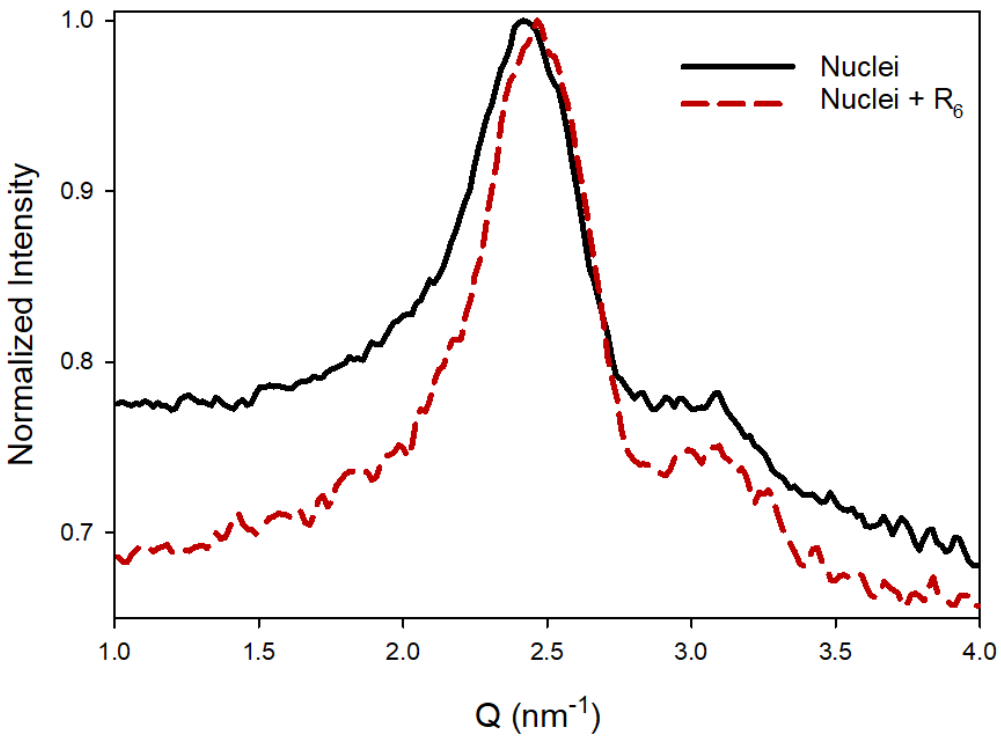

Figure 4.10: SAXS scattering profile of salmon nuclei. R_6 addition to the salmon nuclei results in both a reduction of the low Q values and a shift of the Bragg reflection to higher scattering vector, Q.

R_6. The Bragg peak for native salmon nuclei shows a Q value of ~2.42 nm^{-1}. The addition of R_6 to the nuclei results in a slight shift of the Bragg reflection to Q ~2.47 nm^{-1} as well as a significant narrowing of the peak width. Specifically, the scattering intensity from low Q (or more loosely packaged DNA) is significantly reduced. Also, there is an increase in the higher order reflection (Q~3.1 nm^{-1}) after the addition of the hexa-arginine peptide. Both of these effects are consistent with a tightening up of the DNA packaging within the R_6 treated sperm nuclei and an increase in the long-range order of the condensate. Using only the Bragg reflections, the interaxial spacing can be seen to decrease from D_{int} of 30.0 Å to 29.4 Å (± 0.15 Å). [29]

Section 4.4: Discussion

Through recent advances in the understanding of the susceptibility of sperm DNA to damage and its relationship to both male infertility and adverse genetic outcomes, the importance of the understanding of the mechanisms behind spermatic DNA damage, or conversely, processes protecting sperm DNA, have begun to be more appreciated. Current conventional semen analysis procedures focus primarily on descriptive analysis of the ejaculated semen (count, mobility, etc.), but fail to effectively describe the integrity of the sperm chromatin. [78, 80] Previous studies have shown that there is a correlation between protamine levels and greater incidences of DNA damage present in spermatozoa, thus the analysis of precise levels of underprotamination as it relates to DNA packaging and DNA damage is critical. [9] Our study has defined levels of underprotamination in terms of N/P ratio, which allows for a more exact quantification and description of various levels of protamination. We have also described the types and extent of the DNA damage present at each distinct protamination level.

Our studies have shown that complete DNA condensation occurs at N/P: 1.1, slightly higher than the expected value of N/P: 1.0, this effect occurs regardless of DNA length. Condensation studies performed at physiological salt concentrations, 150 mM NaCl, showed that DNA was not completely condensed by protamine until N/P: 1.50. Our data is consistent with prior published results showing that a greater concentration of protamine is needed to condense DNA in environments with higher ionic content. [105]

It is thought that protamine-DNA in vivo exists at N/P: 1.0, this value is slightly at odds with our reconstituted condensation studies. Possible reasons for this discrepancy could either be an effect of error within our UV-Vis assay, or that sperm DNA in mature nuclei is not completely charge compensated and exists in a slightly underprotaminated state. It is doubtful that the protamine-DNA condensates formed in our reconstituted samples exist in the distinct toroids

present within mature sperm nuclei, failure to form these distinct toroid structures could result in the requiring of greater amounts of protamine to completely condense the DNA.

Protamine packaging shows itself to be an effective protection mechanism for DNA against free radical damage. The prevalence of single and double-strand breaks, as well as base damage, can be decreased substantially with the condensation of the DNA by protamine. A possible mechanism behind this protection ability is that DNA buried deep within the protamine-DNA condensate cannot be easily accessed by the radical species and that only the DNA present on the outer surface of the condensate is subjected to radical damage. Naked plasmid DNA is accessible by the radicals for the entire length of the plasmid, hence showing a greater amount of damage. Other published data suggests that protamine and related cationic peptides could play the role of an antioxidant and can absorb the radical species protecting the DNA from damage. [145] In this case, protamine-DNA at N/P > 2.0 would contain a significant free fraction of protamine and would possess substantial antioxidant capabilities. This was not consistent with our damage assay as shown in Figure 4.5

Levels of protamination correlate directly with the amount of damage present in the protamine DNA condensate. Our data describes the extent of DNA single-strand nicks, double-strand breaks and base damage to the protamine protected DNA as compared to naked DNA. Through the application of protamine, we are able to substantially decrease the prevalence of DNA lesions present on the damaged DNA. Analysis of protamine-DNA condensates at low N/P ratios shows that small decreases in protamination can have a large effect on the amount of damage present on the DNA. Condensation of DNA by protamine at N/P 2.0 nearly eliminates the presence of DNA double-strand breaks from the plasmid. This is quite significant in that DNA double-strand breaks have been shown to result in cellular apoptosis and instability within the

cell on the genetic level. [146]. The presence of such DNA lesions within sperm nuclei would hinder male fertility potential and could result in genetic disruptions in the fertilized embryo [147]

The addition of hexa-arginine, a small cationic peptide, increases the packaging density for both reconstituted protamine-DNA condensates as well as actual sperm nuclei. Condensates consisting of only R_6 have been shown to have a greater packing density than that of protamine-DNA, where R_6 and Protamine-DNA have an interaxial spacing of 28.6 Å and 29.3 Å (± 0.15 Å) respectively. Our SAXS data shows that the addition of the R_6 to the protamine-DNA increases its packaging density. This increase in density hinders the ability for oxidative species to access the condensed DNA, resulting in a decrease in DNA damage.

The ability of the R_6 to cross the nuclear membrane and integrate itself into actual sperm nuclei is substantial in that it has the potential for numerous other applications. Attachment of a fluorescent label to the R_6 could be used as a method to label sperm with poorly condensed sperm chromatin allowing for better sperm selection when undertaking assisted reproductive techniques such as Intra Cytoplasmic Sperm Injection (ICSI). Such a label could also act as a marker for use in studies involving chromatin remodeling processes within the testis or observing sperm chromatin de-condensation post-fertilization.

Section 4.5: Conclusions And Future Work

Protamine has long been thought to play a role in protecting spermatic DNA from damaging agents. The relationship between low levels of protamine and increased amounts of damage has been shown; however, the exact quantification of the levels of underprotamination have been poorly described. Our study accurate defines the exact ratio of protamine to DNA and the resulting degrees of damage present on the DNA at those precise ratios. We have shown that underprotaminated DNA can be further condensed by the application of a small cationic peptide,

hexa-arginine. This increase in packaging density has a direct effect on the prevalence and the extent of DNA damage within the condensate. The binding of this hexa-arginine can be observed not only through the resulting increase in packaging density via SAXS measurements, but through a decrease in CMA3 fluorescence

Future work into this study will entail using hexa-arginine to actually sort out underprotaminated sperm from fully protaminated sperm samples. The preceding R_6- salmon sperm nuclei binding experiments will be repeated using sperm from animals with more complicated protamine systems, such as bull, horse, and human. The effect of hexa-arginine in animals possessing two forms of protamine, P1, and P2 will also be observed. The ability and kinetics for hexa-arginine to cross into intact sperm, as opposed to isolated nuclei will be determined. The effect of peptides of different lengths and net charges will also be explored.

Chapter 5: Effect of Disulfide Bonds on Sperm Chromatin

Section 5.1: Introduction

Section 5.1.1: Introduction into Bull Sperm Chromatin Packaging

During spermatogenesis, somatic chromatin is remodeled, and DNA histones are first replaced with transition proteins, and then with short arginine-rich peptides known as protamines. [148] These protamines, with their large number of basic residues, compact the entire paternal genome into a space upwards of $1/20^{th}$ the volume of the somatic nucleus. [131] This massive compaction results in some of the tightest DNA packaging in nature and results in a near-crystalline hexagonal array. [12, 16, 149] This massive compaction serves not only to facilitate easy transport of the paternal genome to the ovum, but also is thought necessary to protect the sperm genome from damage, oxidative or otherwise. [20, 150] While the protamines of insects, birds, fish, reptiles and most marsupials lack cysteines, the protamines of eutherian mammals (which includes all placental mammals excluding marsupials and monotremes) all contain multiple cysteine residues. These cysteines are readily oxidized by to form inter- and intramolecular disulfide bridges that link the protamines together and stabilize the mammalian sperm chromatin complex during the final stages of spermatogenesis. [26] Typically, due to the high cationic charge of protamine, such as salmon protamine, the protein in an aqueous solution would result in an intrinsically disordered protein structure. [151] In bull chromatin, however, experiments suggest that the intramolecular disulfide bonds result in the formation of a unique hairpin shape for the protamines as depicted in Figure 5.1. In addition, it was shown that intermolecular disulfide bonds form between adjacent protamine hairpins resulting in a rigid protamine network throughout the bull sperm chromatin.[26, 27, 152]

Prior studies by the DeRouchey lab have suggested that despite the large cationic charge of bull protamine, this hairpin structure is actually critical for proper chromatin remodeling in bull

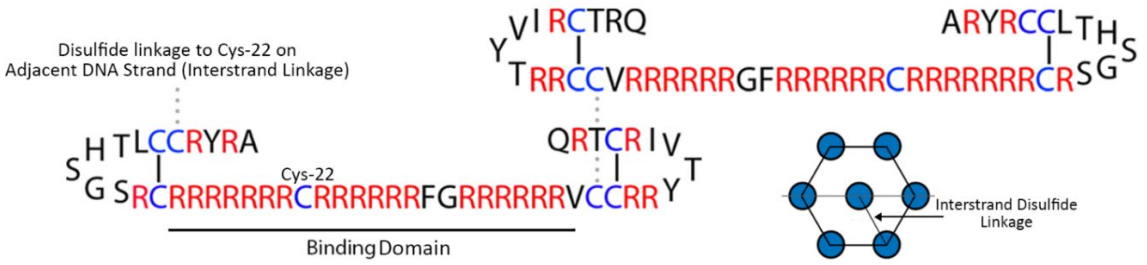

Figure 5.1: Bull protamine forms both inter and intramolecular disulfide bonds. This forms a hairpin dimer with disulfide linkages between protamines on adjacent DNA strands.

sperm nuclei. Small-angle X-ray scattering (SAXS) studies showed that bull sperm nuclei in a reducing environment of dithiothreitol (DTT) exhibited a progressive increase in the DNA interaxial spacing over the course of several days. [29] The tight protamine-DNA packaging

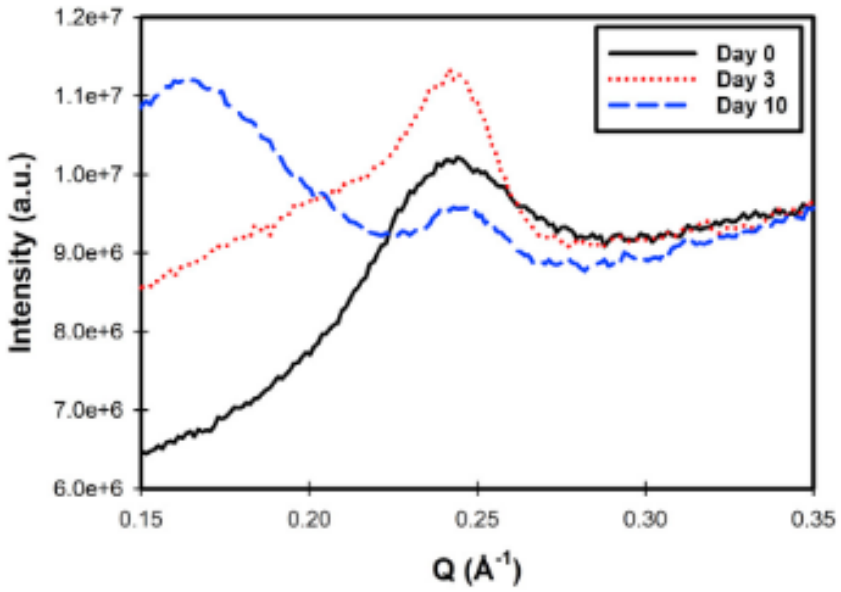

Figure 5.2: SAXS data from Hutchinson et al. Showing incubation of bull sperm in DTT results in a massive growth in the DNA interaxial spacing, suggesting that the disulfide bond reduction results in complete denaturation of the sperm nuclei. Image reprinted Hutchison, J.M., D.C. Rau, and J.E. DeRouchey, *Role of Disulfide Bonds on DNA Packaging Forces in Bull Sperm Chromatin.* Biophysical Journal, 2017. **113**(9): p. 1925-1933. [29]

ultimately changed to a looser, more liquid-crystalline structure as evidenced by the low q peak in the Day 10 (blue dashed line) curve in Figure 5.2. Data shown was also in the presence of an osmotic stressing solution of PEG-water. Without the PEG stressing solution, the DNA in the bull sperm nuclei was observed to completely dissociate upon full reduction of the inter and intramolecular disulfide bonds with a corresponding complete loss of Bragg scattering. [29]

This lack of DNA binding by reduced bull protamine is in stark contrast to the numerous studies showing that piscine protamine, which lack both cysteine residues and the hairpin motif, can condense DNA even at low protamine/DNA ratios. [105, 153] The protamines of avian species, as well as amphibians and some marsupials lack cysteines in their protamine primate sequences as well. [10] We have also observed that piscine protamine/DNA packaging is unaffected by DTT. In this chapter, we have strived to better elucidate the importance of the protamine hairpin motif in eutherian sperm nuclei. Prior studies by the DeRouchey lab have shown that the addition of uncharged amino acids to polycation peptides both increased the repulsive intermolecular forces while decreasing to a lesser extent the long-range attractive forces. [86] Using hexa-arginine peptides of the form ($R_3A_xR_3$), it was shown that each alanine addition resulted in an increased equilibrium spacing between DNA helices. Extrapolating these results, it was predicted that peptides with a net charge approaching 50% or less would not be able to condense DNA.

As shown in Figure 5.3, the primary sequence of salmon protamine is 32 amino acid residues long, of which 21 are arginines. [11] This results in 66% of the residues in the salmon protamine being cationic. Bull protamine contains 50 amino acid residues in its primary sequence, of which 26 are arginine, resulting in 52% of the residues being cationic. [24] Upon forming the hairpin structure, bull protamine appears to move the less charged tails at the amino and carboxyl ends out of the way and creating an arginine-rich DNA binding domain (between Cys-14 and Cys-39) with a higher local cationic charge density.. [10] We note that this DNA binding domain is

nearly identical to the piscine protamines like salmon, with ~26 residues and containing 19 arginine residues (73% charged). Our hypothesis for this work is that the formation of the hairpin results in a higher local percent cationic charge for the DNA binding domain that is nearly identical to the piscine protamines. However, loss of the intramolecular disulfide bonds, would enable the entire bull protamine molecule to interact with the DNA. This unfolded molecule has a net cationic charge of 52% thus leading to an inability to properly package DNA.

.

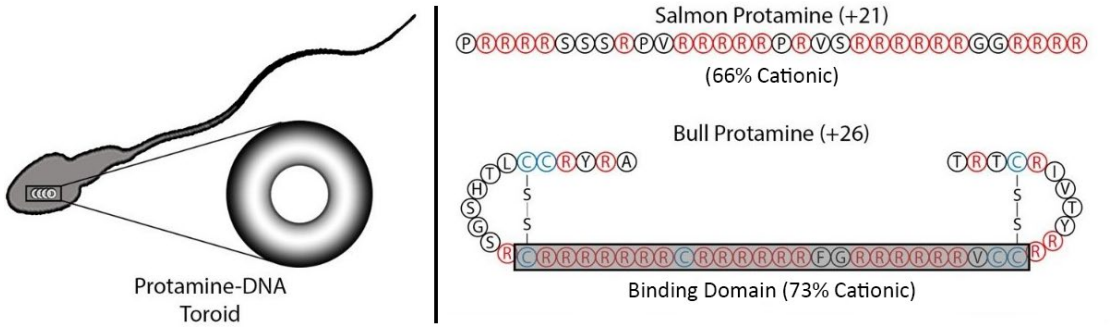

Figure 5.3: Formation of the bull protamine hairpin increases the percent cationic charge of the protamine binding domain. This binding domain is similar in percent cationic charge to salmon protamine.

Typically for in vitro studies of DNA condensation, it is known that multivalent cations of charge +3 or higher typically are capable of condensing DNA. With bull protamine being +26, it would be generally assumed that it should have no problem, with or without the hairpin formation to condense DNA. However, we will show in this chapter that once the disulfide linkages are cleaved, reducing the local cationic charge to closer to 50% cationic charge, results in greatly diminished effective DNA condensation. While the hairpin has only been experimentally observed in bull protamine, we will also show through multiple sequence alignment analysis that the locations of the cysteines in eutherian protamines are the most highly conserved feature among

all species suggesting that the hairpin secondary structure may be a universal feature in eutherian animals. [154]

Section 5.1.2 Sperm Nuclear Vacuoles

In order to appreciate the significance of a selection of the findings in this study, a brief discussion on sperm nuclear vacuoles is needed.

Sperm nuclear vacuoles are small nuclear inclusion bodies present within the sperm head of mature spermatozoa. Sperm nuclear vacuoles typically appear as circular, well-defined structures, with smooth edges. These vacuoles vary in size but are typically small and appear on both the anterior and posterior of the sperm head (Figure 5.4). [155-158] Sperm that contains fewer than two nuclear vacuoles taking up less than 4% of the total sperm head are considered to be normal sperm morphology. [159] These vacuole structures appear to exist within the sperm

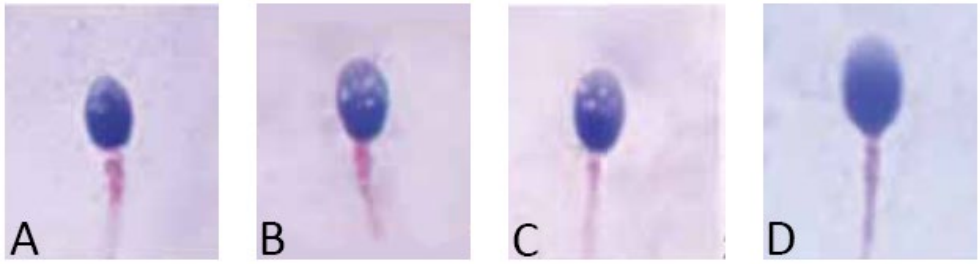

Figure 5.4: Sperm Nuclear Vacuoles: Panels A, B and C show sperm heads with several nuclear vacuoles. Panel D shows sperm with normal morphology. Images adapted from [81]

chromatin, and often appear as ‘voids’ or ‘holes’ within the sperm nuclei, depending on sperm staining or imaging method is used. [156, 160] Smaller vacuoles can exist either on the surface of the sperm nucleus or deep within the sperm chromatin, while large vacuoles often appear as concavities within the sperm head. [161] Sperm nuclear vacuoles are often implicated in poor

male fertility potential, where vacuolated sperm used in Intra Cytoplasmic Sperm Injection (ICSI) have resulted in poor embryo development and greater incidences of spontaneous abortion. [162, 163]

The exact composition or nature of these vacuoles is poorly understood. Many studies have been undertaken to describe the origin or makeup of these vacuoles, and have resulted in multiple, sometimes conflicting, results. [164, 165] In general, there is a consensus that sperm nuclear vacuoles originate within the sperm chromatin itself and are not due to defects in either the sperm outer membrane or the acrosome, the digestive enzyme containing cap present on mature sperm. [166, 167] Sperm nuclear vacuoles are thought to be either the result of poor sperm chromatin condensation during spermatogenesis or the product of DNA damage and fragmentation to the spermatic DNA. [164, 168]

Sperm containing large nuclear vacuoles have been shown to have deficiencies in protamination levels, as observed through the CMA3 assay, a commonly used indicator of protamine status. [168] Sperm containing prominent nuclear vacuoles have been shown to contain a large fraction of residual DNA histones, indicated through aniline blue staining. [169] This suggests that sperm nuclear vacuoles are the direct result of sperm chromatin remodeling failure.

Greater levels of DNA damage has been found in sperm containing large nuclear vacuoles. [170] Analysis by the terminal deoxynucleotidyl transferase dUTP nick end labeling assay (TUNEL), an assay used to detect DNA strand breaks, found that sperm containing nuclear vacuoles had a greater incidence of DNA double-strand breaks than non-vacuolated sperm. [171] Acridine orange staining also found greater levels of DNA fragmentation in vacuolated sperm as compared to morphologically normal sperm. [171] These findings suggest that sperm nuclear vacuoles are an indicator of poor sperm chromatin integrity and are the result of increased amounts of DNA

damage to the sperm chromatin. It is generally known that the protamination state and prevalence spermatic DNA damage are related, so it is quite possible that both these hypotheses on the cause and makeup of sperm nuclear vacuoles are coupled. [172]

Section 5.2: Materials and Methods

Section 5.2.1: Materials

Percoll was purchased from GE Healthcare. CHAPS (3-[(3- Cholamidopropyl) dimethylammonio]-1-propanesulfonate), Iodoacetamide, crystal violet, and thiourea was purchased from Acros Organics. PMSF, (phenylmethylsulfonyl fluoride) and salmon protamine chloride, HCl, ethidium bromide, calf thymus DNA, Dextran Sulfate from *Leuconostoc spp*. (avg molecular weight 9,000-20,000) and iodoacetic acid was purchased from Sigma-Aldrich. Dithiothreitol, urea, glacial acetic acid and acetone were purchased from VWR. 40% acrylamide solution and 0.5M EDTA stock were purchased from Fisher BioReagents. Nonidet, guanidinium chloride and trichloroacetic acid were purchased from Ameresco. 1M Tris-Cl stock was purchased from Mediatech. 5M NaCl stock was purchased from Promega. 3-bromopropylamine hydrochloride was purchased from Alfa Aesar. Ficoll-400 was purchased from OmniPur. Glycerol was purchased from Fisher. AcquaStain was purchased from Bulldog Biolabs. Propidium iodide and Hoechst 33342 and methyl iodide were provided by Dr. Pheobe Glazer and DiO was provided by Dr. Chris Richards, both of University of Kentucky Department of Chemistry. Bull sperm straws were purchased from CattleVisions LLC. Horse sperm and epididymal samples was provided by Dr. Barry Ball from the University of Kentucky Department of Equine Science. All reagents were used without alteration, except where noted.

Section 5.2.2: Bull/Horse Sperm Nuclei Separation

0.75 mL of thawed bull sperm in extender was centrifuged at 700g at room temperature for 15 minutes and the resulting supernatant was removed leaving an intact sperm pellet.

All subsequent solutions were stored on ice during the cleaning procedure. All centrifugations were performed at 5°C. Buffer A (150 mM NaCl, 20 mM Tris-Cl, 2 mM EDTA, 1 mM PMSF) was created prior to use and stored at room temperature, apart from the PMSF, which was added immediately prior to performing the cleanup procedure. All other solutions were created immediately before performing the nuclei clean up.

The sperm pellet was suspended in a solution of 1x buffer A and 250 mM sucrose. The resulting suspension centrifuged for 5 minutes at 5000g and the supernatant was discarded. The sperm pellet was then resuspended in 1x buffer A and passed through a 22 gauge needle several times to shear off sperm tails from the intact sperm. The sample was then centrifuged at 2000g for 5 minutes and the supernatant was discarded. The shearing was repeated using fresh buffer A for a total of 2 washings. The sperm pellet was resuspended in a solution of 0.5x Buffer A and 50% Percoll. The sample was then sonicated on ice using 'Sonic Dismembrator' for 10 seconds at 35% amplitude a total of 10 sonications, waiting 2 minutes between each sonication. The resulting suspension was then centrifuged at 14,000g for 20 minutes, discarding the resulting supernatant. The sperm pellet was then incubated at 37°C in 100 mM, Tris-Cl, 10 mM CHAPS and 20% glycerol for 30 minutes. After incubation, the solution was centrifuged at 2000g for 5 minutes, discarding the supernatant. Nuclei pellet was washed 2 times by vortexing in 150 mM NaCl, 10 mM Tris-Cl and 0.02% NP-40, and centrifuged at 2000g for 5 minutes, decanting the supernatant between washings. Nuclei were stored in the refrigerator in the washing solution until needed.

Section 5.2.3: Propidium Iodide Staining

All microscopy images were acquired using an Olympus IX71 inverted fluorescent microscope. Sample magnification was 600x using either an oil or water immersion objective. Cell stains were viewed through the following excitation/barrier filter wavelengths: DiO: 450/515 nm, Hoechst 33342: 361/420 nm, PI: 535/590 nm. Images were captured by an 'Andor Zyla sCMOS' camera controlled by the Micro-Manager ImageJ plug-in. Images were captured in grayscale, then colored in photoshop.

Sperm nuclei were separated from intact sperm as previously described. Sperm nuclei were smeared on a glass coverslip using a sterilized wire loop and let dry under air. Once dried, the nuclei were fixed to the coverslip by immersion in 95% ethanol for 20 minutes at -20 °C, then dried under air at room temperature. Propidium iodide (PI) was dissolved in 10 mM Tris-Cl to a final concentration of 30 µM. [158] PI was introduced to the top of the fixed nuclei and were incubated for 20 minutes at room temperature in the dark. After incubation, PI was removed, and the nuclei were rinsed with DI water 3 times then imaged.

Section 5.2.4: DiO and Hoechst 33342 Staining

Hoechst 33342 was dissolved in 1x PBS to a final concentration of 8.1 µM. Bull nuclei were fixed to a coverslip using 95% ethanol as previously described. Hoechst 33342 was introduced to the fixed nuclei and incubated at room for 20 minutes. After incubation, nuclei were rinsed 3 times using 1x PBS. DiO was dissolved in DMSO and diluted with 1x PBS to a final concentration of 1 µM, then introduced to the Hoechst stained nuclei. The sample was incubated for 30 minutes at 37°C. The sample was rinsed 3 times with 1x PBS then imaged as previously described. All staining procedures were done in the dark.

Section 5.2.5: DTT Decondensation Assay

Isolated sperm nuclei were fixed to a coverslip and labeled with PI as previously described. DTT decondensation solution was prepared to a final concentration of 400 mM DTT, 150 mM NaCl, 8 mM EDTA, pH 8.2-8.4. The solution was prepared immediately prior to use. The DTT solution was added to the top of labeled nuclei and allowed to incubate for 180 minutes, a picture of the nuclei was taken every 3-5 minutes to record the decondensation process. Images were collated and edited in photoshop and saved as a movie. The decondensation process was repeated using isolated salmon and isolated horse sperm nuclei. Nuclei area was quantified using ImageJ. Nuclei area was determined across 5 distinct nuclei for the horse trial, 53 distinct nuclei for the salmon trial and 5 distinct nuclei for the bull trial. Nuclei area for each species was averaged and standard error was calculated. Bull and salmon decondensation pictures obtained with Jacquelyn Rhinehart.

Section 5.2.6: Bull Protamine Separation

Purified bull sperm nuclei were incubated in a solution of 2M urea, 1M NaCl, 1M guanidinium chloride and 50 mM dithiothreitol until nuclei were completely dissolved. The nuclei solution was then sonicated on ice using a 'Sonic Dismembrator' for 10 seconds at 35% amplitude. 6M HCl was added to nuclei solution to a final concentration of 0.96M and incubated on ice for 20 minutes to precipitate out the DNA. DNA was pelleted by centrifugation at 10,000g for 10 minutes at 5°C. The resulting protamine rich supernatant was decanted, and sodium acetate was added to a final concentration of 1.15M.

Protamines were purified by centrifugation in an Amicon Ultra-2 Centrifugal filter, 3K NMWL, for a total of 2 centrifugations at 4000g for 30 minutes at room temperature, adding 1 mL 10 mM Tris-Cl to the protamines before each centrifugation. The resulting retentate was removed and the final volume was adjusted to 500 µL, 1M NaCl in 10 mM Tris buffer.

The protamine solution was trichloroacetic acid (TCA) precipitated. 100 µL 100% TCA was added to the protamine solution and incubated on ice for 20 minutes. Protamines were pelleted by centrifugation at 14,000g for 15 minutes at 5°C, and the resulting supernatant was then discarded. Protamines were washed with 150 µL of 25% TCA and the centrifugation was repeated. After discarding the supernatant, the protamines were precipitated using cold acidified acetone (acetone with 1 mM HCl). Protamines were pelleted by centrifugation and the acetone supernatant was discarded. Protamines were dried and stored in 150 mM NaCl, 10 mM Tris-Cl. Protamine concentration was determined using a Qubit protein assay per manufacturer's instructions.

Section 5.2.7: PAGE Analysis of Separated Protamines

Separated protamines were visualized by gel electrophoresis using an acid-urea gel. [97] Gel was made to a final concentration of 20% polyacrylamide (5% crosslinker), 2.5M urea, 0.9M acetic acid, using thiourea and H_2O_2 as an initiator. [173] Gels were degassed for 10 minutes prior to polymerization. Each protamine sample well contained approximately 1-2 µg protamine in 5 µL solution, 0.9M acetic acid, and 8% Ficoll 400. Gels were run at 130 volts, 4 mAmps, for 120-180 minutes with the current reversed using 0.9 M acetic acid as a running buffer. The gel was stained using AcquaStain (Bulldog Bio) and photographed using a BioRad Gel Doc XR gel documentation system.

Section 5.2.8: Protamine Cysteine Alteration

Solid protamines were dissolved in 20 µL of 100 mM Tris-Cl, pH 8.4 and 20 mM DTT and incubated in the refrigerator overnight. Samples were combined with 100 mM Tris-Cl, pH 8.4, and methyl iodide to a final concentration of 50 mM MeI and a final volume of 150 µL. Samples were

incubated for at least 2 hours in the dark at room temperature. Methylated protamines were concentrated using a 3k NMWL centrifuge filter and TCA precipitated as previously described. Protamine methylation was confirmed by PAGE analysis as previously described. Any protamines not fully methylated were subsequently re-methylated using the same procedure. Protamines were stored in 150 mM NaCl, 10 mM Tris-Cl until needed. Carboxylation and carbamidomethyl reactions were performed in the same manner, with 50 mM Iodoacetic acid and Iodoacetamide used for their respective modifications. Propylamination of sperm protamines was completed using 70 mM 3-bromopropylamine [174-176]

Section 5.2.9: Altered Protamine Ethidium Bromide Displacement Assays

Calf thymus DNA was dissolved in 150 mM NaCl, 10 mM Tris-Cl overnight. The DNA concentration was determined by UV-Vis, where DNA concentration at A_{260}=1 is 50 µg/mL. [177] Ethidium bromide was added to DNA at a 1 to 10 molar ratio of ethidium bromide to DNA base pair. [104] Protamine was added stepwise to ethidium bromide/DNA at increments at of N/P: 0.25. DNA was incubated at room temperature for at least 5 minutes between measurements, the volume of protamine added was less than 2% of the total solution volume. Fluorescence was measured at λ_{ex}=520 and λ_{em}=595. Data was reported as relative fluorescence $(F-F_0)/(F_{Max}-F_0)$, where F is the sample emission intensity, F_0 is the emission intensity of ethidium bromide without DNA, F_{Max} is the emission intensity of only DNA and ethidium bromide. Exclusions assays were repeated 3 times, data was averaged, and standard error was calculated.

Section 5.2.10: Sperm Nuclei Salt Challenge Assay

Salmon sperm nuclei were cleaned by procedure discussed in section 4.2.5 then placed in 2 mL of 10 mM Tris-Cl. 5M NaCl Stock was added to salmon nuclei suspension at 40 µL intervals.

After each addition, salmon nuclei were mixed thoroughly and let rest for a minimum of 5 minutes. After resting, the sample was centrifuged at 11000g for 15 minutes, the resulting supernatant was measured for A_{260} value. The supernatant was returned to the salmon nuclei mixture and NaCl addition was repeated. UV-Vis spectrophotometer was blanked using a solution of the same salt molarity between measurements. Assay was repeated 3 times; results were averaged, and standard error was calculated.

Bull nuclei were isolated as previously discussed, bull nuclei were placed in 600 µL Tris-Cl buffer, 5M NaCl stock was added to the suspension in 200 and 400 µL increments. The sample was let rest and centrifuged as discussed above. Sample supernatant was measured for A260 value, using an appropriate blank for each measurement. Absolute NaCl molarity was calculated for each NaCl addition, and data was graphed as NaCl molarity vs. A_{260} value. Assay was repeated 3 times; results were averaged, and standard error was calculated.

Section 5.2.11: Protamine-DNA Particle Stability Assay

pUC19 plasmid was combined with bull protamine to a final N/P ratio of 2.0 and allowed to condense for a minimum of 15 minutes. Dextran sulfate in 10 mM Tris-Cl was added at 15 µg increments. DTT was added to the final concentrations indicated, total sample volume was 14 µL. Samples were heated for 30 minutes at 60 °C. 2 µL 6X loading dye was added to each sample then introduced into a 1.0% agarose gel. The gel was created using 1x TAE buffer. The gel was run for 90 minutes at 95 volts, 70 mAmps in 1x TAE. The gel was stained in ethidium bromide in 1x TAE, 2.5 µg/mL for 30 minutes, then destained for 20 minutes in pure 1x TAE. The sample was imaged in a Bio-Rad Gel Doc imaging system.

Section 5.2.12: Cysteine Sequence Alignment

Sequence alignment was performed by Christian Powell and Dr. Hunter Moseley of the University of Kentucky Institute for Biomedical Informatics, the complete procedure can be found in [178]

Section 5.2.13: CMA3 Analysis of Isolated Bull Sperm Nuclei

Bull sperm nuclei were isolated as previously discussed. Samples were labeled for CMA3 fluorescence as described in section 4.2.6. Sample images were obtained as described in section 5.2.3. Images were colored in photoshop.

Section 5.2.14: Analysis of Horse Epididymal Samples:

Horse sperm nuclei were separated from horse epididymal sections using the procedure described in section 5.2.2. Horse epididymal nuclei were stained and imaged using the procedure listed in section 5.2.3. SAXS analysis of epididymal nuclei was performed by the procedure described in section 4.2.5

Section 5.3 Results

Section 5.3.1: Microscopy Studies of Bull and Horse Nuclei

Figure 5.5 and 5.6 shows the results of the nuclei cleanup procedure for both horse and bull. By subjecting the bull and horse sperm nuclei to an extensive cleanup procedure, intact sperm nuclei are able to be separated from the sperm flagellum and other organelles. Treatment with CHAPS detergent solubilizes both the sperm plasma membrane and the acrosome. [179] Despite the CHAPS treatment, the sperm nuclear envelope remains intact around the sperm nuclei as seen by staining the nuclei with DiO, a lipophilic stain. Observing the nuclei using

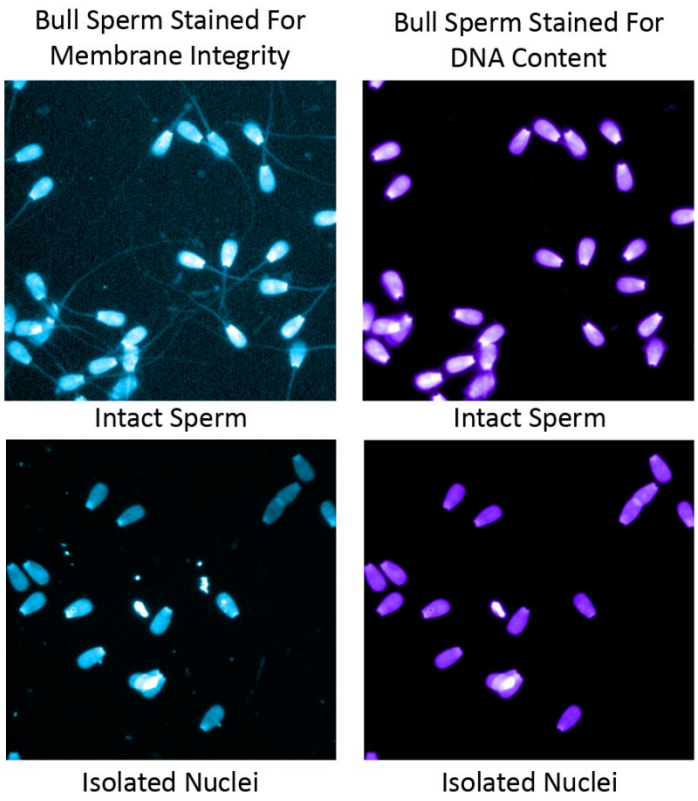

Figure 5.5: Bull nuclei stained for DNA content (Hoechst 33342) and membrane integrity (DiO). The nuclear membrane is present but not impermeant.

propidium iodide, a DNA selective stain, shows that the DNA within the horse and bull sperm nuclei are still intact and have not been compromised during the cleanup procedure to any

observable degree. Propidium iodide is known to not penetrate fully intact plasma membrane, so the fact that we observe DNA staining with PI and DiO is evidence that the nuclear membrane is present but not impermeant. Bull sperm nuclei appear to be approximately three to four times the size of the horse sperm nuclei, consistent with prior published results. [180, 181]

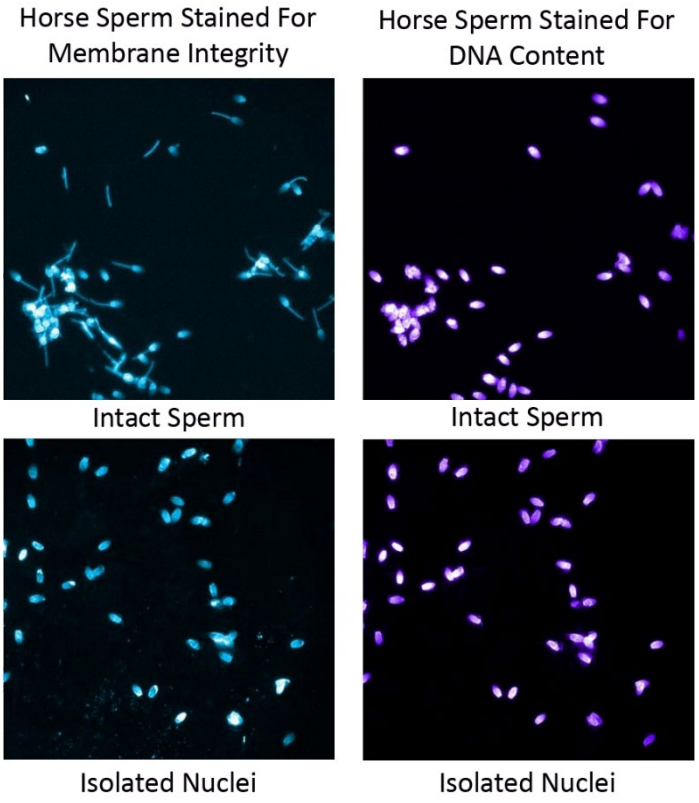

Figure 5.6: Horse nuclei stained for DNA content (Hoechst 33342) and membrane integrity (DiO). The nuclear membrane is present but not impermeant.

Section 5.3.2: DTT Mediated Decondensation Of Sperm Nuclei

Incubation of bull sperm nuclei in a bathing solution of DTT, NaCl, and EDTA initially results in the formation of small inclusion bodies within the sperm nucleus reminiscent of sperm nuclear vacuoles (Figure 5.7). These vacuoles form almost immediately following treatment with DTT and are clearly visible after 10 minutes of incubation (Figure 5.7, left panel). Such vacuoles

are indicative of the DNA inside the nuclei decondensing. As the vacuoles grow and the nuclei decondense, the DNA presses against the sperm nuclear envelope causing the nuclei to swell (Figure 5.7, right panel). Salmon nuclei are unaffected by this DTT mediated decondensation as shown in Figure 5.7, bottom panels. A 2-hour incubation

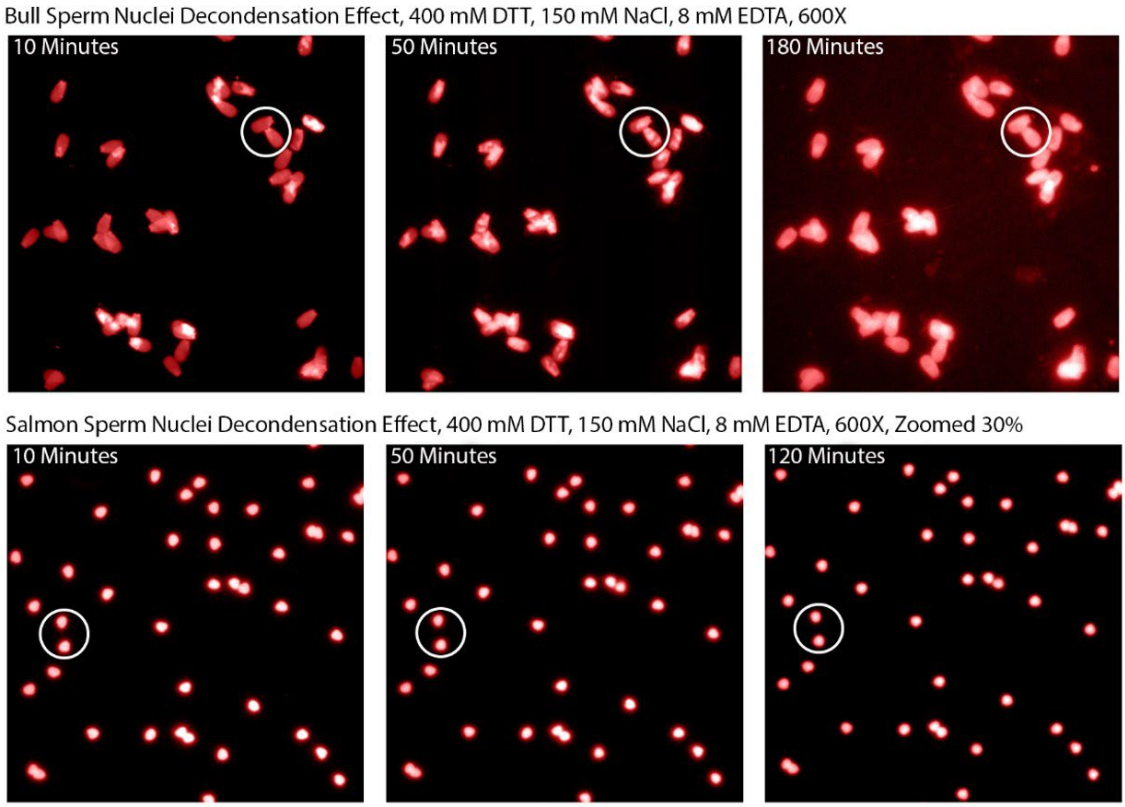

Figure 5.7: DTT incubation breaks disulfide bonds within the protamine of bull sperm nuclei, decondensing the DNA. As a result, the DNA pushes against the nuclear membrane, causing the nuclei swell. Salmon nuclei, which contain no cysteines within their protamine sequence, are unaffected. Both bull and salmon nuclei are labeled with propidium iodide

results in no visible changes to the salmon sperm nuclei, implying that they are retaining their nuclear integrity.

Shearing away the sperm nuclear membrane, by wicking away the DTT bathing solution using a Kimwipe, results in the rapid decondensation of the bull sperm nuclei, essentially causing them to 'explode'. This releases the free DNA into the DTT bathing solution and is evident by a

complete loss of structure to the bull sperm nuclei (Figure 5.8, top panels). Salmon nuclei subjected to the same DTT treatment are completely unaffected by the reducing environment and shows neither vacuole formation, nuclei swelling, or nuclei decondensation even when subjected to shearing trauma. (Figure 5.8, bottom panel).

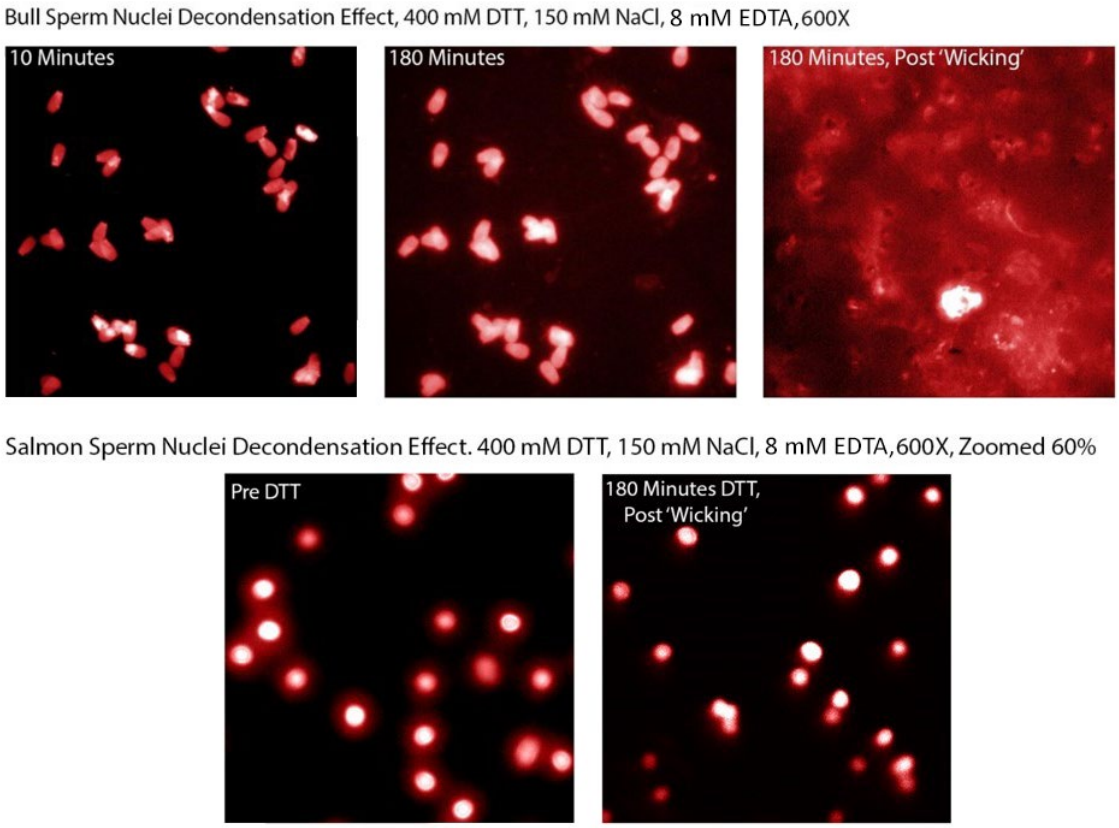

Figure 5.8: Bull sperm nuclei after DTT treatment rapidly decondense when subjected to mechanical trauma by 'wicking away' the DTT bathing solution. Again, salmon sperm nuclei are unaffected. Both bull and salmon nuclei are labeled with propidium iodide

Horse sperm nuclei show a similar effect as the bull sperm nuclei when allowed to incubate in the DTT reducing solution. Horse sperm nuclei in the DTT bathing solution exhibits a progressive swelling of the nuclei as incubation time increases. Formation of the nuclear vacuole inclusion bodies is less obvious in the horse sperm nuclei. This is due either to their smaller size, making the presence of the vacuoles less obvious, or that the presence of the second form of

protamine (P2) present in horse but not bull, is affecting the formation of the vacuoles. While many mammals, including humans, mice, and primates are known to have both P1 and P2, the exact ratio of P1 to P2 is species dependent. In horse, the P1/P2 ratio is approximately 75/25.

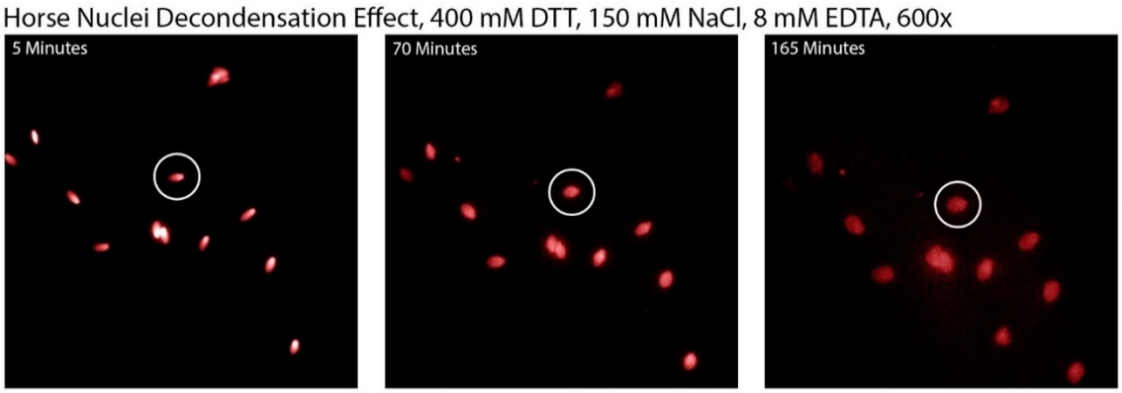

Figure 5.9: Horse sperm nuclei subjected to DTT treatment show similar swelling as bull sperm nuclei. Horse sperm nuclei contain two forms of protamine, P1 and P2. Despite this extra protamine, horse nuclei still decondenses in the presence of DTT. Nuclei are labeled with propidium iodide

By quantifying the area of the decondensing sperm nuclei, a better idea of the progress of the decondensation relative to time can be obtained. Bull sperm nuclei over the course of 180 minutes swell approximately 1.8 times in size. Salmon nuclei show a slight decrease in size during

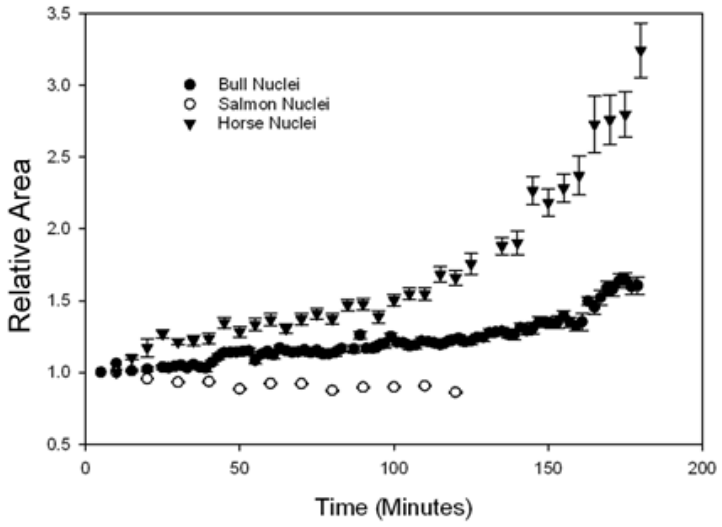

Figure 5.10: Quantification of sperm nuclei size during the decondensation procedure. Size is reported as relative area, where the initial nuclear size is 1.

the DTT incubation, most likely due to slight photobleaching of the nuclei, making the nuclei appear smaller. Horse nuclei swell to upwards of 3.5 times their initial size, suggesting that they are especially susceptible to DTT mediated decondensation. This data is shown in Figure 5.10.

Section 5.3.3: Alteration of Protamine Cysteine

Incubation of native bull protamine in DTT results in the reduction of the disulfide bonds between protamine cysteines, allowing them to be accessible to various alkylating agents. By alkylating the protamine cysteine, the sulfur is 'capped', preventing re-formation of the disulfide bond. By performing this capping reaction on all 7 bull protamine cysteines, the formation of both

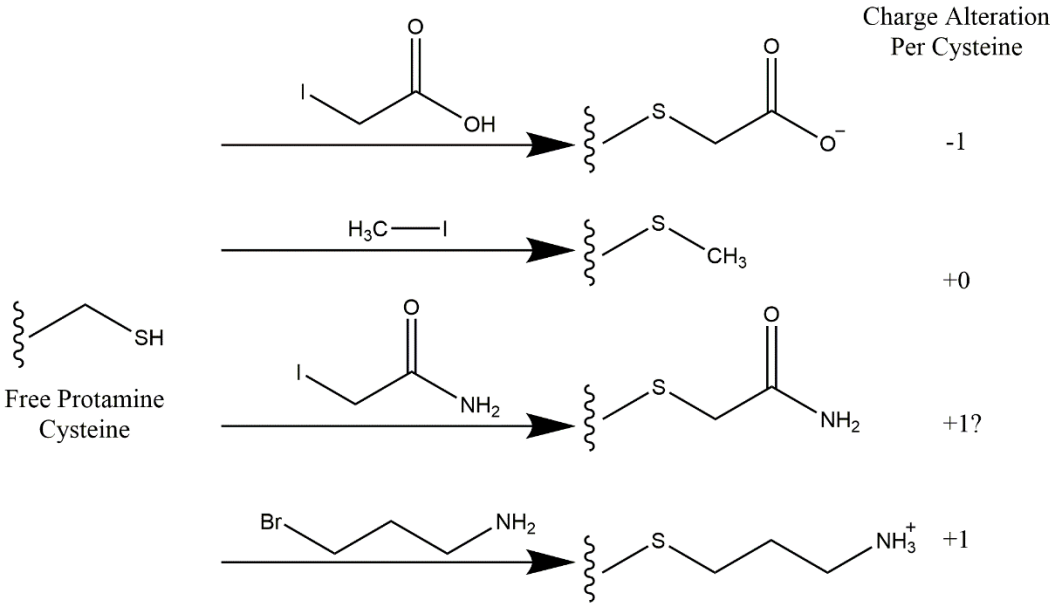

Figure 5.11: Protamine cysteine 'capping' reaction summary. Each capping reaction alters the net charge of the protamine cysteine and also prevents the formation of disulfide bonds.

the protamine hairpin can be prevented, as well as the formation of the intermolecular disulfide bonds. By selecting the alkylating agents shown in Figure 5.11, either an anionic, cationic, or neutral charge can be imparted onto the protamine cysteine by the capping reaction. This allows

for modification of not only the ability to form the hairpin but also the percent cationic charge for in-vitro binding experiments.

Both the concentration dependence of the alkylating reagent as well as the reaction progress can be monitored by gel electrophoresis. The reaction of denatured protamine and methyl iodide results in the addition of a methyl group to the thiol on the protamine cysteine This can be seen in Figure 5.13. Unaltered protamine, not denatured in DTT, forms multiple intermolecular disulfide bonds. This results in the formation of an extensive protamine network which increases the size of the protein, making it unable to enter the gel as seen in the first lane on the far left of Figure 5.13. Despite not being present in DTT, a small fraction of the protamine exists as the single protamine hairpin and is observed as a fast-moving band towards the bottom of the gel. The prominent band midway through the gel is suspected to be the protamine-protamine dimer.

As the cysteine methylates, the protamine loses its ability to form disulfide bonds, causing more protamine to migrate into the gel. As the reactant concentration increases, eventually all seven of the protamine cysteines methylate, and the protein exists solely as the denatured methylated product. This product migrates in its entirety at the same rate and is seen as one prominent band in the gel, with only a small fraction of the protamine existing as the heterodimer as seen in lane 5. Herring protamine sulfate acts as a control and migrates faster through the gel than the bull protamine due to its smaller molecular weight. The reaction progress for all four alkylating agents can be seen in Figure 5.12-5.19. The reaction was repeated for a total of two alkylations on all products to confirm that no disulfide bonds were present in any of the altered protamines.

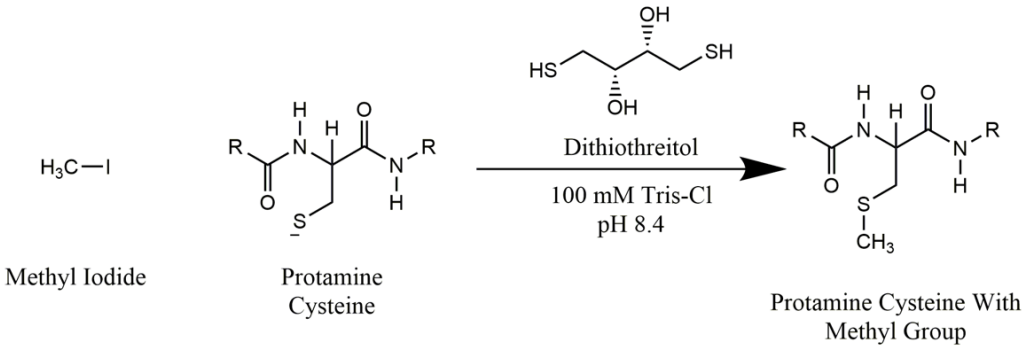

Figure 5.12: Methylation of protamine cysteine prevents disulfide bond formation

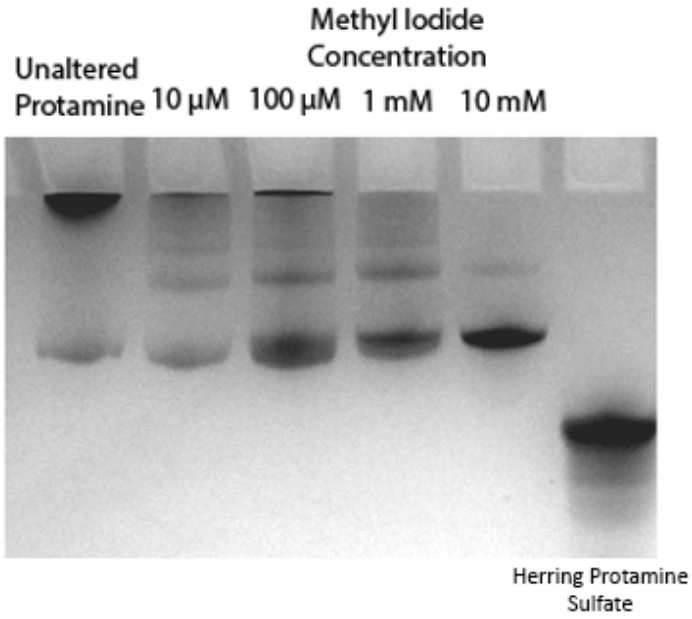

Figure 5.13 Gel analysis of the progress of the protamine methylation reaction.

Figure 5.12 and Figure 5.13 shows the addition of a methyl group to the protamine cysteine, preventing disulfide bond formation. As the concentration of methyl iodide increases, a greater fraction of the disulfides methylate. Protamine without the formation of any disulfide bonds can easily enter the PAGE gel.

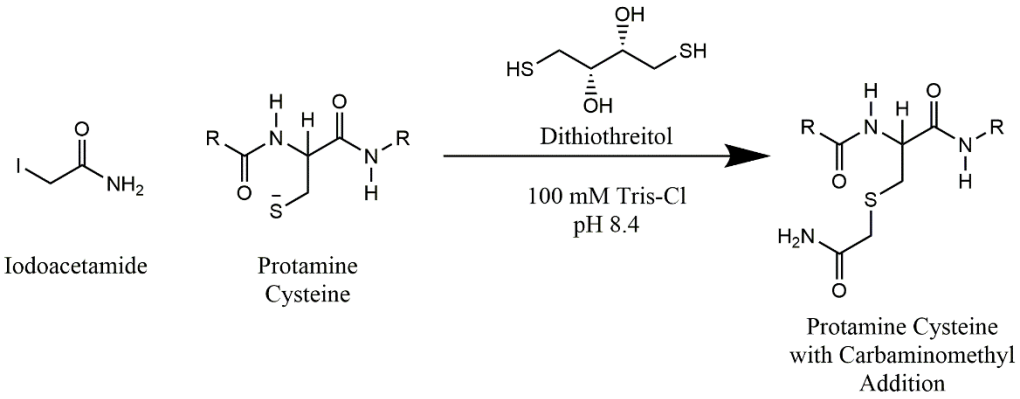

Figure 5.14: Carbamidomethyl addition prevents disulfide bond formation.

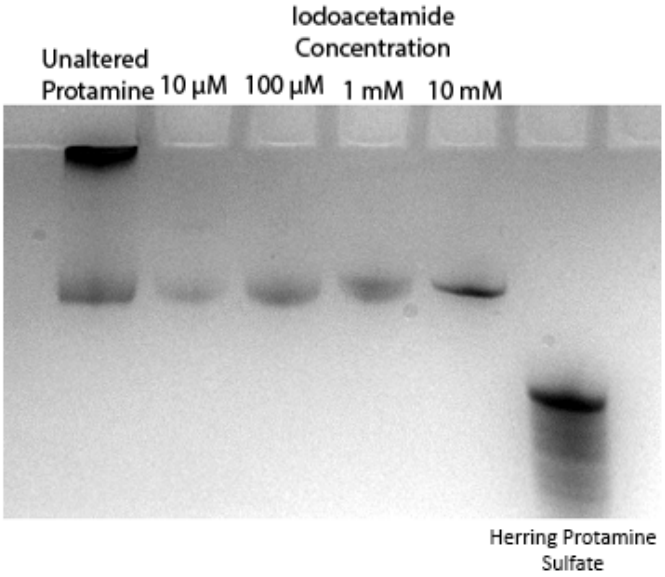

Figure 5.15: Gel analysis of the reaction progress of protamine carbamidomethyl addition

Figures 5.14 and 5.15 shows the addition of a carbamidomethyl group to the protamine cysteine. Again, this prevents the formation of the protamine disulfide bond network.

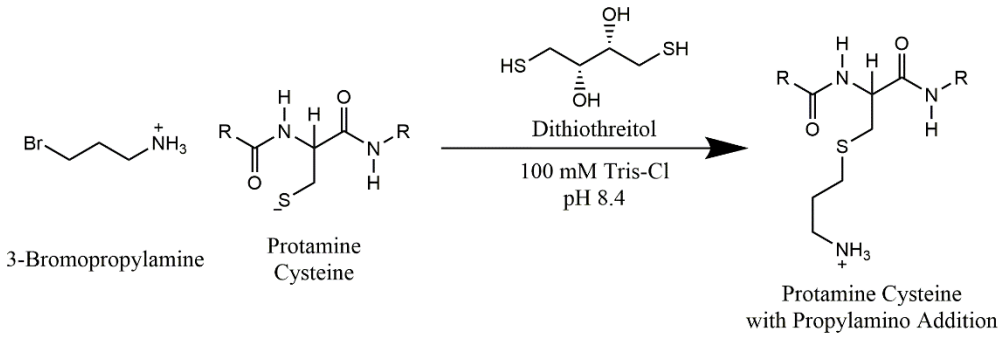

Figure 5.16 Addition of a propylamino group prevents disulfide bond formation and adds a cationic charge to the cysteine

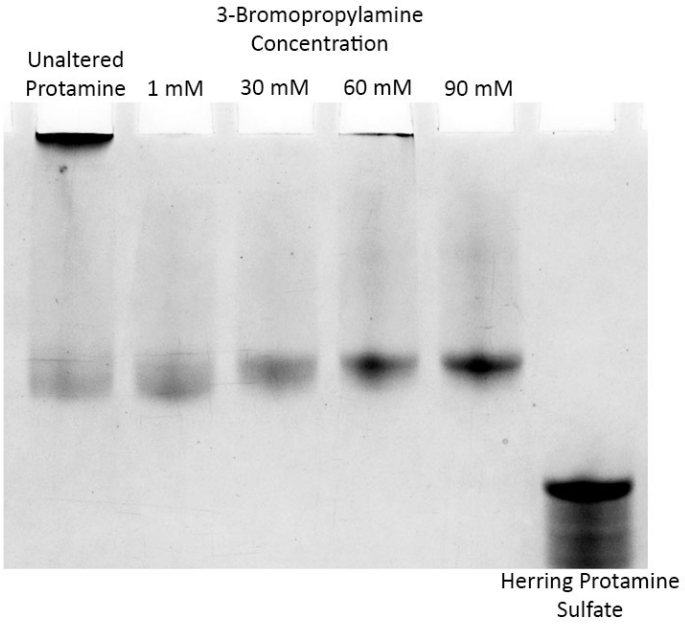

Figure 5.17: Gel analysis of the progress of protamine propylamino addition

Figures 5.16 and 5.17 shows the effect of a propylamino addition on the protamine cysteine. In order for the reaction to go to completion, a greater concentration of reactant was needed. The 'streak' present in the gel above the protamine band is indicative of sperm cellular debris present in the sperm nuclei suspension prior to the protamine separation.

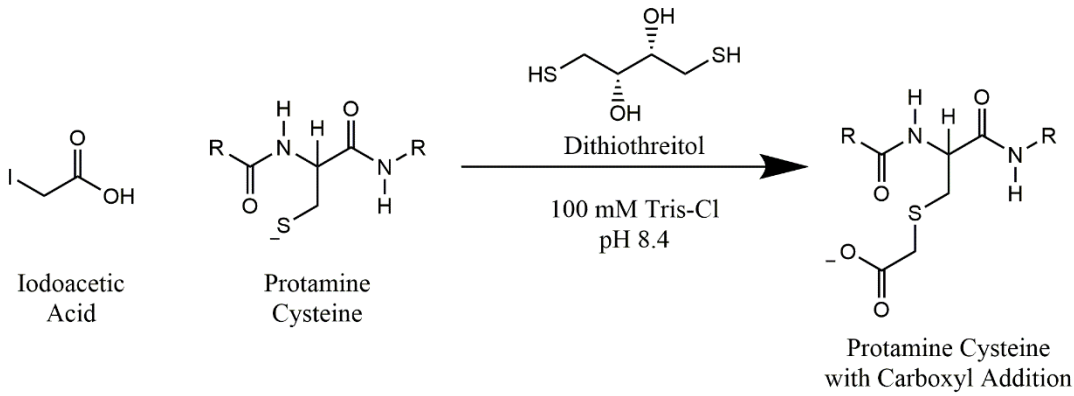

Figure 5.18: Addition of a carboxyl group prevents disulfide bond formation and adds an anionic charge to the cysteine

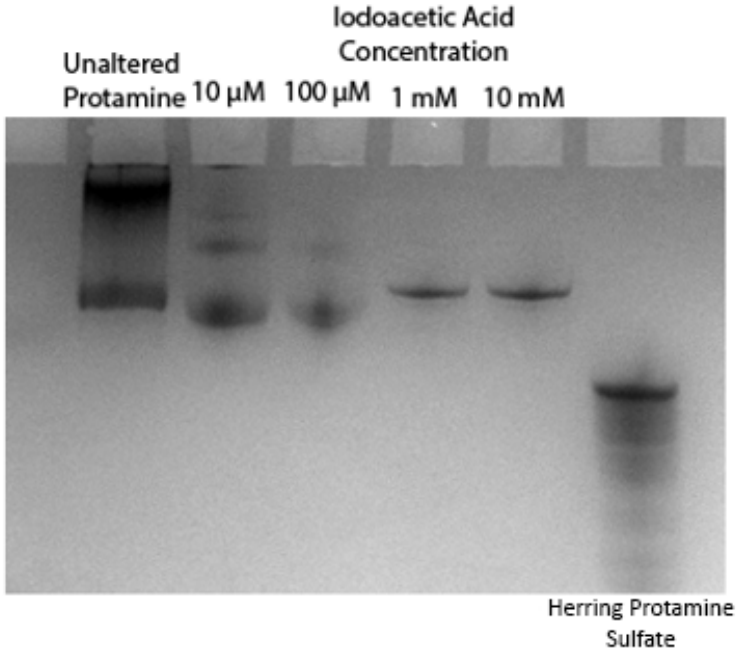

Figure 5.19: Gel analysis of the progress of protamine carboxyl addition

Figures 5.18 and 5.19 shows the effect of a carboxyl addition to the protamine cysteine. Again, showing the effect of preventing the formation of the disulfide bond network within the protamine.

As previously discussed, bull protamine without the presence of the hairpin has a percent cationic charge of 52%. Through the addition of a propylamino group to the protamine cysteine, the net cationic charge of the native protamine as increased by +7, bringing the percent cationic charge to 66%. This is the same cationic charge percentage on salmon protamine. Addition of the carbamidomethyl group also appears to be adding a +7 cationic charge, this result is unexpected as the terminal amino group on the carbamidomethyl group is typically deprotonated. The justification for this observation will be discussed in a subsequent section below. Addition of a carboxyl group to the protamine cysteines adds 7 anionic charges to the native protamine, resulting in a net cationic charge of +19, reducing the percent cationic charge to 38%. Methylating the cysteines impart a neutral charge to the protamine, keeping the net cationic charge at +26 and the percent cationic charge at 52%. A summary of these charge alterations as well as their respective molecular weight changes to the protamine can be seen in table 5.1. A comparison of the altered protamine migration differences across a PAGE gel can be seen in Figure 5.20

Table 5.1: Summary of bull protamine net cationic charge, percent cationic charge, and molecular weight changes

Protamine Alteration	**Percent Cationic Charge**	**Net Cationic Charge**	**Molecular Weight Change**
Salmon Protamine	66%	+21	N/A
Unaltered Protamine Hairpin	73%	+26	N/A
Methylation	52%	+26	+105
Carbamidomethyl	66% ?	+33 ?	+413
Propylamination	66%	+33	+413
Carboxylation	38%	+19	+406

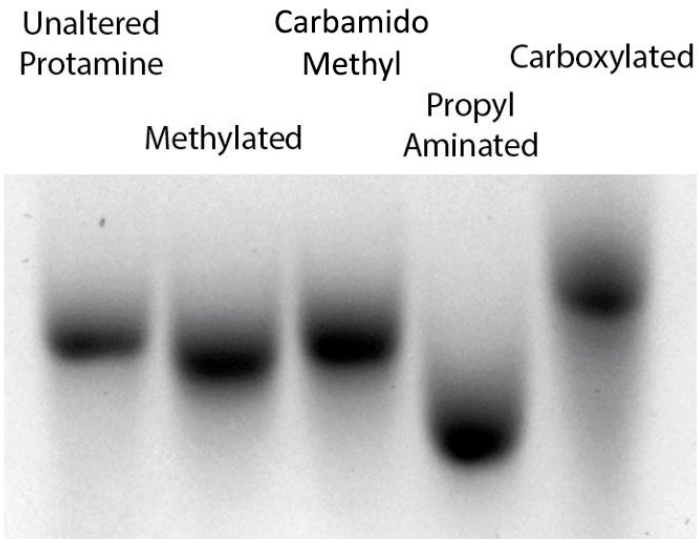

Figure 5.20: Migration differences of altered protamines is dependent on charge density as well as molecular weight. Propylaminated protamine has a higher cationic charge then carboxylated protamine, resulting in a difference in migration rates.

Section 5.3.4 Ethidium Bromide Displacement Assays of Altered Protamines

Titration of protamine into ethidium bromide intercalated DNA results in progressive binding of the DNA by the protamine. As protamine binding occurs, intercalated ethidium bromide is displaced from the DNA, reducing fluorescence. Data is graphed as relative fluorescence vs. N/P ratio.

It was previously shown that isolated bull protamine, upon removal of DTT reducing agent, quickly reforms the intramolecular disulfide bonds to reform the hairpin structure. [26] To examine the effect of the hairpin formation on DNA condensation, we performed an ethidium bromide exclusion assay comparing DNA condensation for reconstituted bull protamine hairpin to bull protamine with full methylated cysteines that prevent the formation of any disulfide linkages (Figure 5.21). Focusing on the biologically relevant protamine/DNA charge ratio of N/P 1.0, we observe that the bull protamine hairpin/DNA complex exhibits 20% relative fluorescence. By preventing the formation of the inter and intramolecular disulfide bonds and subsequently the

formation of the hairpin, the binding ability of the protein decreases nearly 60%, despite the net cationic charge to remaining the same.

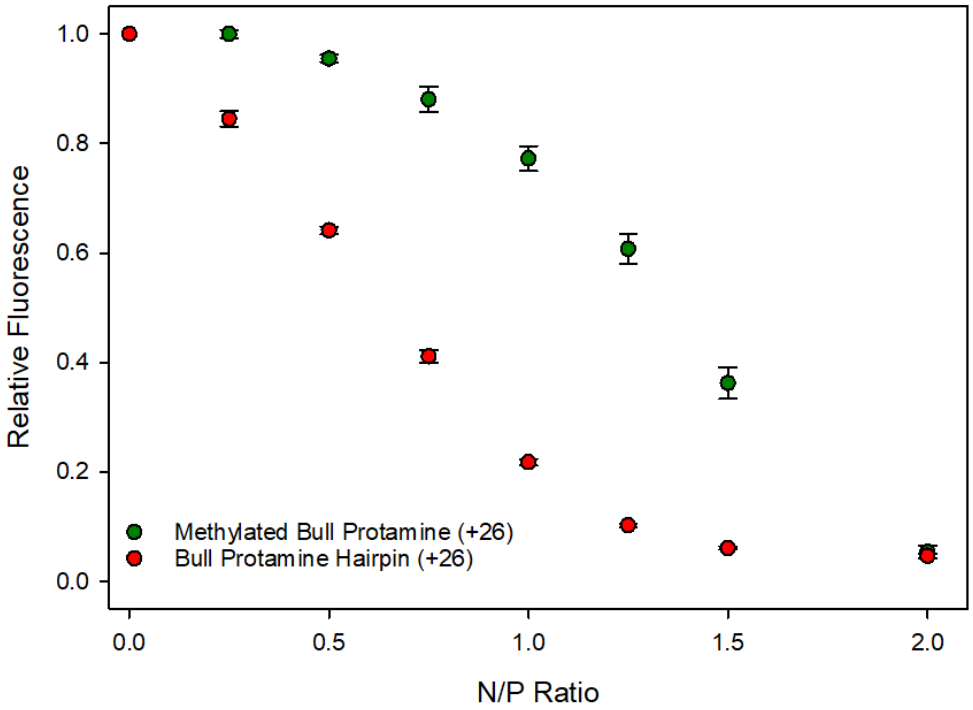

Figure 5.21 Preventing disulfide formation in bull protamine reduces bull protamine binding ability by upwards of 60% at the physiologically relevant N/P ratio of 1.0. Values are given as mean ± standard error (n = 3).

Next, we examined the effect of altering the protamine percent cationic charge on DNA binding ability of the protamine using the reactions described in Figure 5.11. By carboxylation of the seven cysteine residues of the bull protamine, we could synthesize an intrinsically disordered, polyampholytic protamine (26 arginines and 7 carboxylic acids) reducing the net cationic charge to 38%. As shown in Figure 5.22, protamine binding of DNA by carboxylated-protamine is nearly completely prevented despite the net +19 charge of the carboxylated protamine. Propylamination of the bull cysteines increases the percent cationic charge to 66%, the same as salmon protamine and both protamines exhibit similar binding curves.

Curiously, the addition of the carbamidomethyl group results in a similar binding curve as both the salmon protamine and the propylaminated bull protamine, suggesting that it has similar cationic charge as well. Typically, the amine on the carbamidomethyl group is deprotonated, resulting in it being an uncharged functional group. If this is the case, it should bind more similarly to the methylated protamine. However, it is clearly binding as if it has a similar cationic charge to the salmon protamine. One possible explanation for this observation lies in the unique characteristics of the amide group. Amide groups have a resonance structure, which results in delocalized charged between the oxygen of the carbonyl and the nitrogen. This results in a partial

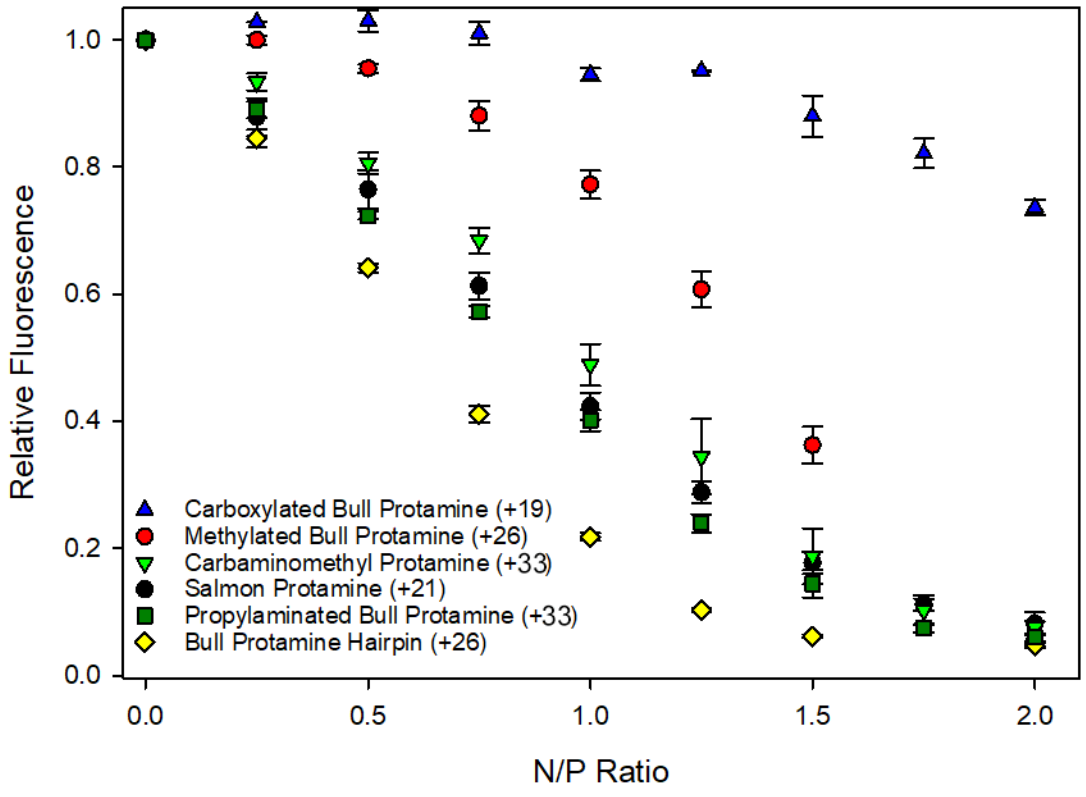

Figure 5.22: Altering protamine percent cationic charge changes its binding ability. Reduction of the percent cationic charge to 38% (carboxylated prot.) nearly completely eliminates protamine binding. By increasing the percent cationic charge to 66% results in a binding curve identical to that of salmon protamine (carbamidomethyl, propylaminated prot.) Values are given as mean ± standard error (n = 3).

positive charge on the amide nitrogen. (Figure 5.23) This resonance structure and resulting positive charge could be influencing the binding of the protamine with the carbamidomethyl addition resulting it to bind like salmon protamine. It should be noted that the binding ability of the carbamidomethyl protamine is approximately 10% worse than the 66% cationic charged protamines.

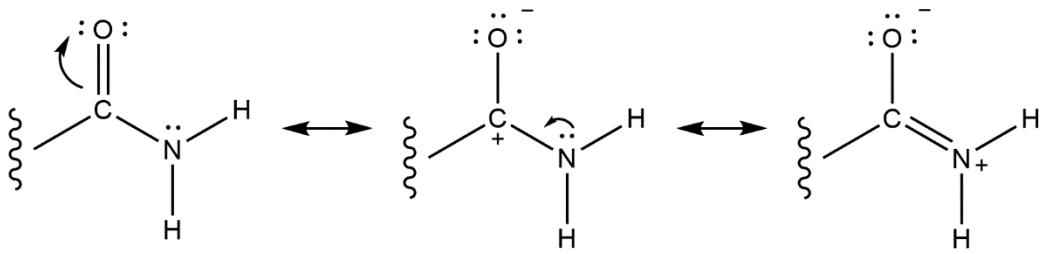

Figure 5.23: Amide resonance structures result in the formation of a partial positive charge on the amide nitrogen.

Section 5.3.5: Protamine P1 Sequence Alignment

Sequence alignments performed by Christian Powell (University of Kentucky Institute for Biomedical Informatics), show that within the sperm protamine P1 sequence sample set, 8 positions were determined to be highly conserved across 179 different eutherian mammal P1 sequences. A majority, >79.4%, of these positions contained cysteine residues; these conserved residues were found to be in position 48, 7, 47, 59, 17, 38, 29 and 6. Of these conserved positions, 5 were within 1 position of an intermolecular crosslinking region, specifically positions 7, 17, 47, 48, 59. One notable outlier for the sequence alignment is that in human protamine P1, the cysteine residue in position 17 is replaced with a tyrosine residue. A selected portion of the sequence alignment is shown in Figure 5.24; the complete sequence alignment can be found in Appendix A.

```
Etheria Protamine P1
                                10        20        30        40        50        60        70
                  5    39         6         8         7        21         0         4
HSP1_HUMAN        MARYRCCRSQ --SRSRYY-R ---Q-RQRSR -RRRRRSCQT RRRAMRCCRP R--YR---PR -CRRH-----
HSP1_BOVIN        MARYRCCLTH --SGSRCR-R ---RRRRRCR -RRRRRFGRR RRR-RVCCRR ---YT--VIR -CTRQ-----
HSP1_HORSE        MARYRCCRSQ --SQSRCR-R ---RRRRRCR -RRRRRSVRQ RR---VCCRR ---YT--VLR -CRRRR----
HSP1_MOUSE        MARYRCCRSK --SRSRCR-R ---R-RRRCR -RRRRRCCRR RRR--RCCRR RRSYT---IR -CKKY-----
HSP1_RAT          MARYRCCRSK --SRSRCR-R ---R-RRRCR -RRRRRCCRR RRR--RCCRR RRSYT---FR -CKRY-----
HSP1_ORCOR        MARNRC-RSP --SQSRCR-R ---P-RRRCR --RRIRCCRR QRR--VCCRR ---YT--TTR -CARQ-----
HSP1_PIG          MARYRCCRSH --SRSRCR-P ---R-RRRCR -RRRRRCCPR RRR-AVCCRR ---YT--VIR -CRRC-----
HSP1_GORGO        MARYRCCRSQ --SRSRCY-R ---Q-RQTSR -RRRRRSCQT QRRAMRCCRR R--NR---LR -RRKH-----
HSP1_SHEEP        MARYRCCLTH --SRSRCR-R ---RRRRRCR -RRRRRFGRR RRR-RVCCRR ---YT--VVR -CTRQ-----
HSP1_CAPHI        MARYRCCLTH --SRSRCR-R ---RRRRRCR -RRRRRFGRR RRR-RVCCRR ---YT--VVR -CTRQ-----
```

Figure 5.24: Protamine P1 sequence alignment shows that cysteine placement in mammalian P1 is highly conserved, suggesting that the protamine hairpin is present in species other than bull. Sequence alignment performed by Christian Powell (University of Kentucky Institute for Biomedical Informatics) Image adapted from [178]

Section 5.3.6: Effect of Disulfide Bond Formation on Bull Nuclei Stability

The bull protamine hairpin and intermolecular disulfide bonds confer substantial levels of stability to the sperm nuclei as compared to the sperm nuclei of species lacking these disulfide bonds. The effects of this added stability are exhibited in Figures 5.25 and 5.26. In Figure 5.25, the

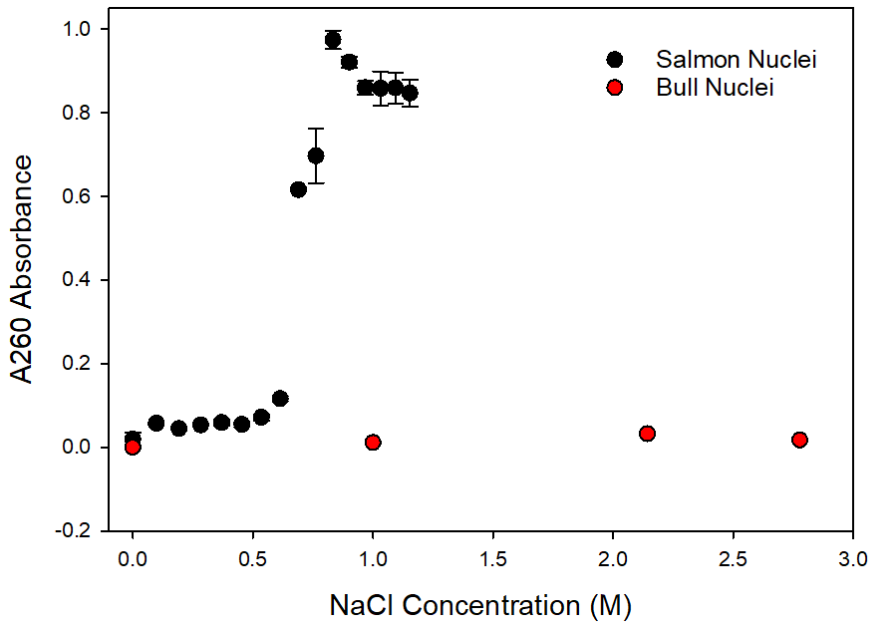

Figure 5.25: Titration of salt into whole sperm nuclei results in decondensation of salmon nuclei, bull nuclei are not affected.

effect of ionic content, in the form of excessive NaCl concentration, on nuclei stability is shown. Salmon nuclei in the presence of 600 mM NaCl rapidly dissociate, resulting in a large increase in A_{260} (DNA) absorbance. Bull nuclei subjected to the same conditions are stable in NaCl in concentrations as high as 4M. (absorbance data from 3M to 4M NaCl not shown).

The rigidity afforded by the disulfide bond network can be better observed by challenging bull protamine hairpin-DNA condensates to a decondensing agent, in this case, in the form of dextran sulfate, a large anionic polymer. In Figure 5.26, bull protamine-DNA condensates are created at N/P: 2.0, with an absolute protamine content of 158 ng bull protamine per condensate. After the addition of 105 μg of dextran sulfate, 665X the amount of protamine, the protamine-

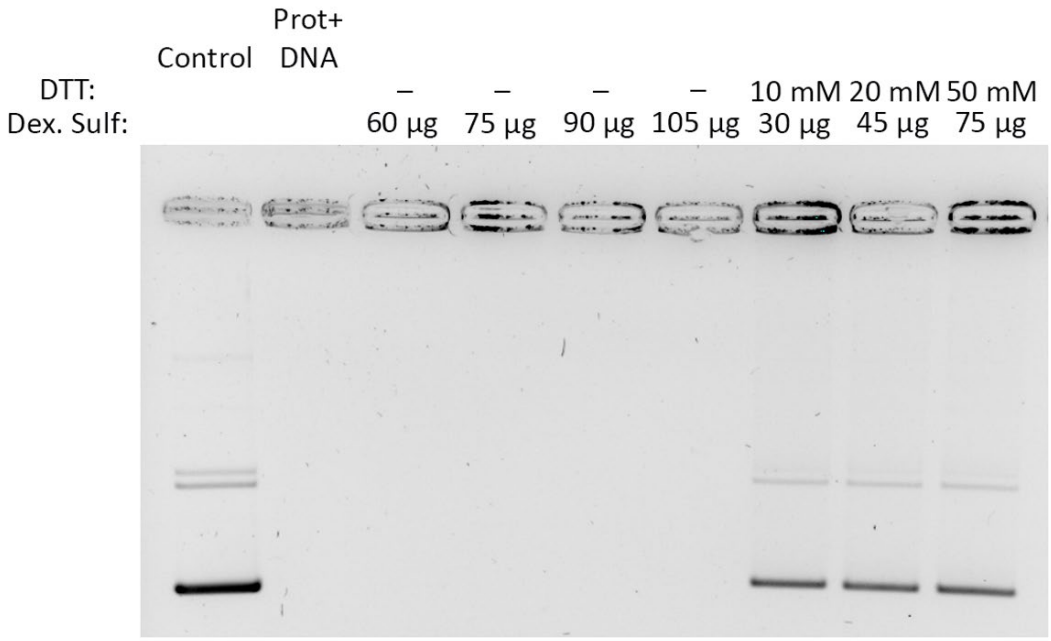

Figure 5.26: Despite a large excess of a competitor anion, bull protamine/DNA condensates remain stable. DTT addition causes immediate breakdown of the condensate.

DNA condensate remains intact, unaffected by the anionic polymer consistent with the reforming of the inter-protamine disulfide bonds resulting in an insoluble crosslink network. Small amounts of DTT added to the condensate, in addition to the dextran sulfate, results in an immediate

breakdown of the condensate, and the subsequent release of the DNA similar to dissociation by salmon protamine-DNA condensates, discussed in detail in chapter 4. The bull protamine hairpin is only slightly more cationic than salmon protamine, such a large excess of dextran sulfate should be to dissociate a bull protamine condensate, however, the formation of the intermolecular DNA disulfide network instills massive rigidity to the chromatin making such an anionic challenge ineffective.

Section 5.3.7: Observation of Sperm Nuclear Vacuoles in DTT Incubated Nuclei

DTT induced decondensation of bull sperm chromatin results in the formation of small circular inclusion bodies. These inclusion bodies are similar in both structure and appearance to sperm nuclear vacuoles. The inclusion bodies appear as regions of brighter fluorescence within the sperm chromatin. Isolated bull nuclei consist only of sperm DNA and the nuclear envelope (Figure 5.5). Since propidium iodide is a DNA selective stain, the increase in fluorescence must originate within the sperm chromatin and not the nuclear envelope. By comparison of the size and shape of the DTT induced inclusion bodies to published photos of confirmed sperm nuclear vacuoles, shown in Figure 5.27, the resemblance between the DTT induced inclusions and the confirmed sperm nuclear vacuoles is quite clear. This strongly suggests that the inclusion bodies formed by DTT induced decondensation are indeed sperm nuclear vacuoles.

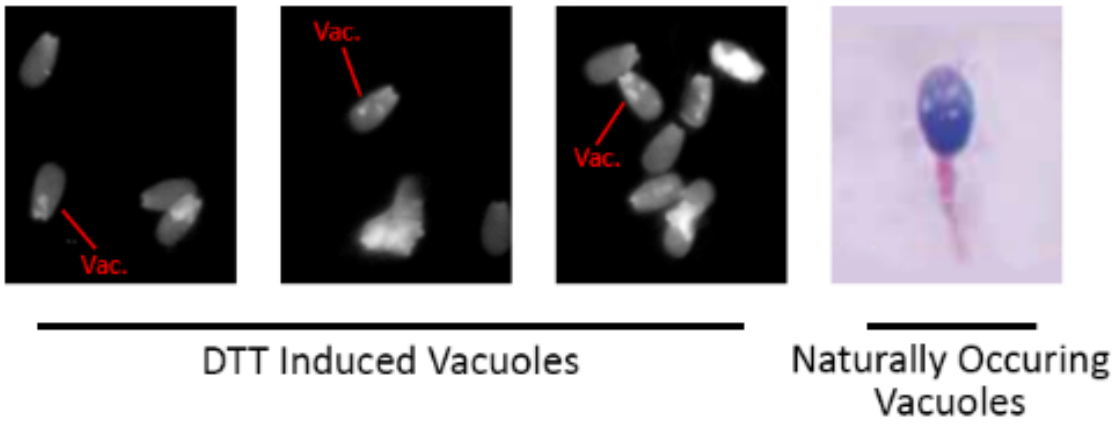

Figure 5.27: Comparison of DTT induced vacuole to published images of sperm nuclear vacuoles. Structures in both published confirmed vacuoles and DTT induced vacuoles are similar in appearance. Published image obtained from [81]

Section 5.3.8: Evidence of Sperm Nuclear Vacuoles in CMA3 Stained Nuclei

Evidence of sperm nuclear vacuoles can be seen in bull sperm nuclei which have been stained with CMA3, a stained typically used to determine levels of protamination within mature sperm nuclei. CMA3 is a fluorescent molecule which competes with protamine to bind DNA. Once

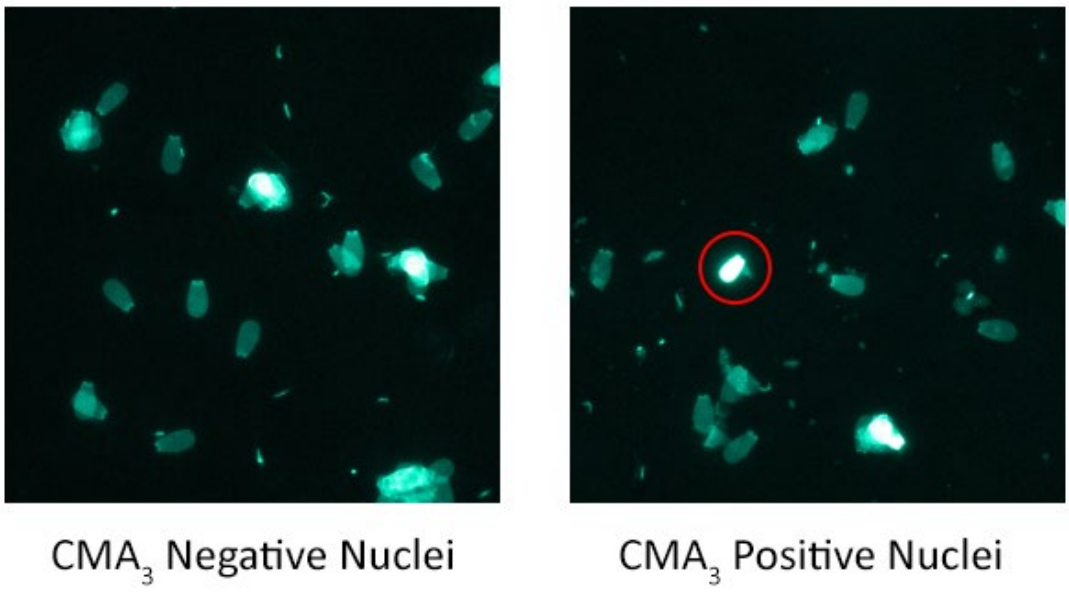

Figure 5.28: CMA3 stained isolated bull nuclei. CMA3 positive nuclei is indicated with the red circle. CMA3 positivity indicates underprotamination within the nuclei.

bound, the level of fluorescence exhibited by the CMA3 greatly increases. CMA3 positive nuclei appear much brighter than their CMA3 negative counterparts. Low levels of protamine within sperm nuclei result in greater amounts of poorly condensed DNA, this leads to increased CMA3 binding and fluorescence.

Both CMA3 positive and CMA3 negative nuclei are shown in Figure 5.28. Poorly protaminated nuclei afford better binding by the CMA3 and result in greater levels of fluorescence. As expected, nearly all the mature nuclei are fully protaminated and bind the CMA3 quite poorly. CMA3 positive nuclei are quite sporadic, implying that a vast majority of mature sperm nuclei are highly compacted and likely fully protaminated.

Figure 5.29 shows a CMA3 positive nuclei that has been enlarged for better observation of the sperm chromatin. Within the nuclei, we see structures within the chromatin that are similar in size and shape to the inclusion bodies seen within bull sperm nuclei in the process of DTT mediated decondensation. These structures are also similar in appearance to the published

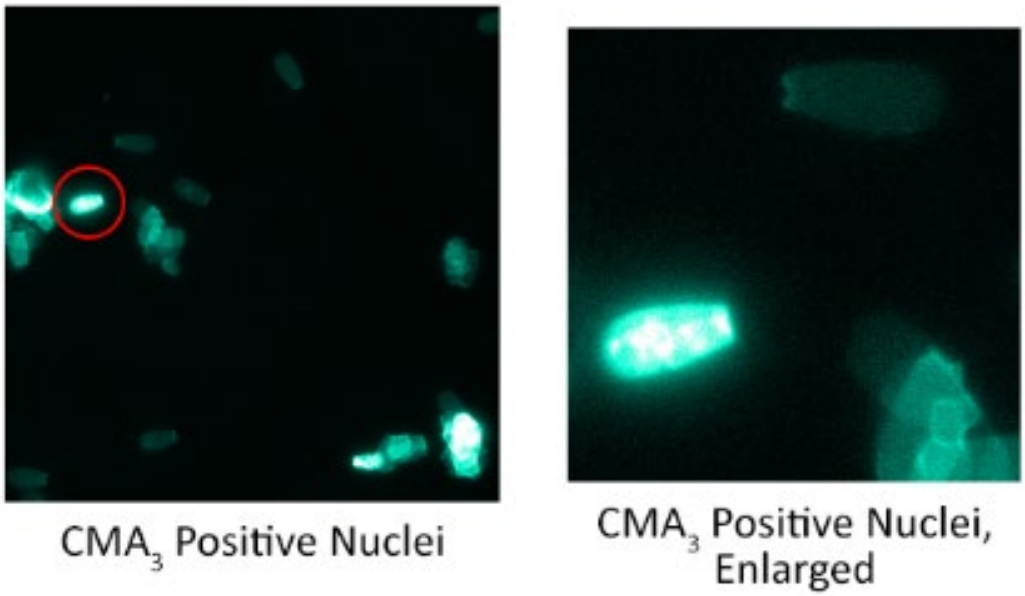

Figure 5.29: CMA3 positive nuclei, enlarged for detail. Notice the structures similar to nuclear vacuoles present in the CMA3 positive nuclei.

pictures of confirmed sperm nuclear vacuoles. This again shows that poorly condensed DNA results in the formation of chromatin inclusions resembling sperm nuclear vacuoles.

Section 5.3.9: Observation and Analysis of Horse Sperm Epidydimal Samples

It is known that sperm maturation concludes as the sperm travel from the testis through the 3 main sections of the epididymis, the caput (head), the corpus (body) and the corpus (tail). [182] One major hallmark of this maturation is the formation of disulfide bonds between the protamines within the sperm chromatin. [35] Here, we sought to isolate immature sperm cells from the three main sections of the epididymis and isolate their respective nuclei. After isolating the sperm nuclei, we stained the nuclei to determine the integrity of the nuclear membrane as well as the DNA content, we then determined the DNA interaxial spacing by SAXS measurements within the sperm chromatin.

Section 5.3.9.1: Microscope Studies of Horse Epididymal Sperm

Figure 5.30 – 5.32 shows the results of sperm nuclei isolation from sperm cells obtained from the caput, corpus, and cauda sections of the horse epididymis. These nuclei are expected to be immature and exist in varying stages of maturation. In Figures 5.30 – 5.32, we see that despite the nuclei being immature, they are still quite well formed and possess the sperm nuclear membrane present in the mature ejaculated samples previously shown in Figure 5.6. The chromatin within the nuclei is quite compact and stains well. These samples were obtained from epididymal tissue suspensions as opposed to ejaculated semen, the source of the sperm used in the majority of this study. Because of this, the samples are not as ‘clean’ as the other sperm samples used in this study. Therefore, the resulting pictures show a greater degree of aberrant staining and cellular debris.

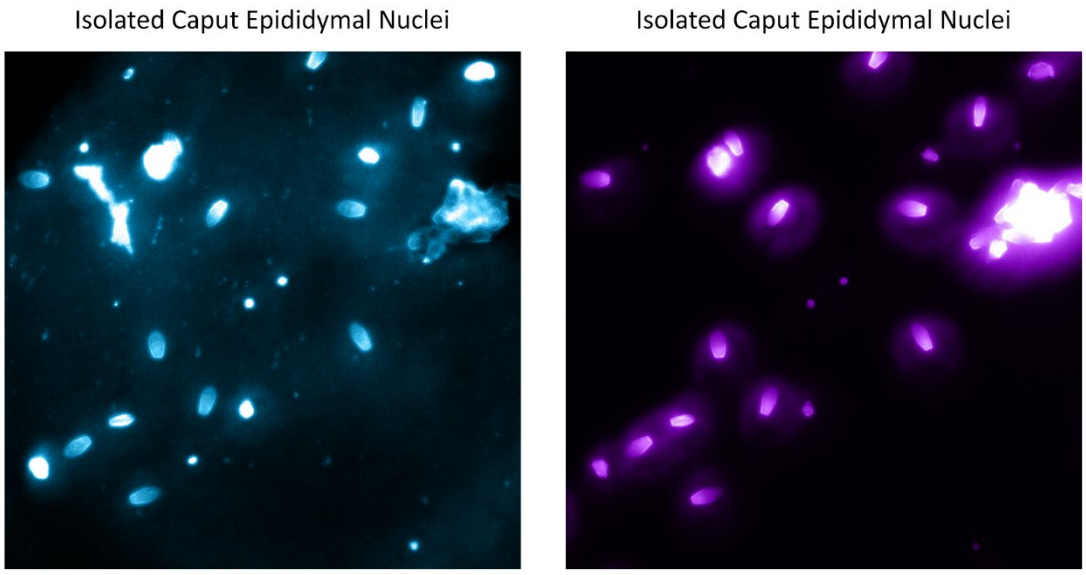

Figure 5.30: Caput epididymal nuclei, stained for membrane integrity (DiO) and DNA content. (Hoechst 33342)

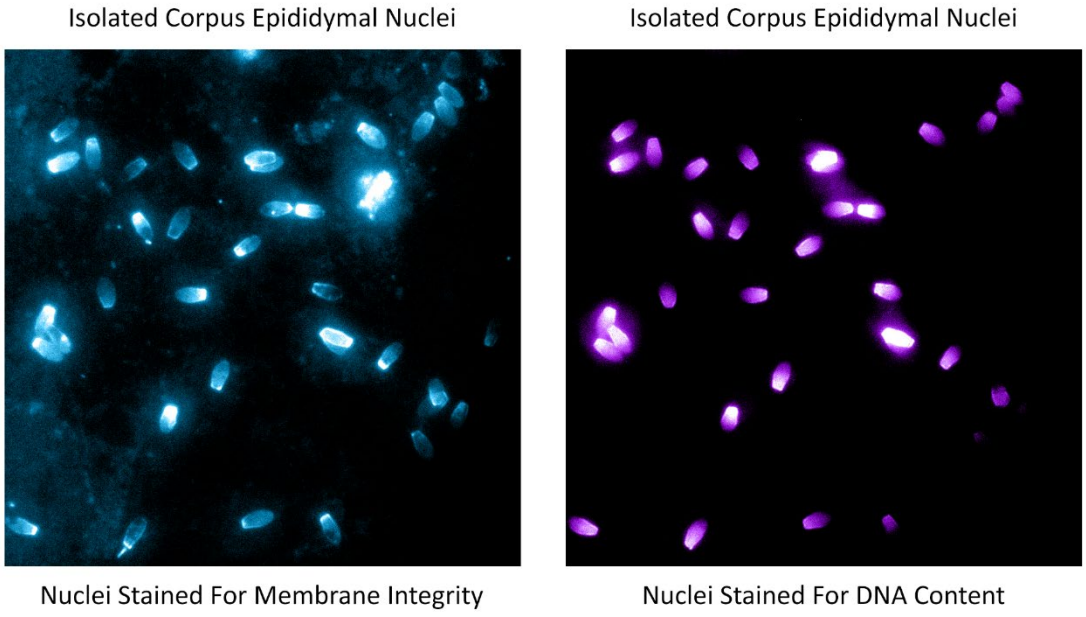

Figure 5.31: Corpus epididymal nuclei, stained for membrane integrity (DiO) and DNA content. (Hoechst 33342)

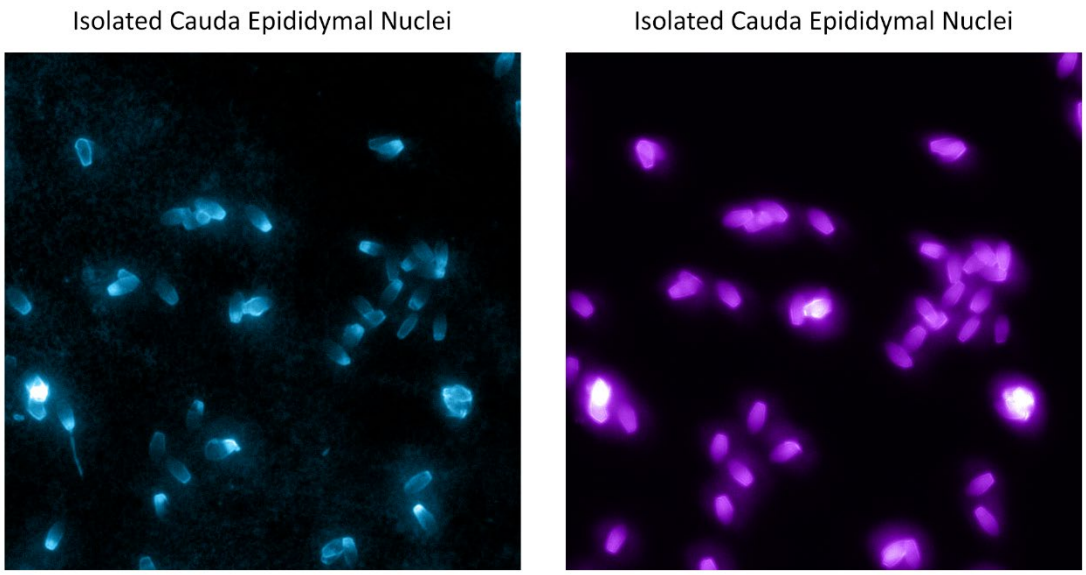

Figure 5.32: Cauda epididymal nuclei, stained for membrane integrity (DiO) and DNA content (Hoechst 33342).

Section 5.3.9.2: SAXS Analysis of Horse Epididymal Nuclei

By performing SAX analysis on nuclei obtained from the three different sections of the epididymis, the effect of sperm maturation on interaxial spacing within the sperm chromatin can be seen. The results of the SAXS analysis and resulting Bragg and interaxial spacings are shown in Figure 5.32 and Table 5.4.

Table 5.4: Bragg and Interhelical spacing of sperm nuclei across the epididymis

Epididymal Section	**D-Bragg (Å) ± 0.15 Å**	**D-Int (Å) ± 0.15 Å**
Caput	26.7	30.8
Corpus	26.3	30.4
Cauda	26.1	30.1

.

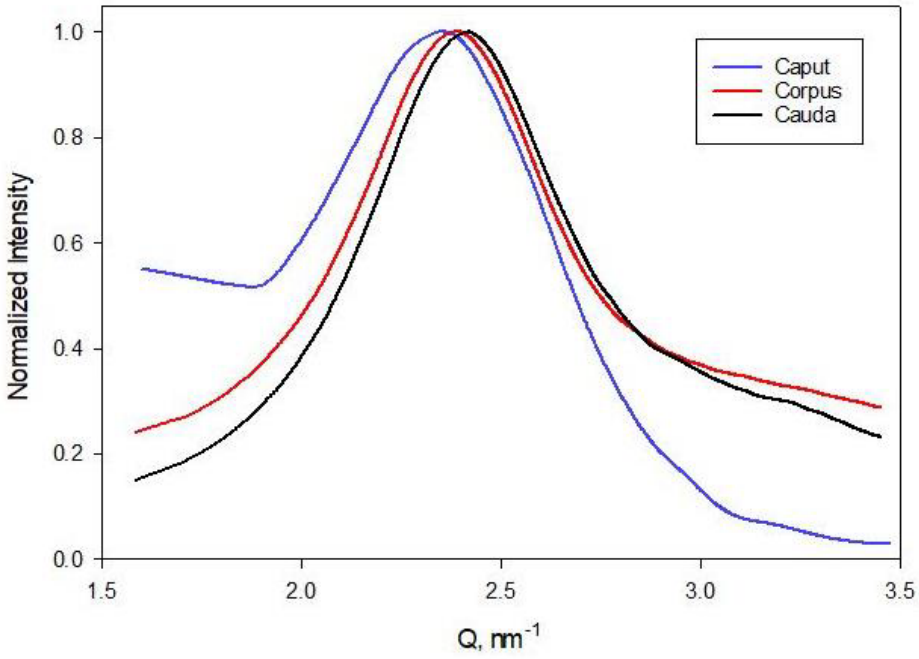

Figure 5.33: SAXS analysis of epididymal samples show a progressive decrease in interaxial spacing as sperm travel through the epididymis. Showing that the nuclei are 'tightening up' during epididymal transit.

In Figure 5.33 we see a clear shift in the scattering vector, Q, as the sperm progress through the epididymis. This shift in scattering peak correlates to a decrease in interaxial spacing between the DNA helixes within the sperm chromatin, showing that as sperm traverse the epididymis, the sperm chromatin gets packed tighter.

Section 5.4: Discussion

Section 5.4.1 Effect of Percent Cationic Charge on DNA Condensation

Initial inquiries into the amino acid composition of sperm nuclear proteins, now known as protamines, showed that mammalian protamines contained a significant fraction of cysteines not present in piscine protamines. [183, 184] It has since been shown experimentally that in bull sperm protamine, these cysteines function in disulfide bonding and result in the formation of a

hairpin shape, as well as an intermolecular disulfide bond network. Our data shows that this hairpin structure is critical for effective DNA condensation and that failure for this structure to form results in a complete decondensation of the sperm chromatin and a loss of integrity within the sperm nucleus. This trend is apparent both in actual bull sperm nuclei as well as reconstituted bull protamine-DNA samples. Based on prior studies with mixed charge peptides, we have proposed that the hairpin is required for condensation as it enables a higher local cationic charge to be formed in the binding domain region which interacts with DNA phosphates.

Our data also highlights the importance of the percent cationic charge as opposed to the net cationic charge of a protein. By modifying the percent cationic charge of actual bull protamine, we can substantially affect the binding ability of the protamine. This effect most obvious in the studies comparing bull protamine with and without the hairpin motif. By preventing the formation of the hairpin, we reduce the binding ability of the protein by upwards of 60% in reconstituted bull protamine-DNA samples. Disulfide bond reduction in actual nuclei results in a complete loss of chromatin integrity. The prior hypothesized percent cationic charge needed to allow for complete DNA condensation is ~50%; our data supports this value. [86] Methylated bull protamine has a percent cationic charge of 52%, just over the needed value of 50%, explaining why we are able to see small amounts of DNA binding in the reconstituted methylated protamine-DNA samples. By further reducing the percent cationic charge to 38% through carboxylation, we are able to completely prevent DNA condensation by bull protamine.

This leads to the question as to why bull and other mammals expend the metabolic energy to create this disulfide bond hairpin and subsequent disulfide network, whereas other species, such as fish, lack this secondary structure. Multiple possibilities exist for this added complexity, first being that the inter and intramolecular disulfide bonds instill rigidity to the sperm chromatin and protect the DNA from damage. [18] Sperm live in an extremely oxidatively damaging

environment; numerous radical sources are present in close proximity to the sperm DNA. [185] Radical sources include the numerous mitochondria in the sperm midsection and the H_2O_2 needed for effective capacitation, a normal part of sperm physiology. [186] These radical sources can easily damage the paternal genome. As all DNA repair mechanisms are turned off in the mature sperm nucleus, preventing damage to the paternal genome is particularly critical to ensure both reproductive success and health of the offspring. [185] Greater incidences of compromised damage within spermatic DNA has been shown to be linked to decreased fertility levels and greater incidences of spontaneous abortion of the fertilized embryo. [187] Compromised spermatic DNA is suspected to correlate to a greater incidence of genetic disease in a mature offspring. [188] By having a rigid disulfide network, access of radicals to the DNA can be hindered, allowing for a greater likelihood for the genetic material remaining intact.[189]

The effect that the protamine hairpin and subsequent disulfide network has on the rigidity of the sperm chromatin is shown in Figure 5.25-5.26. Both bull sperm nuclei and bull protamine-DNA condensates are completely resistant to decondensation by both excessive ionic content and the addition of a competitor anion. Samples containing salmon protamine are easily dissociated by both competitor anions and excess salt. Physiological salt concentrations are 150 mM, salmon sperm nuclei complete dissociate at approximately 600 mM, clearly showing how important it is for biological systems to regulate their ionic content. Massive amounts of competitor anion, some 665x the amount when compared to protamine, which will easily break apart condensates made of salmon protamine are completely ineffective in dissociating condensates consisting of bull protamine. This is again showing the effect that interstrand disulfide bonds have in conferring strength to the DNA-protamine polyplex.

By requiring the protamine hairpin for DNA condensation, greater levels of control are afforded to the organism during chromatin remodeling. This can ensure correct compaction of

the paternal genome and correct formation of the intermolecular disulfide bonds. During chromatin remodeling, it is possible that disulfide bonds could form between neighboring protamine molecules prior to complete binding of the protamine to the sperm DNA. (misformed intermolecular disulfide bonds) This would result in a greater level of disorder within the sperm nucleus, rending the nucleus more susceptible to damage or other fertility issues. By requiring the formation of the hairpin, the entire chromatin remodeling process can be essentially slowed down, as no binding of protamine to the DNA will occur until the hairpin is completely formed. The hairpin formation essentially ensures complete protamine binding to the DNA before the formation of inter-protamine bonds. Mis-formed disulfide bonds between protamine molecules will not condense DNA without the hairpin and could either be reformed correctly via a cellular process, or removed from the sperm nucleus in its entirety. Sperm nuclei in bull exist in a sterically strained environment, so a greater level of control would be needed to form this strained network. [29] Eutherian sperm chromatin retains this cysteine fraction as the intermolecular disulfides confer substantial stability to the sperm nucleus. The protamine hairpin has only been experimentally proven in bull; however, our extensive multiple sequence analysis performed in collaboration with the lab of Dr. Hunter Moseley (UK -Dept of BioInformatics) shows near perfect alignment of cysteine residues in the P1 protamine across 179 different species. This strongly suggests that the protamine hairpin, as well as the intermolecular disulfide network, is universal among eutherian mammals. This cysteine alignment is present in the protamine P1 sequences of species who have two forms of protamine, P1, and P2. This includes mice, horses as well as humans. [138] Human protamine P1 is unique in that the cysteine on position 17 has been substituted for a tyrosine residue, implying that a tyrosine-cysteine bond is needed to create the hairpin. Such a bond is known as a tyrosine-cysteine crosslink and is a unique copper catalyzed

bond. (Figure 5.34) [190, 191] Such a substitution could be evidence of a greater level of cellular regulation present in human sperm chromatin remodeling.

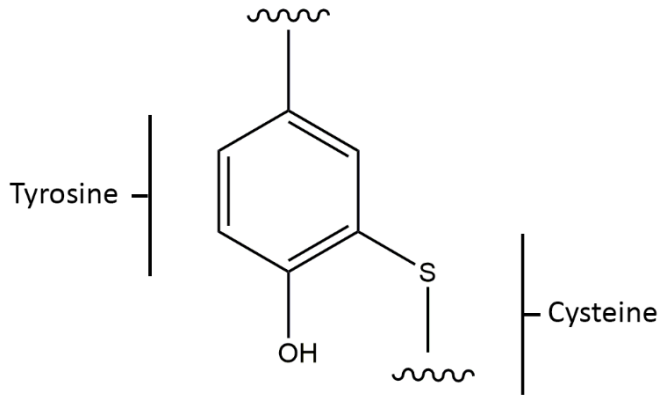

Figure 5.34: Tyrosine-Cysteine crosslinks are potentially present in human protamine P1.

Section 5.4.2: Appearance of Sperm Nuclear Vacuoles Within DTT Treated Sperm Nuclei

The appearance of inclusion bodies within the sperm nuclei after DTT incubation resembling sperm nuclear vacuoles is quite significant. As previously discussed, the exact nature and etiology of sperm nuclear vacuoles is currently unclear. Our data suggests that vacuoles are the product of poorly formed disulfide bonds within the sperm chromatin. The relationship between DTT incubation and sperm vacuole formation was first reported by Bedford et al in 1973, here, the authors incubated intact sperm with DTT and sodium dodecyl sulfate and saw the formation of vacuole-like structures. [192] Our data shows that vacuole structures can be formed solely with incubation of sperm nuclei with DTT. DTT only breaks disulfide bonds and does not significantly damage DNA, therefore the vacuoles must be the effect of disulfide bond reduction within the sperm nuclei. One possible explanation for the etiology of sperm nuclear vacuoles is that misformed disulfide bonds within the sperm nuclei cause small points of DNA decondensation This non-condensed DNA exists in a different packaging state, is more susceptible

to damage than its condensed counterpart. This explains the two main hypotheses concerning sperm nuclear vacuoles. The vacuoles are the product of poor sperm chromatin packaging, this poorly packaged sperm is more susceptible to damage and thus shows greater levels of sperm DNA fragmentation. Sperm with greater incidences of DNA damage or poor chromatin integrity will have a decreased fertility potential, a possible explanation for the link between sperm nuclear vacuoles and infertility. The detection of vacuole-like structures in CMA3 stained bull nuclei strengthens the argument that vacuoles are the result of poorly formed disulfide bonds. Since CMA3 is specific for poorly protaminated or condensed DNA, the fact that CMA3 positive nuclei would show vacuole-like structures suggests that poorly condensed, CMA3 positive, nuclei contain poorly formed disulfide bonds.

Section 5.4.3 SAXS Analysis on Horse Epidydimal Samples

Formation of disulfide bonds within sperm nuclei is thought to both protect the condensed DNA from damage and add stability and structure to the sperm chromatin. Disulfide bond formation occurs as sperm travel through the epididymis, during this transit the DNA within the sperm nuclei is transcriptionally inactive and all DNA repair mechanisms are turned off. [182] Therefore, all DNA damage sustained to the DNA will remain until fertilization occurs. Forming these disulfide bonds, the distance between the helices decreases, potentially limiting access of any damaging agents to the spermatic DNA, thereby protecting the paternal genome.

Section 5.5 Conclusions and Future Work

We have shown in a protamine model that the percent cationic charge is more critical than net cationic charge when determining the condensing ability of protein. Bull protamine creates a unique hairpin secondary structure and effectively increases the percent cationic charge

of the DNA binding domain on the protamine. With the formation of this hairpin, the DNA binding domain increases its percent cationic charge above 50% allowing it to effectively condense DNA. This hairpin shape in protamine appears to be universal amongst eutherian mammals. Formation of intermolecular disulfide bonds results in the formation of a rigid protamine network which allows for bull chromatin to be resistant to decondensation by excessive ionic content and an anionic challenge. This rigid network potentially shields the paternal genome from aberrations. Misformed disulfide bonds within the bull sperm nuclei result in the formation of sperm nuclear vacuoles. These vacuoles are visible evidence of poor sperm DNA condensation and likely result in a greater likelihood of the sperm DNA to be susceptible to damage.

Future work into this project will entail performing X-Ray analysis into protamine-DNA condensates created using both the protamine hairpin and methylated bull protamine. This will allow for a more accurate description of the packaging state of sperm nuclei deficient in disulfide bond formation. Subjecting bull protamine-DNA in varying packaging states to damaging agents will allow for a better understanding of how disulfide bond formation within bull chromatin protects the paternal genome from damage. More advanced microscopy techniques such as differential interference contrast microscopy will be used to better characterize and determine the etiology of the sperm nuclear vacuole structures. Direct labeling techniques of the free thiols within sperm epididymal samples will be performed to discern the effect of disulfide bond formation on DNA interaxial spacing.

Summary and Future Directions

Summary

In this study, we have strived to describe the effect that cation makeup has on its ability to condense DNA. We have compared the DNA condensing ability of long cations and short cations of varying final packaging densities by UV-Vis and ethidium bromide exclusion assays. We have shown that long cations are better at condensing DNA than short cations, regardless of cation makeup. DNA condensed by polycations is afforded protection from damaging agents, we have shown that longer cations instill greater amounts of protection than their shorter counterparts. Packing density also plays a role in the susceptibility of condensed DNA to damage, where greater packing densities result in greater levels of DNA protection.

Low levels of protamine, underprotamination, has been associated with greater levels of DNA damage within sperm nuclei. We have described different levels of underprotamination in terms of N/P ratio. By creating DNA condensates in vitro at these differing levels of underprotamination and subjecting them to AAPH damage, we were able to describe the prevalence of DNA damage present in condensates at differing levels underprotamination. Underprotaminated condensates can be further condensed by use of small cationic peptides. These cationic peptides increase the packing density of the underprotaminated condensate.

Disulfide bond formation is critical within eutherian sperm nuclei. We have shown that the disulfide bond formation within bull nuclei serves to not only create a DNA binding domain but in fact, increases the effective percent cationic charge of the protamine DNA binding domain. This binding domain is the portion of the protamine which interacts with DNA, and the percent cationic charge of this binding domain is critical. Through alterations in the percent cationic charge of bull protamine, we have shown that a percent cationic charge of 50% is necessary for a protein to effectively condense DNA. These disulfide bonds instill a great amount of stability and rigidity

to bull sperm chromatin. Through these disulfide bonds, the sperm chromatin is resistant to dissociation via excessive ionic content as well as competitor anions. The cysteine residues within eutherian mammalian protamine are highly conserved, suggesting that the bull protamine hairpin is universal.

Disulfide bond reduction in bull sperm chromatin results in the appearance of structures similar in appearance to sperm nuclear vacuoles. Our data suggests that these vacuoles are the result of poor disulfide bond formation, which results in small points of decondensed sperm DNA.

Future Directions

Future directions into the topics presented in this study will include a more detailed analysis of sperm maturation as the immature sperm travel through the epididymis. Correlation of sperm inter and intramolecular disulfide bond formation to DNA interaxial spacing within maturing sperm in the epididymis will be determined. Determination of phosphorylation levels of protamine during sperm maturation will allow for a complete description of the maturation process of the sperm nucleus post meiosis.

The discussion of protamine in this study focused nearly in its entirety on protamine P1 found in either bull or salmon sperm nuclei. Future studies will delve into describing both the structure and condensation properties of the protamine present in species which contain two forms of protamine, P1, and P2. This includes humans, horses, and mice. The structure of sperm chromatin containing P1 and P2 will most likely be more complicated than bull sperm chromatin. The structure of protamine P2 has yet to be conclusively proven, through the determination of the protamine P2 structure, insight into the relationship between protamine P1 and P2 and the resulting chromatin structure will be ascertained.

Mature spermatozoa have been shown to contain a significant fraction of zinc. The exact function and etiology behind this zinc fraction has yet to be conclusively proven, but possibly plays a role in the formation of a zinc finger motif within protamine P2. The nature and function of zinc within sperm chromatin and its relation to sperm processes will help elucidate the relationship between zinc and protamine P2.

Appendix: Complete Protamine P1 Sequence Alignment.

Below is the complete sequence alignment for all protamine P1 sequences discussed in Section 5.3.5 in this study. All sequence Alignments were performed by Christian Powell of the University of Kentucky Institute for Biomedical Informatics. [178]

```
Rank                 82          5           7          6          31          4
A0A2K5CXY9_AOTNA MARHRCCRSR SQSRSRR--D R---QKRRCR -TPRRRSCRR RTA-RRCGRR R---YKPRCR RN-------- --------
Q64412_CAVPO     MARYRCCRSP --SRSRC--R R---RRRRFY -RRRRRCHRR RRRLYQTSRS S---YHL--- ---------- --------
HSP1_RHIFE       MARYSCCRSH --SRSRS--R R---RRQRCR -RRRRRSCGR RRR--ACYRR YTVRYRRRRR RR-------- --------
HSP1_HIPCO       MARYRCCRSH --SRSRC--R R---RRRRSR -RRRRRSCGR RRR--AGYRR Y-T---VRYR RRR------- --------
C8C436_PLAMN     MARNRCCRSQ --SRSRC--R R---PKRGCR -SRRRRCYQR RRR--VCCRR Y---TTIRCA RQ-------- --------
A8IYB4_PHYCD     MARNRCCRSQ --SRSRC--R R---PRRRCR -SPRRRRYQR RRR--VCCRR Y---TVTRCA RQ-------- --------
C8C438_KOGBR     MARNRCCRSQ --SRGRC--R R---PRRRYR -SPRRRRYQR RRR--VCCRR S---TTMRCA SQ-------- --------
C8C437_KOGSI     MARNRCCRSQ --SRGRC--R R---PRRRCR -SPKRRRYQR RRR--VCCRR S---ATMRCA SQ-------- --------
C8C439_EUBAS     MARNRCCRSQ --SRSRR--R R---PRQRCR -SQRRRCCRR RRR--VCCRR Y---TTVRCA RR-------- --------
B1ACJ8_EUBJA     MARNRCCRSQ --SRSRR--R R---PRQRCR -SQRRRCCRR RRR--VCCRR Y---TTVRCA RR-------- --------
B1ACJ7_BALMY     MARNRCCRSQ --SRSRR--R R---PRQRCR -SQRRRCCRR RRR--VCCRR Y---TTVRCA RR-------- --------
C8C440_EUBGL     MARNRCCRSQ --SRSRR--R R---PRQRCR -SQRRRCCRR RRR--VCCRR Y---TTVRCA RR-------- --------
B1ACJ6_CAPMR     MARNRCCRSQ --SRSRR--R R---PRQRCR -SQRRRCCRR RRR--VCCRR Y---TTVRCA RQ-------- --------
B1ACI8_MEGNO     MARNSCCRSP --SRSRR--R R---PRQRRR -SQRRRCCQR RRR--VCCRR Y---TTVRCA RQ-------- --------
B1ACI9_BALPH     MARNSCCRSP --SRSRR--R R---PRQRRR -SQRRRCCQR RRR--VCCRR Y---TTVRCA RQ-------- --------
B1ACJ0_BALMU     MARNTCCRSP --SRSRR--R R---PRQRCR -SQRRRCCRR RRR--VCCRR Y---TTVRCA RQ-------- --------
B1ACJ5_ESCRO     MARNSCCRSP --SRSRR--R R---PRQRCR -SQRRRCCRR RRR--VCCRR Y---TTVRCA RQ-------- --------
B1ACJ2_BALED     MARNSCCRSP --SRSRR--R R---PRQRCR -SQRRRCCRR RRR--VCCRR Y---TTVRCA RQ-------- --------
B1ACJ1_BALBO     MARNSCCRSP --SRSRR--R R---PRQRCR -SQRRRCCRR RRR--VCCRR Y---TTVRCA RQ-------- --------
B1ACJ4_BALAC     MARNSCCRSP --SRSRR--R R---PRQRCR -SQRRRCCRR RRR--VCCRR Y---TTVRCA GQ-------- --------
B1ACJ3_BALBN     MARNSCCRSP --SRSRR--R R---PRQRCR -SQRRRCCRR RRR--VCCRR Y---TTVRCA GQ-------- --------
A8IYB7_ZIPCA     MARNRCCRGQ --SQSRR--R R---PRRRYR -SRRRQCCQK RRR--VCCRR Y---TATRCA RQ-------- --------
C8C435_BERBI     MARNRCCRSQ --SQSRR--R R---PRRRNR -SRRRQCCQR RRR--VCCRR Y---TAIRCA RQ-------- --------
C8C432_MESGR     MARNTCCRSQ --SQSRR--R R---PRRRYR -SRRKQCCQK RRR--VCCRR Y---TAIRCA RQ-------- --------
C8C434_TASSH     MARNRCCRSQ --SQSRR--R R---PRRRYR -SRRRQCCQK RRR--VCCRR Y---TAIRCA RQ-------- --------
C8C433_MESBI     MARNRCCRSQ --SQSRR--R R---PRRRYR -SRRRQCCQK RRR--VCCRR Y---TAIRCA RQ-------- --------
C8C431_MESPE     MARNRCCRSQ --SQSRR--R R---PRRRYR -SRRKQCCQK RRR--VCCRR Y---TAIRCA RQ-------- --------
B4YVM7_ORCOR     MARNR-CRSP --SQSRC--R R---PRRRCR --RRIRCCRR QRR--VCCRR Y---TTTRCA RQ-------- --------
HSP1_ORCOR       MARNR-CRSP --SQSRC--R R---PRRRCR --RRIRCCRR QRR--VCCRR Y---TTTRCA RQ-------- --------
C8C426_GRAGR     MARNR-CRSP --SQSRC--R R---PRRRYR --RRRQCCRR RRR--VCCRR Y---TTTRCA RQ-------- --------
B4YVM8_PSECS     MARNR-CRSP --SQSRC--R R---PRRRYR --RRRQCCRR RRR--VCCRR Y---TTTRCA RQ-------- --------
C8C425_GLOMA     MARNR-CRSP --SQSRC--R R---PRRRYR --RRRQCCRR RRR--VCCRR Y---TTTRCA RQ-------- --------
C8C424_FERAT     MARNR-CRSP --SQSRC--R R---PRRRYR --RRRRCCRR RRR--VCCRR Y---TTTRCA RQ-------- --------
F5CBD0_PENEL     MARNR-CRSP --SQSRC--R R---PRRRYR --RRRRCCRR RRR--VCCRR Y---TTTRCA RQ-------- --------
C8C423_LAGAC     MARNR-CRSP --SQSRC--R R---PRRRCL --RRRRCCRR RRR--VCCRR Y---TTTRCA R--------- --------
F5CBC9_CEPCM     MARNR-CRSP --SQSRC--R R---PRRRCR --RRRRCCRR RRR--VCCRR Y---ATTRCA RQ-------- --------
F5CBC8_LAGAL     MARNR-CRSP --SQSRC--R R---PRRRCR --RRRRCCRR RRR--VCCRR Y---TTTRCA SQ-------- --------
C8C421_TURTR     MARNR-CRSP --SQSRC--R R---PRRRCR --RRRLCCRR RRR--VCCRR Y---TTTRCA RQ-------- --------
F5CBC0_TURAD     MARNR-CRSP --SQSRC--R R---PRRRCR --RRRLCCRR RRR--VCCRR Y---TTTRCA RQ-------- --------
B4YVN1_STECO     MARNR-CRSP --SQSRC--R R---PRRRCR --RRRLCCRR RRR--VCCRR Y---TTTRCA RQ-------- --------
F5CBD1_9CETA     MARNR-CRSP --SQSRC--R R---PRRRCR --RRRRCCRR RRR--VCCRR Y---TTTRCA RQ-------- --------
F5CBC1_STELO     MARNR-CRSP --SQSRC--R R---PRRRCR --RRRRCCRR RRR--VCCRR Y---TTTRCA R--------- --------
F5CBB9_DELCA     MARNR-CRSP --SQSRC--R R---PRRRCR --RRRRCCRR RRR--VCCRR Y---TTTRCA R--------- --------
F5CBC3_STEAT     MARNR-CRSP --SQSRC--R R---PRRRCR --RRRRCCRR RRR--VCCRR Y---TTTRCA R--------- --------
F5CBC4_SOUCH     MARNR-CRSP --SQSRC--R R---PRRRCR --RRRRCCRR RRR--VCCRR Y---TTTRCA RQ-------- --------
F5CBC6_SOTFL     MARNR-CRSP --SQSRC--R R---PRRRCR --RRRRCCRR RRR--VCCRR Y---TTTRCA R--------- --------
B4YVM9_STEBR     MARNR-CRSP --SQSRC--R R---PRRRCR --RRRRCCRR RRR--VCCRR Y---TTTRCA RQ-------- --------
C8C422_LISBO     MARNR-CRSP --SQSRC--R R---PRRRCR --RRRRCCRR RRR--VCCRR Y---TTTRCA RQ-------- --------
B4YVN0_DELDE     MARNR-CRSP --SQSRC--R R---PRRRCR --RRRRCCRR RRR--VCCRR Y---TTTRCA R--------- --------
F5CBC7_LAGOL     MARNR-CRSP --SQSRC--R R---PRRRCR --RRRRCCRR RRR--VCCRR Y---TTTRCA R--------- --------
F5CBC2_STEFR     MARNR-CRSP --SQSRC--R R---PRRRCR --RRRRCCRR RRR--VCCRR Y---TTTRCA R--------- --------
F5CBC5_LAGHO     MARNR-CRSP --SQSRC--R R---PRRRCR --RRRRCCRR RRR--VCCRR Y---TTTRCA R--------- --------
F5CIP3_LIPVE     MARNR-CRSP --SQSRG--R R---PRRKYR -SRRRRCCQR RRR--VCCRR Y---TTMRCA KQ-------- --------
A8IYB2_PONBL     MARNR-CRSP --SQNRG--R R---PRRRYR -SRRRRCCQR RRR--VCCRR Y---TSVRCA RQ-------- --------
A8IYA9_INIGE     MARNR-CRSP --SQSRG--R R---PRRRYR -SRRRRCCQR RRR--VCCRR Y---TTVRCA RQ-------- --------
C8C429_MONMO     MARTR-CRSP --SQSRG--R R---PRRRYR -SKRRRCCQR RRR--VCCRR Y---TTTRCA RQ-------- --------
C8C430_DELLE     MARNR-CRSP --SQSRG--R R---PRRRYR -SKRRRCCQR RRR--VCCRR Y---TTTRCA RQ-------- --------
H2NQ55_PONAB     MARYRCCRSQ --SQSRC--C R---RRQRCH -RRRRRCCQT RRRAMRCCRR R---YRLRCR RH-------- --------
HSP1_PONPY       MARYRCCRSQ --SQSRC--C R---RRQRCH -RRRRRCCQT RRRAMRCCRR R---YRLRCR RH-------- --------
Q3MN80_HUMAN     MARYRCCRSQ --SRSRY--Y R---QRQRSR -RRRRRSCQT RRRAMRCCRP R---YRPRCR RH-------- --------
HSP1_HUMAN       MARYRCCRSQ --SRSRY--Y R---QRQRSR -RRRRRSCQT RRRAMRCCRP R---YRPRCR RH-------- --------
A0A2I3GMT3_NOMLE ---------- ---------- ---------- -RRRRRSCQT RRRAMRCCRP R---YRLRRR RH-------- --------
HSP1_HYLLA       MARYRCCRSQ --SRSRC--Y R---RGQRSR -RRRRRSCQT RRRAMRCCRP R---YRLRRR RH-------- --------
A0A2I3RG75_PANTR MARYRCCRSQ --SRSRC--Y R---QRQRSR -RRKRQSCQT QRRQHRSCRR R---KRRSCR HRRRHRRGLP APPPCPAC
HSP1_GORGO       MARYRCCRSQ --SRSRC--Y R---QRQTSR -RRRRRSCQT QRRAMRCCRR R---NRLRRR KH-------- --------
A0A2J8L9Y2_PANTR MARYRCCRSQ --SRSRC--Y R---QRQRSR -RRKRQSCQT QRRAMRCCRR R---SRMRRR RH-------- --------
HSP1_PANTR       MARYRCCRSQ --SRSRC--Y R---QRQRSR -RRKRQSCQT QRRAMRCCRR R---SRMRRR RH-------- --------
HSP1_PANPA       MARYRCCRSQ --SRSRC--Y R----QRRSR -RRKRQSCQT QRRAMRCCRR R---SRLRRR RH-------- --------
```

```
F7VJK6_LOXAF     MARYRCCRSR --SRSRCR-S R---RRRRSH -RRRRRCARR RRRTRRGCRR R---YSLRRR RY-------- --------
A8IYA4_ANTAM     MARYRCCLTH --SRSRCRPR R---RRRRCR -KLRRRFCRR PRR-RVCCRR Y---TAIRCT R--------- --------
HSP1_GALVR       MARYRCCR-- --SRSRC--R R---RRRSCR -RRRR--CRR RRA-RRSCRR R---YSLRCC RRY------- --------
Q1KZY7_ELACE     MARYRCCLTH --SRSRCR-R R---RRRRCH -RRRKRFGRR RRR-RVCCRR Y---TVVRCT RQ-------- --------
A8IYA7_9CETA     MARYRCRLTH --SRSGCR-R R---RRRRCR -RRRRRFCRR RRR-RVCCRR Y---TVVRCT RQ-------- --------
D5K1R5_BOVIN     MARYRCCLTH --SGSRCR-R R---RRRRCR -RXRRRFGRR RRR-RVCCRR Y---TVIRCT RQ-------- --------
A0A193KZW0_9CETA MARYRCCLTH --SGSRCR-R R---RRRRCR -RRRRRFGRR RRR-------- R--------- ---------- --------
B8Y880_BOVIN     MARYRCCLTH --SGSRCR-R R---RRRRCR -RRRRRFGRR RRR-RVCCRR Y---TVIRCT RQ-------- --------
A0A068B2A1_BOSIN MARYRCCLTH --SGSRCR-R R---RRRRCR -RRRRRFGRR RRR-RVCCRR Y---TVIRCT RQ-------- --------
HSP1_BOVIN       MARYRCCLTH --SGSRCR-R R---RRRRCR -RRRRRFGRR RRR-RVCCRR Y---TVIRCT RQ-------- --------
E2ICF7_CAPHI     MARYRCCLTH --SRSRCR-R R---RRRRCR -RRRRRFGRR RRR-RVCCRR Y---TVVRCT RQ-------- --------
C5IFA1_SHEEP     MARYRCCLTH --SRSRCR-R R---RRRRCR -RRRRRFGRR RRR-RVCCRR Y---TVVRCT RQ-------- --------
W5QJA5_SHEEP     ------CR-- --------R- R---RRRRCR -RRRRRFGRR RRR-RVCCRR Y---TVVRCT RQ-------- --------
A8IYA2_OVIDA     MARYRCCLTH --SRSRCR-R R---RRRRCR -RRRRRFGRR RRR-RVCCRR Y---TVVRCT RQ-------- --------
HSP1_CAPHI       MARYRCCLTH --SRSRCR-R R---RRRRCR -RRRRRFGRR RRR-RVCCRR Y---TVVRCT RQ-------- --------
HSP1_SHEEP       MARYRCCLTH --SRSRCR-R R---RRRRCR -RRRRRFGRR RRR-RVCCRR Y---TVVRCT RQ-------- --------
G3SMV3_LOXAF     MARYRCCRSR --SRSRC--R S---RRRRSH -RRRRRSCRS RRR--RCCRR R--------- HR-------- --------
A0A2R8PK40_CALJA MARYRCCRSQ --SRSRC--Y R---QRRRGR -RRRRRSCRR RRA-SRCCRR R---YKLPCR RY-------- --------
HSP1_SAGIM       MARYRCCRSQ --SRSRC--Y R---QRRRGR -RRRRRTCRR RRA-SRCCRR R---YKLTCR RY-------- --------
F7VJK5_ERIEU     MARYRCCRSQ --SRSRC--S RRRYRRRRCR -RRRRRSCRR RRR-RACCRY R---Y----R RY-------- --------
H0VAL2_CAVPO     MARYRCCRSP --SRSRC--R R---RRRRFY -RRRRRCHRR RRR--GCCRR R---YTRRCK RY-------- --------
HSP1_CAVPO       MARYRCCRSP --SRSRC--R R---RRRRFY -RRRRRCHRR RRR---CCRR R---YTRRCK RY-------- --------
HSP1_RABIT       MVRYRCCRSQ --SRSRC--R R---RRRRCR -RRRRRCCQR RRV-RKCCRR T---YTLRCR RY-------- --------
Q9GKQ0_ATESP     MARYRCCRSR --SRSRC--Y R---QRPRCR -RRRRRSCRR RRG-SRCCRR R---YRLRRR RY-------- --------
HSP1_ALOSE       MARYRCCRSR SLSRSRC--Y R---QRPRCR -RRRRRSCRR PRA-SRCCRR R---YRLRRR RY-------- --------
A0A2K6TB39_SAIBB MARYRCCRSR --SRSRC--Y R---RRRRCR -TRRRRCCRR RRA-RRCCRR R---YKLRCR RY-------- --------
HSP1_SAISC       MARYRCCRSR --SRSRC--Y R---RRRRCR -TRRRRCCRR RRA-RRCCRR R---YKLRCR RY-------- --------
A0A2K5R6E5_CEBCA MARYRCCRSR --SRSRC--Y R---QRRRCR -RRRRRCRSR RAR--RCCRR R---YRLRCR RY-------- --------
B5TJZ8_SIGHI     MARYRCCRSK --SRSRC--R R---RRRRCR -RRRRRCCRR RRR--RCCRR R-RTYTLRCK KY-------- --------
C3U1R2_MUSPA     MARYRCCRSK --SRSRC--R R---RRRRCR -RRRRRCCRR RRQ--RCCRR R-RSYTIRCK KY-------- --------
C3U1Q6_MUSMB     MARYRCCRSK --SRSRC--R R---RRRRCR -RRRRRCCRR RRR--RCCRR R-RSYTIRCK KY-------- --------
Q8CEM2_MOUSE     MARYRCCRSK --SRSRC--R R---RRRRCR -RRRRRCCRR RRR--RCCRR R-RSYTIRCK K--------- --------
C3U1Q8_MUSMC     MARYRCCRSK --SRSRC--R R---RRRRCR -RRRRRCCRR RRR--RCCRR R-RSYTIRCK KY-------- --------
C3U1R5_MUSSP     MARYRCCRSK --SRSRC--R R---RRRRCR -RRRRRCCRR RRR--RCCRR R-RSYTIRCK KY-------- --------
C3U1Q7_MUSCO     MARYRCCRSK --SRSRC--R R---RRRRCR -RRRRRCCRR RRR--RCCRR R-RSYTIRCK KY-------- --------
C3U1R4_MUSSI     MARYRCCRSK --SRSRC--R R---RRRRCR -RRRRRCCRR RRR--RCCRR R-RSYTIRCK KY-------- --------
C3U1R3_MUSMA     MARYRCCRSK --SRSRC--R R---RRRRCR -RRRRRCCRR RRR--RCCRR R-RSYTIRCK KY-------- --------
C3U1R0_MOUSE     MARYRCCRSK --SRSRC--R R---RRRRCR -RRRRRCCRR RRR--RCCRR R-RSYTIRCK KY-------- --------
C3U1Q9_MOUSE     MARYRCCRSK --SRSRC--R R---RRRRCR -RRRRRCCRR RRR--RCCRR R-RSYTIRCK KY-------- --------
A3KMD0_MOUSE     MARYRCCRSK --SRSRC--R R---RRRRCR -RRRRRCCRR RRR--RCCRR R-RSYTIRCK KY-------- --------
HSP1_MOUSE       MARYRCCRSK --SRSRC--R R---RRRRCR -RRRRRCCRR RRR--RCCRR R-RSYTIRCK KY-------- --------
C3U1R1_9MURI     MARYRCCRSK --SRSRC--R R---RRRRCR -RRRRRCCQR RRR--RCCRR R-RSYTIRCK KY-------- --------
HSP1_RAT         MARYRCCRSK --SRSRC--R R---RRRRCR -RRRRRCCRR RRR--RCCRR R-RSYTFRCK RY-------- --------
C3U1S7_APOSY     MARYRCCRSK --SRSRC--R R---RRRRCR SRRRRRCCRR RRR--RCCRR R-RSYTIRCK RY-------- --------
A0A2K5I3S6_COLAP MARYRCRRSQ --SRSRC--C R---QRRRCR -RRRRQRFRA RKRAMRCCRR R---YRLRCR RY-------- --------
HSP1_COLGU       MARYRCRRSQ --SRSRC--C R---QRRRCR -RRRRQRFRA RKRAMRCCHR R---YRLRCR RY-------- --------
F7VJK8_OTOGA     MARYRCCRSQ --SRSRC--R R---RRRRCR -RRRRRCCRR RRR--RCCRR R---YRLRCR RY-------- --------
HSP1_PILBA       MARYRCCRSQ --SRSRC--C R---RRRRCR -RRRRQRCRA RRTAMRCCRR R---YRRRCR RY-------- --------
HSP1_NASLA       MAKSRCCGSQ --SRSRC--C R---PRQRCR -RRRRRSCRA RRRAMRCCRR R---YRLRCR RY-------- --------
S4SNH6_SEMEN     -------RSQ --SRSRC--C R---PRRRCR --RRRRSCRA RRRATRCCRR R---YRLRCK RY-------- --------
HSP1_TRAJO       MARYRRCRSQ --SRSRC--C R---PRRRCR -RRRRQSCRA RRRATRCCRR R---YRLRCR RY-------- --------
L0CM34_TRAPH     MARYRCCRSQ --SRSRC--C R---PRRRCR -RRRRRSCRA RRRATRCCRR R---YRL-SR RY-------- --------
HSP1_TRAPH       MARYRCCRSQ --SRSRC--C R---PRRRCR -RRRRRSCRA RRRATRCCRR R---YRL-SR RY-------- --------
L0CNC1_TRAPH     MARYRCCRSQ --SRSRC--C R---PRRRCR -RRRRRSCRA RRRATRCCRR R---YRLRSR RY-------- --------
L0CM39_9PRIM     MARYRCCRSQ --SRSRC--C R---PRRRCR -RRRRRSCRA RRRATRCCRR R---YRLRSR RY-------- --------
HSP1_TRAOB       MARYRCCRSQ --SRSRC--C R---PRRRCR -RRRRRSCRA RRRATRCCRR R---YRLRSR RY-------- --------
HSP1_TRACR       MARYRCCRSQ --SRSRC--C R---PRRRCR -RRRRRSCRA RRRATRCCRR R---YRLRSR RY-------- --------
A0A2K6PXN1_RHIRO MARYRCCRSQ --SRSRC--C R---PRRRCR -RRRRRSCRA RRRAMRCCRR R---YRLRCR RY-------- --------
A0A2K6LMP4_RHIBE MARYRCCRSQ --SRSRC--C R---PRRRCR -RRRRRSCRA RRRAMRCCRR R---YRLRCR RY-------- --------
HSP1_TRAFR       MARYRCCRSQ --SRSRC--C R---PRRRCR -RRRRRSCRA RRRATRCCRR R---YRLRCR RY-------- --------
HSP1_TRAPL       MARYRCCRSQ --SRSRC--C R---PRRRCR -RRRRRSCRA RRRATRCCRR R---YRLRCR RY-------- --------
HSP1_TRAGE       MARYRCCRSQ --SRSRC--C R---PRRRCR -RRRRRSCRA RRRATRCCRR R---YRLRCR RY-------- --------
HSP1_TRAVT       MARYRRCRSQ --SRSRC--C R---PRRRCR --RRRRSCRA RRRATRCCRR R---YRLRCR RY-------- --------
HSP1_SEMEN       MARYRRCRSQ --SRSRC--C R---PRRRCR --RRRRSCRA RRRATRCCRR R---YRLRCR RY-------- --------
S4SLP0_TRAJO     ---------- --------C R---PRRRCR -RRRRRSCRA RRRATRCCRR R---YRLRCR RY-------- --------
S4SNK2_9PRIM     -------RSQ --SRSRC--C R---PRRRCR --RRRRSCRA RRRATRCCRR R---YRLRCR RY-------- --------
S4SM07_TRAJO     -------RSQ --SRSRC--C R---PRRRCR -RRRRRSCRA RRRATRCCRR R---YRLRCR RY-------- --------
S4SLR0_SEMEN     -------RSQ --SRSRC--C R---PRRRCR --RRRRSCRA RRRATRCCRR R---YRLRCR RY-------- --------
S4SLN4_9PRIM     -------RSQ --SRSRC--C R---PRRRCR --RRRRSCRA RRRATRCCRR R---YRLRCR RY-------- --------
A0A0D9R7P5_CHLSB MARYRCCRSQ --SRSRC--C R---QRRRCR -RRRRRRCRA RRRAMKYCRR R---YRLRCR RY-------- --------
A0A096MLL5_PAPAN MARYRCCRSQ --SRSRC--C R---QRRRCR -RRRRRRCRA RRRAMRCCRR R---YRLRCR RY-------- --------
A0A2K5LCN6_CERAT MARYRCCRSQ --SRSRC--C R---QRRRCR -RRRRRRCRA RRRAMRCCRR R---YRLRCR RY-------- --------
A0A2K5ZQV8_MANLE MARYRCCRSQ --SRSRC--C R---QRRRCR -RRRRRRCRA RRRAMRCCRR R---YRLRCR RY-------- --------
G7NPN0_MACMU     MARYRCCRSQ --SRSRC--C R---RRRRCR -RRRRRRCRA RRRAMRCCRR R---YRLRCR RY-------- --------
G7Q0H9_MACFA     MARYRCCRSQ --SRSRC--C R---RRRRCR -RRRRRRCRA RRRAMRCCRR R---YRLRCR RY-------- --------
A0A2K6DMS0_MACNE MARYRCCRSQ --SRSRC--C R---RRRRCR -RRRRRRCRA RRRAMRCCRR R---YRLRCR RY-------- --------
HSP1_PAPCY       MARYRCCRSQ --SRSRC--C R---RRRRCR -RRRRRRCRA RRRAMRCCRR R---YRLRCR RY-------- --------
HSP1_MACMU       MARYRCCRSQ --SRSRC--C R---RRRRCR -RRRRRRCRA RRRAMRCCRR R---YRLRCR RY-------- --------
Q4R6L4_MACFA     MARYRCCSQ --SRSRC--C R---RRRRCR -RRRRRRCRA RRRAMRCCRR R---YRLRCR RY-------- --------
F7VJK3_FELCA     MARYRCCRSH --SRSRC--R R---RRRRCR -RRRRRCCRR PRK-RVCSRR Y---RVGRCR RR-------- --------
A8IYC1_POTPR     MARYRCCRSH --SRSRC--R P---RRRRCR -RRRRRCCPR RRR-AVCCRR Y---TVIRCR RC-------- --------
```

```
HSP1_PIG          MARYRCCRSH --SRSRC--R P---RRRRCR -RRRRRCCPR RRR-AVCCRR Y---TVIRCR RC-------- --------
HSP1_OTOHE        MARYRCCRSR --SRSRC--R R---RRRKCY -RRRRRCSRK RRR-RVCCRR Y---TVMRCR RR-------- --------
A8IYB9_HIPAM      MARYRCCRSP --SRSRC--R R---QRRRCR -RRRRRCCRQ RRR-RVCCRR Y---TMVRCT RQ-------- --------
C8C444_HEXLI      MARYRCCRSP --SRSRC--R R---QRRRCR -RRRRRCCRQ RRR-RVCCRR Y---TMVRCT RQ-------- --------
A0A0M4LXH7_EQUAS  MARYRCCRSQ --SQSRCR-R R---RRRRCR -RRRRRCVRR RR---VCCRR Y---TVLRCR RRR------- --------
HSP1_EQUAS        MARYRCCRSQ --SQSRCR-R R---RRRRCR -RRRRRCVRR RR---VCCRR Y---TVLRCR RRR------- --------
F7DCW3_HORSE      MARYRCCRSQ --SQSRCR-R R---RRRRCR -RRRRRSVRQ RR-------- ---------- ---------- --------
HSP1_HORSE        MARYRCCRSQ --SQSRCR-R R---RRRRCR -RRRRRSVRQ RR---VCCRR Y---TVLRCR RRR------- --------
HSP1_HYPSA        MARYRRCR-- --SRSRC--R R---RRRRCH -RRRRRCCRR RRRRRACCRR Y------RCR RR-------- --------
HSP1_NEOBU        MARYRRCR-- --SRSRC--R R---RRRRCH -RRRRRCCRR RRRRRACCRR Y------RCR RR-------- --------
HSP1_RHIHA        MARYRCCRSR --SRSRC--R P---RRRRCR -RRRRRCCRR RRR--VCCRR Y----SARCR RRR------- --------
HSP1_MURCY        MARYRCCR-- --SRSRC--R R---RRRRCH -RRRRRCSRR RRR-RVCCRR Y---TVIRCR RR-------- --------
HSP1_MORME        MARYRCCRSP --SRSRC--R R---RRRRCR -RRRRRSCRR RRR--VCCRR Y----TVRCR RR-------- --------
HSP1_MONRE        MARYRCCRSP --SRSRC--R R---RRRRCR -RRRRRCCRR RRR--VCCRR Y----TVRCR RR-------- --------
HSP1_DESRO        MARYRCCRSP --SRSRC--R R---RRRRCR -RRRRRCCRR RRR--VCCRR Y----TVRCR RR-------- --------
HSP1_PTEPA        MARYRCCRSP --SRSRC--R R---RRRRCR -RRRRRCCRR RRR--VCCRR Y----TVRCR RR-------- --------
F7VJK7_MYOLU      MARYRCCR-- --SRSRC--R R---RRRRCY -RRRRRCCRR RRRRRVCCRR Y-----SRCR RR-------- --------
HSP1_MYODA        MARYRCCR-- --SRSRC--R R---RRRRCY -RRRRRCCRR RRRRRVCCRR Y-----SRCR RR-------- --------
HSP1_GLABE        MARYRCCR-- --SRSRC--R R---RRRRSY -RRRRRCCRR RRR-RVCCRR Y-----VRCR RR-------- --------
HSP1_NATST        MARYRCCRSQ --SRSRC--R P---RRRRCR -TRRRRCCRR RRR-RVCCRR Y---TVVRCR RR-------- --------
HSP1_CHIMC        MARYRCCRSQ --SRSRC--R R---RRRRCR -TRRRRCCRR RRR-RVCCRR Y---TVVRCR RR-------- --------
HSP1_EPTFU        MARYRCCR-- --SRSRC--R R---RRRRCY -RRRRRCCRR RRR-RVCCRR Y---TVIRCR RR-------- --------
HSP1_EPTBR        MARYRCCR-- --SRSRC--R R---RRRRCY -RRRRRCCRR RRR-RVCCRR Y---TVIRCR RR-------- --------
HSP1_CORTO        MARYRCCRSQ --SRSRC--R R---RRRRCY -RRRRRCCRR RRR-RVCCRR Y-----TRVR RR-------- --------
HSP1_PLEAU        MARYRCCRSQ --SRSRC--R R---RRRRCY -RRRRRCCRR RRR-RVCCRR Y---TVVRCR RR-------- --------
F7VJK4_CANLF      MARYRCCRSQ --SRSRC--R R---RRRRCR -RRRRRCCRR RRR-RVCCRR Y---TVVRCR RR-------- --------
HSP1_PTEHP        MARYRCCRSQ --SRSRC--R R---RRRRCR -RRRRRCCRR RRR--VCCRR Y----TVRCR RRR------- --------
```

REFERENCES

1. Reginald Garrett, C.G., Michal Sabat, *Biochemistry*. 5th Edition ed. 2013: Brooks/Cole.
2. Razin, S.V. and A.A. Gavrilov, *Chromatin without the 30-nm fiber Constrained disorder instead of hierarchical folding.* Epigenetics, 2014. **9**(5): p. 653-657.
3. Porter, I.M., G.A. Khoudoli, and J.R. Swedlow, *Chromosome condensation: DNA compaction in real time.* Current Biology, 2004. **14**(14): p. R554-R556.
4. *Somatic Chromatin Remodeling Image adapted from, http://images.slideplayer.com/19/5919803/slides/slide_17.jpg.*
5. Annunziato, A.T., *DNA Packaging: Nucleosomes and Chromatin.* Nature Education 2008. **1**(26).
6. Miller, D., M. Brinkworth, and D. Iles, *Paternal DNA packaging in spermatozoa: more than the sum of its parts? DNA, histones, protamines and epigenetics.* Reproduction, 2010. **139**(2): p. 287-301.
7. *Sperm Chromatin: Biological and Clinical Applications in Male Infertility and Assisted Reproduction*. Sperm Chromatin: Biological and Clinical Applications in Male Infertility and Assisted Reproduction, ed. A. Zini and A. Agarwal. 2011. 1-512.
8. Bellastella, G., et al., *Dimensions of human ejaculated spermatozoa in Papanicolaou-stained seminal and swim-up smears obtained from the Integrated Semen Analysis System (ISAS(®)).* Asian journal of andrology, 2010. **12**(6): p. 871-879.
9. Balhorn, R., *Sperm Chromatin: An Overview*, in *Sperm Chromatin: Biological and Clinical Applications in Male Infertility and Assisted Reproduction*

A.Z.a.A. Agarwal, Editor. 2011. p. 3-18.

10. Balhorn, R., *The protamine family of sperm nuclear proteins.* Genome Biology, 2007. **8**(9).
11. Moir, R.D. and G.H. Dixon, *CHARACTERIZATION OF A PROTAMINE GENE FROM THE CHUM SALMON (ONCORHYNCHUS-KETA).* Journal of Molecular Evolution, 1988. **27**(1): p. 8-16.
12. Ward, W.S. and D.S. Coffey, *DNA PACKAGING AND ORGANIZATION IN MAMMALIAN SPERMATOZOA - COMPARISON WITH SOMATIC-CELLS.* Biology of Reproduction, 1991. **44**(4): p. 569-574.
13. Mao, A.H., et al., *Net charge per residue modulates conformational ensembles of intrinsically disordered proteins.* Proceedings of the National Academy of Sciences of the United States of America, 2010. **107**(18): p. 8183-8188.
14. Bianchi, F., et al., *INTERACTION OF HUMAN P1 AND P2 PROTAMINES WITH DNA.* Biochemical and Biophysical Research Communications, 1994. **201**(3): p. 1197-1204.
15. Allen, M.J., E.M. Bradbury, and R. Balhorn, *AFM analysis of DNA-protamine complexes bound to mica.* Nucleic Acids Research, 1997. **25**(11): p. 2221-2226.
16. Brewer, L.R., M. Corzett, and R. Balhorn, *Protamine-induced condensation and decondensation of the same DNA molecule.* Science, 1999. **286**(5437): p. 120-123.
17. Conwell, C.C., I.D. Vilfan, and N.V. Hud, *Controlling the size of nanoscale toroidal DNA condensates with static curvature and ionic strength.* Proceedings of the National Academy of Sciences of the United States of America, 2003. **100**(16): p. 9296-9301.
18. Ward, W.S., *Function of sperm chromatin structural elements in fertilization and development.* Molecular Human Reproduction, 2010. **16**(1): p. 30-36.
19. Akmal, M., et al., *The important role of protamine in spermatogenesis and quality of sperm: A mini review.* Asian Pacific Journal of Reproduction, 2016. **5**(5): p. 357-360.

20. Oliva, R., *Protamines and male infertility.* Human Reproduction Update, 2006. **12**(4): p. 417-435.
21. Castillo, J., et al., *Human sperm chromatin epigenetic potential: genomics, proteomics, and male infertility.* Asian Journal of Andrology, 2015. **17**(4): p. 601-609.
22. Nasr-Esfahani, M.H., et al., *Effect of protamine-2 deficiency on ICSI outcome.* Reproductive Biomedicine Online, 2004. **9**(6): p. 652-658.
23. Gonzalez-Marin, C., J. Gosalvez, and R. Roy, *Types, Causes, Detection and Repair of DNA Fragmentation in Animal and Human Sperm Cells.* International Journal of Molecular Sciences, 2012. **13**(11): p. 14026-14052.
24. Mazrimas, J.A., et al., *A CORRECTED PRIMARY SEQUENCE FOR BULL PROTAMINE.* Biochimica Et Biophysica Acta, 1986. **872**(1-2): p. 11-15.
25. Balhorn, R., *A MODEL FOR THE STRUCTURE OF CHROMATIN IN MAMMALIAN SPERM.* Journal of Cell Biology, 1982. **93**(2): p. 298-305.
26. Vilfan, I.D., C.C. Conwell, and N.V. Hud, *Formation of native-like mammalian sperm cell chromatin with folded bull protamine.* Journal of Biological Chemistry, 2004. **279**(19): p. 20088-20095.
27. Balhorn, R., et al., *IDENTIFICATION OF BULL PROTAMINE DISULFIDES.* Biochemistry, 1991. **30**(1): p. 175-181.
28. Pirhonen, A., A. Linnalakankkunen, and P.H. Maenpaa, *P2 PROTAMINES ARE PHOSPHORYLATED IN-VITRO BY PROTEIN-KINASE-C, WHEREAS P1 PROTAMINES PREFER CAMP-DEPENDENT PROTEIN-KINASE - A COMPARATIVE-STUDY OF 5 MAMMALIAN-SPECIES.* European Journal of Biochemistry, 1994. **223**(1): p. 165-169.
29. Hutchison, J.M., D.C. Rau, and J.E. DeRouchey, *Role of Disulfide Bonds on DNA Packaging Forces in Bull Sperm Chromatin.* Biophysical Journal, 2017. **113**(9): p. 1925-1933.
30. de Vries, M., et al., *Chromatin remodelling initiation during human spermiogenesis.* Biology Open, 2012. **1**(5): p. 446-457.
31. Braun, R.E., *Packaging paternal chromosomes with protamine.* Nature Genetics, 2001. **28**(1): p. 10-12.
32. Rathke, C., et al., *Chromatin dynamics during spermiogenesis.* Biochimica et Biophysica Acta (BBA) - Gene Regulatory Mechanisms, 2014. **1839**(3): p. 155-168.
33. Sullivan, R. and R. Mieusset, *The human epididymis: its function in sperm maturation.* Human Reproduction Update, 2016. **22**(5): p. 574-587.
34. *Testicle Anatomy, https://maleinfertility.org/understanding-male-infertility/anatomy-physiology-male-reproduction/testicular-anatomy.*
35. Ijiri, T.W., et al., *Thiol changes during epididymal maturation: a link to flagellar angulation in mouse spermatozoa?* Andrology, 2014. **2**(1): p. 65-75.
36. Conrad, M., et al., *The nuclear form of phospholipid hydroperoxide glutathione peroxidase is a protein thiol peroxidase contributing to sperm chromatin stability.* Molecular and Cellular Biology, 2005. **25**(17): p. 7637-7644.
37. Bloomfield, V.A., *DNA condensation by multivalent cations.* Biopolymers, 1997. **44**(3): p. 269-282.
38. Wang, Y.W., et al., *DNA condensations on mica surfaces induced collaboratively by alcohol and hexammine cobalt.* Colloids and Surfaces B-Biointerfaces, 2011. **83**(1): p. 61-68.
39. Widom, J. and R.L. Baldwin, *CATION-INDUCED TOROIDAL CONDENSATION OF DNA STUDIES WITH CO3+(NH3)6.* Journal of Molecular Biology, 1980. **144**(4): p. 431-453.

40. DeRouchey, J.E. and D.C. Rau, *Salt effects on condensed protamine-DNA assemblies: anion binding and weakening of attraction.* The journal of physical chemistry. B, 2011. **115**(41): p. 11888-11894.
41. Hakem, R., *DNA-damage repair; the good, the bad, and the ugly.* Embo Journal, 2008. **27**(4): p. 589-605.
42. Dizdaroglu, M. and P. Jaruga, *Mechanisms of free radical-induced damage to DNA.* Free Radical Research, 2012. **46**(4): p. 382-419.
43. Gosalvez, J., E. Tvrda, and A. Agarwal, *Free radical and superoxide reactivity detection in semen quality assessment: past, present, and future.* Journal of Assisted Reproduction and Genetics, 2017. **34**(6): p. 697-707.
44. AbdulSalam, S.F., F.S. Thowfeik, and E.J. Merino, *Excessive Reactive Oxygen Species and Exotic DNA Lesions as an Exploitable Liability.* Biochemistry, 2016. **55**(38): p. 5341-5352.
45. Phaniendra, A., D.B. Jestadi, and L. Periyasamy, *Free Radicals: Properties, Sources, Targets, and Their Implication in Various Diseases.* Indian Journal of Clinical Biochemistry, 2015. **30**(1): p. 11-26.
46. Wagner, H., J.W. Cheng, and E.Y. Ko, *Role of reactive oxygen species in male infertility: An updated review of literature.* Arab Journal of Urology, 2018. **16**(1): p. 35-43.
47. Aitken, R.J., *Reactive oxygen species as mediators of sperm capacitation and pathological damage.* Molecular Reproduction and Development, 2017. **84**(10): p. 1039-1052.
48. deLamirande, E., P. Leclerc, and C. Gagnon, *Capacitation as a regulatory event that primes spermatozoa for the acrosome reaction and fertilization.* Molecular Human Reproduction, 1997. **3**(3): p. 175-194.
49. Di Meo, S., et al., *Role of ROS and RNS Sources in Physiological and Pathological Conditions.* Oxidative Medicine and Cellular Longevity, 2016: p. 44.
50. Walczak-Jedrzejowska, R., J.K. Wolski, and J. Slowikowska-Hilczer, *The role of oxidative stress and antioxidants in male fertility.* Central European journal of urology, 2013. **66**(1): p. 60-7.
51. *DNA Damage Types, Adapted from* https://sites.google.com/site/bi6101dnarepair/damage-detection-response/types-of-dna-damage.
52. Pages, V. and R.P.P. Fuchs, *How DNA lesions are turned into mutations within cells?* Oncogene, 2002. **21**(58): p. 8957-8966.
53. O'Driscoll, M. and P.A. Jeggo, *The role of double-strand break repair - insights from human genetics.* Nature Reviews Genetics, 2006. **7**(1): p. 45-54.
54. Thoms, K.M., C. Kuschal, and S. Emmert, *Lessons learned from DNA repair defective syndromes.* Experimental Dermatology, 2007. **16**(6): p. 532-544.
55. Alshykhly, O.R., A.M. Fleming, and C.J. Burrows, *5-Carboxamido-5-formamido-2-iminohydantoin, in Addition to 8-oxo-7,8-Dihydroguanine, Is the Major Product of the Iron-Fenton or X-ray Radiation-Induced Oxidation of Guanine under Aerobic Reducing Conditions in Nucleoside and DNA Contexts.* Journal of Organic Chemistry, 2015. **80**(14): p. 6996-7007.
56. Suzuki, M., et al., *Calculating Distortions of Short DNA Duplexes with Base Pairing Between an Oxidatively Damaged Guanine and a Guanine.* Molecules, 2014. **19**(8): p. 11030-11044.
57. Shibutani, S., M. Takeshita, and A.P. Grollman, *INSERTION OF SPECIFIC BASES DURING DNA-SYNTHESIS PAST THE OXIDATION-DAMAGED BASE 8-OXODG.* Nature, 1991. **349**(6308): p. 431-434.

58. K.R., S.G., et al., *Mechanism of DNA Binding and Cleavage.* 2014. **2**(1): p. 1-9.
59. Balasubramanian, B., W.K. Pogozelski, and T.D. Tullius, *DNA strand breaking by the hydroxyl radical is governed by the accessible surface areas of the hydrogen atoms of the DNA backbone.* Proceedings of the National Academy of Sciences of the United States of America, 1998. **95**(17): p. 9738-9743.
60. Jain, S.S. and T.D. Tullius, *Footprinting protein-DNA complexes using the hydroxyl radical.* Nature Protocols, 2008. **3**(6): p. 1092-1100.
61. Mehta, A. and J.E. Haber, *Sources of DNA Double-Strand Breaks and Models of Recombinational DNA Repair.* Cold Spring Harbor Perspectives in Biology, 2014. **6**(9).
62. Werber, J., et al., *Analysis of 2,2 '-Azobis (2-Amidinopropane) Dihydrochloride Degradation and Hydrolysis in Aqueous Solutions.* Journal of Pharmaceutical Sciences, 2011. **100**(8): p. 3307-3315.
63. Dion, M.Z., et al., *The Use of a 2,2 '-Azobis (2-Amidinopropane) Dihydrochloride Stress Model as an Indicator of Oxidation Susceptibility for Monoclonal Antibodies.* Journal of Pharmaceutical Sciences, 2018. **107**(2): p. 550-558.
64. Ji, J.A., et al., *Methionine, Tryptophan, and Histidine Oxidation in a Model Protein, PTH: Mechanisms and Stabilization.* Journal of Pharmaceutical Sciences, 2009. **98**(12): p. 4485-4500.
65. Niki, E., et al., *OXIDATION OF LIPIDS .12. INHIBITION OF OXIDATION OF SOYBEAN PHOSPHATIDYLCHOLINE AND METHYL LINOLEATE IN AQUEOUS DISPERSIONS BY URIC-ACID.* Bulletin of the Chemical Society of Japan, 1986. **59**(2): p. 471-477.
66. Hiramoto, K., et al., *DNA BREAKING ACTIVITY OF THE CARBON-CENTERED RADICAL GENERATED FROM 2,2'-AZOBIS(2-AMIDINOPROPANE) HYDROCHLORIDE (AAPH).* Free Radical Research Communications, 1993. **19**(5): p. 323-332.
67. Paul, T., et al., *Strand Cleavage of Supercoiled DNA by Water-Soluble Peroxyl Radicals. The Overlooked Importance of Peroxyl Radical Charge.* Biochemistry, 2000. **39**(14): p. 4129-4135.
68. Shao, J., N.E. Geacintov, and V. Shafirovich, *Oxidative Modification of Guanine Bases Initiated by Oxyl Radicals Derived from Photolysis of Azo Compounds.* Journal of Physical Chemistry B, 2010. **114**(19): p. 6685-6692.
69. Sabeti, P., et al., *Etiologies of sperm oxidative stress.* International journal of reproductive biomedicine (Yazd, Iran), 2016. **14**(4): p. 231-240.
70. Hekmatdoost, A., N. Lakpour, and M.R. Sadeghi, *Sperm chromatin integrity: etiologies and mechanisms of abnormality, assays, clinical importance, preventing and repairing damage.* Avicenna journal of medical biotechnology, 2009. **1**(3): p. 147-160.
71. Marnett, L.J., *Oxyradicals and DNA damage.* Carcinogenesis, 2000. **21**(3): p. 361-370.
72. Ahmadi, A. and S.C. Ng, *Fertilizing ability of DNA-damaged spermatozoa.* Journal of Experimental Zoology, 1999. **284**(6): p. 696-704.
73. Zini, A. and J. Libman, *Sperm DNA damage: clinical significance in the era of assisted reproduction.* Canadian Medical Association Journal, 2006. **175**(5): p. 495-500.
74. EggertKruse, W., et al., *The Acridine Orange test: A clinically relevant screening method for sperm quality during infertility investigation?* Human Reproduction, 1996. **11**(4): p. 784-789.
75. Kazerooni, T., et al., *Evaluation of sperm's chromatin quality with acridine orange test, chromomycin A3 and aniline blue staining in couples with unexplained recurrent abortion.* Journal of Assisted Reproduction and Genetics, 2009. **26**(11-12): p. 591-596.
76. Evenson, D.P., *Sperm Chromatin Structure Assay (SCSA®): 30 Years of Experience with the SCSA®*, in *Sperm Chromatin: Biological and Clinical Applications in Male Infertility*

and Assisted Reproduction, A. Zini and A. Agarwal, Editors. 2011, Springer New York: New York, NY. p. 125-149.
77. Bungum, M., L. Bungum, and A. Giwercman, *Sperm chromatin structure assay (SCSA): a tool in diagnosis and treatment of infertility.* Asian journal of andrology, 2011. **13**(1): p. 69-75.
78. Kumar, N. and A.K. Singh, *Trends of male factor infertility, an important cause of infertility: A review of literature.* Journal of human reproductive sciences, 2015. **8**(4): p. 191-6.
79. Harris, I.D., et al., *Fertility and the aging male.* Reviews in urology, 2011. **13**(4): p. e184-e190.
80. Kliesch, S., *Diagnosis of Male Infertility: Diagnostic Work-up of the Infertile Man.* European Urology Supplements, 2014. **13**(4): p. 73-82.
81. Organization, W.H., *WHO laboratory manual for the examination and processing of human semen*. 5th ed. 2010, Geneva: World Health Organization.
82. Bach, P.V. and P.N. Schlegel, *Sperm DNA damage and its role in IVF and ICSI.* Basic and clinical andrology, 2016. **26**: p. 15-15.
83. Hamada, A., et al., *Unexplained Male infertility: Diagnosis and Management.* International Braz J Urol, 2012. **38**(5): p. 576-594.
84. Agarwal, A. and T.M. Said, *Role of sperm chromatin abnormalities and DNA damage in male infertility.* Human Reproduction Update, 2003. **9**(4): p. 331-345.
85. Bissonnette, F., et al., *Sperm DNA fragmentation: threshold value in male fertility.* Human Reproduction, 2005. **20**(12): p. 3446-3451.
86. DeRouchey, J.E. and D.C. Rau, *Role of Amino Acid Insertions on Intermolecular Forces between Arginine Peptide Condensed DNA Helices IMPLICATIONS FOR PROTAMINE-DNA PACKAGING IN SPERM.* Journal of Biological Chemistry, 2011. **286**(49): p. 41985-41992.
87. Burkel, E., *Introduction to x-ray scattering.* Journal of Physics-Condensed Matter, 2001. **13**(34): p. 7477-7498.
88. Roe, R.J., *Methods of X-ray and neutron scattering in polymer science*. 2000, New York: New York : Oxford University Press.
89. Dong, Y.D. and B.J. Boyd, *Applications of X-ray scattering in pharmaceutical science.* International Journal of Pharmaceutics, 2011. **417**(1-2): p. 101-111.
90. Skoog, D.A., *Principles of instrumental analysis*. 5th ed.. ed, ed. F.J. Holler and T.A. Nieman. 1998, Philadelphia: Philadelphia : Saunders College Pub. : Harcourt Brace College Publishers.
91. Roberts, G.A. and D.T.F. Dryden, *DNA Electrophoresis: Historical and Theoretical Perspectives*, in *DNA Electrophoresis: Methods and Protocols*, S. Makovets, Editor. 2013. p. 1-9.
92. Calladine, C.R., et al., *A STUDY OF ELECTROPHORETIC MOBILITY OF DNA IN AGAROSE AND POLYACRYLAMIDE GELS.* Journal of Molecular Biology, 1991. **221**(3): p. 981-1005.
93. Rabindra Reddy, P. and R. Nomula, *Gel-Electrophoresis and Its Applications*. 2012.
94. Ven Lee, S. and A. Bahaman, *Discriminatory Power of Agarose Gel Electrophoresis in DNA Fragments Analysis*. 2012.
95. Barril, P. and S. Nates, *Introduction to Agarose and Polyacrylamide Gel Electrophoresis Matrices with Respect to Their Detection Sensitivities*. Gel Electrophoresis - Principles and Basics, ed. S. Magdeldin. 2012. 3-14.
96. Adamson, N.J. and E.C. Reynolds, *Rules relating electrophoretic mobility, charge and molecular size of peptides and proteins.* Journal of Chromatography B, 1997. **699**(1-2): p. 133-147.

97. Smith, B.J., *Acetic acid-urea polyacrylamide gel electrophoresis of proteins*, in *Methods in Molecular Biology; Basic protein and peptide protocols*, J.M. Walker, Editor. 1994. p. 39-47.
98. Waterborg, J., *Acetic Acid-Urea Polyacrylamide Gel Electrophoresis of Basic Proteins in The Protein Protocols Handbook*. 1996. p. 83-90.
99. Gusse, M., et al., *EXTRACTION, PURIFICATION AND CHARACTERIZATION OF THE SPERM PROTAMINES OF THE DOG-FISH SCYLLIORHINUS-CANICULUS.* Biochimica Et Biophysica Acta, 1983. **748**(1): p. 93-98.
100. Waring, M.J., *COMPLEX FORMATION BETWEEN ETHIDIUM BROMIDE AND NUCLEIC ACIDS.* Journal of Molecular Biology, 1965. **13**(1): p. 269-&.
101. Kavoosi, G. and S.K. Ardestani, *Gel Electrophoresis of Protein - From Basic Science to Practical Approach*. Gel Electrophoresis - Principles and Basics, ed. S. Magdeldin. 2012. 69-88.
102. Banerjee, A., J. Singh, and D. Dasgupta, *Fluorescence Spectroscopic and Calorimetry Based Approaches to Characterize the Mode of Interaction of Small Molecules with DNA.* Journal of Fluorescence, 2013. **23**(4): p. 745-752.
103. Izumrudov, V.A., M.V. Zhiryakova, and A.A. Goulko, *Ethidium bromide as a promising probe for studying DNA interaction with cationic amphiphiles and stability of the resulting complexes.* Langmuir, 2002. **18**(26): p. 10348-10356.
104. Trubetskoy, V.S., et al., *Quantitative assessment of DNA condensation.* Analytical Biochemistry, 1999. **267**(2): p. 309-313.
105. Toma, A.C., et al., *DNA Condensed by Protamine: A "Short" or "Long" Polycation Behavior.* Biomacromolecules, 2009. **10**(8): p. 2129-2134.
106. Schmid, F.-X., *Biological Macromolecules: UV-visible Spectrophotometry*, in *Encyclopedia Of Life Sciences*. 2001.
107. Tchou, J., et al., *SUBSTRATE-SPECIFICITY OF FPG PROTEIN - RECOGNITION AND CLEAVAGE OF OXIDATIVELY DAMAGED DNA.* Journal of Biological Chemistry, 1994. **269**(21): p. 15318-15324.
108. Reeves, R., *TRANSCRIPTIONALLY ACTIVE CHROMATIN.* Biochimica Et Biophysica Acta, 1984. **782**(4): p. 343-393.
109. Venkatesh, S. and J.L. Workman, *Histone exchange, chromatin structure and the regulation of transcription.* Nature Reviews Molecular Cell Biology, 2015. **16**(3): p. 178-189.
110. Balhorn, R., L. Brewer, and M. Corzett, *DNA condensation by protamine and arginine-rich peptides: Analysis of toroid stability using single DNA molecules.* Molecular Reproduction and Development, 2000. **56**(2): p. 230-234.
111. Ren, X., et al., *Is transcription in sperm stationary or dynamic?* Journal of Reproduction and Development, 2017. **63**(5): p. 439-443.
112. Agarwal, A., et al., *Effect of oxidative stress on male reproduction.* The world journal of men's health, 2014. **32**(1): p. 1-17.
113. Tremellen, K., *Oxidative stress and male infertility - a clinical perspective.* Human Reproduction Update, 2008. **14**(3): p. 243-258.
114. Henkel, R.R. and D.R. Franken, *Sperm DNA Fragmentation: Origin and Impact on Human Reproduction.* Journal of Reproductive Biotechnology and Fertility, 2011. **2**(2): p. 88-108.
115. Takata, H., et al., *Chromatin Compaction Protects Genomic DNA from Radiation Damage.* Plos One, 2013. **8**(10).
116. Ljungman, M. and P.C. Hanawalt, *EFFICIENT PROTECTION AGAINST OXIDATIVE DNA DAMAGE IN CHROMATIN.* Molecular Carcinogenesis, 1992. **5**(4): p. 264-269.

117. Enright, H.U., W.J. Miller, and R.P. Hebbel, *NUCLEOSOMAL HISTONE PROTEIN PROTECTS DNA FROM IRON-MEDIATED DAMAGE.* Nucleic Acids Research, 1992. **20**(13): p. 3341-3346.
118. Sishc, B.J. and A.J. Davis, *The Role of the Core Non-Homologous End Joining Factors in Carcinogenesis and Cancer.* Cancers, 2017. **9**(7).
119. Aoki, V.W., et al., *DNA integrity is compromised in protamine-deficient human sperm.* Journal of Andrology, 2005. **26**(6): p. 741-748.
120. Nili, H.A., H. Mozdarani, and A. Aleyasin, *Correlation of sperm DNA damage with protamine deficiency in Iranian subfertile men.* Reproductive Biomedicine Online, 2009. **18**(4): p. 479-485.
121. Simoes, R., et al., *Use of chromomycin A3 staining in bovine sperm cells for detection of protamine deficiency.* Biotechnic & Histochemistry, 2009. **84**(3): p. 79-83.
122. Vazharova, R. and I. Kremensky, *Individual capacity for DNA repair and maintenance of genomic integrity: a fertile ground for studies in the field of assisted reproduction.* Biotechnology & Biotechnological Equipment, 2016. **30**(3): p. 419-433.
123. Blanc, N.S., et al., *DNA in human and stallion spermatozoa forms local hexagonal packing with twist and many defects.* Journal of Structural Biology, 2001. **134**(1): p. 76-81.
124. Gelbart, W.M., *DNA-PEPTIDE COMPLEXES Regulation of interferon production.* Nature Materials, 2015. **14**(7): p. 661-662.
125. Jergil, B. and G.H. Dixon, *PROTAMINE KINASE FROM RAINBOW TROUT TESTIS . PARTIAL PURIFICATION AND CHARACTERIZATION.* Journal of Biological Chemistry, 1970. **245**(2): p. 425-&.
126. Raspaud, E., et al., *Precipitation of DNA by polyamines: A polyelectrolyte behavior.* Biophysical Journal, 1998. **74**(1): p. 381-393.
127. DeRouchey, J., R.R. Netz, and J.O. Rädler, *Structural investigations of DNA-polycation complexes.* The European Physical Journal E, 2005. **16**(1): p. 17-28.
128. Motta, S., et al., *Nanoscale structure of protamine/DNA complexes for gene delivery.* Applied Physics Letters, 2013. **102**(5).
129. Johnson, P.H. and L.I. Grossman, *ELECTROPHORESIS OF DNA IN AGAROSE GELS - OPTIMIZING SEPARATIONS OF CONFORMATIONAL ISOMERS OF DOUBLE-STRANDED AND SINGLE-STRANDED DNAS.* Biochemistry, 1977. **16**(19): p. 4217-4225.
130. Prevette, L.E., et al., *Intrinsic Dynamics of DNA-Polymer Complexes: A Mechanism for DNA Release.* Molecular Pharmaceutics, 2012. **9**(9): p. 2743-2749.
131. Coffey, D.S., W. Steven Ward, and D.S. Coffey, *DNA Packaging and Organization in Mammalian Spermatozoa: Comparison with Somatic Cell.* Biology of reproduction., 1991. **44**(4): p. 569-574.
132. Aitken, R.J., et al., *Relative impact of oxidative stress on the functional competence and genomic integrity of human spermatozoa.* Biology of Reproduction, 1998. **59**(5): p. 1037-1046.
133. Oliva, R. and G.H. Dixon, *VERTEBRATE PROTAMINE GENES AND THE HISTONE-TO-PROTAMINE REPLACEMENT REACTION.* Progress in Nucleic Acid Research and Molecular Biology, 1991. **40**: p. 25-94.
134. Manochantr, S., C. Chiamchanya, and P. Sobhon, *Relationship between chromatin condensation, DNA integrity and quality of ejaculated spermatozoa from infertile men.* Andrologia, 2012. **44**(3): p. 187-199.

135. Evgeni, E., K. Charalabopoulos, and B. Asimakopoulos, *Human sperm DNA fragmentation and its correlation with conventional semen parameters.* Journal of reproduction & infertility, 2014. **15**(1): p. 2-14.
136. Zhang, X.Y., M. San Gabriel, and A. Zini, *Sperm nuclear histone to protamine ratio in fertile and infertile men: Evidence of heterogeneous subpopulations of spermatozoa in the ejaculate.* Journal of Andrology, 2006. **27**(3): p. 414-420.
137. Evenson, D.P., K.L. Larson, and L.K. Jost, *Sperm chromatin structure assay: Its clinical use for detecting sperm DNA fragmentation in male infertility and comparisons with other techniques.* Journal of Andrology, 2002. **23**(1): p. 25-43.
138. Dogan, S., et al., *Sperm Protamine-Status Correlates to the Fertility of Breeding Bulls.* Biology of Reproduction, 2015. **92**(4).
139. Aoki, V.W., et al., *Protamine levels vary between individual sperm cells of infertile human males and correlate with viability and DNA integrity.* Journal of Andrology, 2006. **27**(6): p. 890-898.
140. Bizzaro, D., et al., *In-situ competition between protamine and fluorochromes for sperm DNA.* Molecular Human Reproduction, 1998. **4**(2): p. 127-132.
141. Manicardi, G.C., et al., *DNA strand breaks in ejaculated human spermatozoa: comparison of susceptibility to the nick translation and terminal transferase assays.* Histochemical Journal, 1998. **30**(1): p. 33-39.
142. McILVAINE., T.C., *A BUFFER SOLUTION FOR COLORIMETRIC COMPARISON.* Journal of Biological Chemistry, 1921. **49**: p. 183-186.
143. Czene, S. and M. Harmsringdahl, *DETECTION OF SINGLE-STRAND BREAKS AND FORMAMIDOPYRIMIDINE-DNA GLYCOSYLASE-SENSITIVE SITES IN DNA OF CULTURED HUMAN FIBROBLASTS.* Mutation Research-DNA Repair, 1995. **336**(3): p. 235-242.
144. Schmidt, N., et al., *Arginine-rich cell-penetrating peptides*. 2010. p. 1806-1813.
145. Wang, Y.G., et al., *Purification and characterization of antioxidative peptides from Salmon protamine hydrolysate.* Journal of Food Biochemistry, 2008. **32**(5): p. 654-671.
146. Davis, A.J. and D.J. Chen, *DNA double strand break repair via non-homologous end-joining.* Translational Cancer Research, 2013. **2**(3): p. 130-143.
147. Spano, M., et al., *The significance of sperm nuclear DNA strand breaks on reproductive outcome.* Current Opinion in Obstetrics & Gynecology, 2005. **17**(3): p. 255-260.
148. Wouters-Tyrou, D., et al., *Nuclear basic proteins in spermiogenesis.* Biochimie, 1998. **80**(2): p. 117-128.
149. Santi, S., et al., *NUCLEAR MATRIX INVOLVEMENT IN SPERM HEAD STRUCTURAL ORGANIZATION.* Biology of the Cell, 1994. **81**(1): p. 47-57.
150. Khara, K.K., et al., *Human protamines and male infertility.* Journal of assisted reproduction and genetics, 1997. **14**(5): p. 282-290.
151. Sautiere, P., et al., *PRIMARY STRUCTURE OF A PROTAMINE ISOLATED FROM THE SPERM NUCLEI OF THE DOG-FISH SCYLLIORHINUS-CANICULUS.* European Journal of Biochemistry, 1981. **119**(2): p. 251-255.
152. Balhorn, R., M. Corzett, and J.A. Mazrimas, *FORMATION OF INTRAPROTAMINE DISULFIDES INVITRO.* Archives of Biochemistry and Biophysics, 1992. **296**(2): p. 384-393.
153. Raspaud, E., et al., *Solubility and charge inversion of complexes of DNA and basic proteins.* Physical Review Letters, 2006. **97**(6).
154. Adroer, R., et al., *NUCLEOTIDE-SEQUENCE OF THE PROTAMINE P1 GENE FROM THE WHALE ORCINUS-ORCA PREDICTS A UNIQUE N-TERMINAL AMINO-ACID MOTIF.* Nucleic Acids Research, 1992. **20**(3): p. 609-609.

155. Vanderzwalmen, P., et al., *Blastocyst development after sperm selection at high magnification is associated with size and number of nuclear vacuoles.* Reproductive Biomedicine Online, 2008. **17**(5): p. 617-627.
156. Tanaka, A., et al., *Human sperm head vacuoles are physiological structures formed during the sperm development and maturation process.* Fertility and Sterility, 2012. **98**(2): p. 315-320.
157. Cassuto, N.G., et al., *Correlation between DNA defect and sperm-head morphology.* Reproductive Biomedicine Online, 2012. **24**(2): p. 211-218.
158. Zhu, W.J. and J. Li, *A simple sperm nuclear vacuole assay with propidium iodide.* Andrologia, 2015. **47**(7): p. 779-785.
159. Setti, A.S., et al., *The prevalence of sperm with large nuclear vacuoles is a prognostic tool in the prediction of ICSI success.* Journal of Assisted Reproduction and Genetics, 2014. **31**(3): p. 307-312.
160. Boitrelle, F., et al., *Small human sperm vacuoles observed under high magnification are pocket-like nuclear concavities linked to chromatin condensation failure.* Reproductive Biomedicine Online, 2013. **27**(2): p. 201-211.
161. Boitrelle, F., et al., *Large human sperm vacuoles observed in motile spermatozoa under high magnification: nuclear thumbprints linked to failure of chromatin condensation.* Human Reproduction, 2011. **26**(7): p. 1650-1658.
162. Berkovitz, A., et al., *Does the presence of nuclear vacuoles in human sperm selected for ICSI affect pregnancy outcome?* Human Reproduction, 2006. **21**(7): p. 1787-1790.
163. Ghazali, S., et al., *Large nuclear vacuoles in spermatozoa negatively affect pregnancy rate in IVF cycles.* International Journal of Reproductive Biomedicine, 2015. **13**(7): p. 425-432.
164. Pastuszek, E., et al., *An investigation of the potential effect of sperm nuclear vacuoles in human spermatozoa on DNA fragmentation using a neutral and alkaline Comet assay.* Andrology, 2017. **5**(2): p. 392-398.
165. Lavolpe, M., et al., *Relationship Between Sperm DNA Fragmentation and Nuclear Vacuoles.* Jornal Brasileiro De Reproducao Assistida, 2015. **19**(2): p. 70-74.
166. Boitrelle, F., et al., *The nature of human sperm head vacuoles: a systematic literature review.* Basic and clinical andrology, 2013. **23**: p. 3-3.
167. Gatimel, N., et al., *Sperm cephalic vacuoles: new arguments for their non acrosomal origin in two cases of total globozoospermia.* Andrology, 2013. **1**(1): p. 52-56.
168. Franco, J.G., et al., *Large nuclear vacuoles are indicative of abnormal chromatin packaging in human spermatozoa.* International Journal of Andrology, 2012. **35**(1): p. 46-51.
169. Perdrix, A., et al., *Assessment of acrosome and nuclear abnormalities in human spermatozoa with large vacuoles.* Human Reproduction, 2011. **26**(1): p. 47-58.
170. Skowronek, F., et al., *DNA sperm damage correlates with nuclear ultrastructural sperm defects in teratozoospermic men.* Andrologia, 2012. **44**(1): p. 59-65.
171. Franco, J.I.G., et al., *Significance of large nuclear vacuoles in human spermatozoa: implications for ICSI.* Reproductive Biomedicine Online, 2008. **17**(1): p. 42-45.
172. Simon, L., et al., *Relationships between human sperm protamines, DNA damage and assisted reproduction outcomes.* Reproductive Biomedicine Online, 2011. **23**(6): p. 724-734.
173. Hurley, C.K., *ELECTROPHORESIS OF HISTONES - MODIFIED PANYIM AND CHALKLEY SYSTEM FOR SLAB GELS.* Analytical Biochemistry, 1977. **80**(2): p. 624-626.

174. Hermanson, G.T., *Bioconjugate Techniques, 1st Edition*. Bioconjugate Techniques, 1st Edition. 1996. 1-729.
175. Friedman, M., L.H. Krull, and J.F. Cavins, *CHROMATOGRAPHIC DETERMINATION OF CYSTINE AND CYSTEINE RESIDUES IN PROTEINS AS S-BETA-(4-PYRIDYLETHYL)CYSTEINE.* Journal of Biological Chemistry, 1970. **245**(15): p. 3868-&.
176. Grant, G.A., *Modification of Cysteine.* Current Protocols In Protein Science, 2017. **15.1**: p. 15.1.1-15.1.23.
177. Schmid, F.-X., *Biological Macromolecules: UV-Visible Spectrophotometry.* Encyclopedia of Life Sciences, 2001.
178. Christian D. Powell, D.K., Jason DeRouchey, Hunter N.B. Moseley, , *Evidence of Peroxidase Catalysed Formation of Cysteine-Tyrosine and Dityrosine Cross-Linking in Mammalian Sperm Protamines.* In Preparation, 2019.
179. Nazari, M., M. Kurdi, and H. Heerklotz, *Classifying Surfactants with Respect to Their Effect on Lipid Membrane Order.* Biophysical Journal, 2012. **102**(3): p. 498-506.
180. Phetudomsinsuk, K., et al., *Morphology and head morphometric characters of sperm in Thai native crossbred stallions.* Acta Veterinaria Scandinavica, 2008. **50**.
181. Yaniz, J.L., et al., *A comparative study of the morphometry of sperm head components in cattle, sheep, and pigs with a computer-assisted fluorescence method.* Asian Journal of Andrology, 2016. **18**(6): p. 840-843.
182. Shalgi, R., J. Seligman, and N.S. Kosower, *DYNAMICS OF THE THIOL STATUS OF RAT SPERMATOZOA DURING MATURATION - ANALYSIS WITH THE FLUORESCENT LABELING AGENT MONOBROMOBIMANE.* Biology of Reproduction, 1989. **40**(5): p. 1037-1045.
183. Bellve, A.R., et al., *PURIFICATION AND CHARACTERIZATION OF MOUSE PROTAMINE-P1 AND PROSTAMINE-P2 - AMINO-ACID SEQUENCE OF P2.* Biochemistry, 1988. **27**(8): p. 2890-2897.
184. Frehlick, L.J., et al., *Sperm nuclear basic proteins of two closely related species of Scorpaeniform fish (Sebastes maliger, Sebastolobus sp.) with different sexual reproduction and the evolution of fish protamines.* Journal of Experimental Zoology Part a-Ecological and Integrative Physiology, 2006. **305A**(3): p. 277-287.
185. Noblanc, A., et al., *DNA oxidative damage in mammalian spermatozoa: where and why is the male nucleus affected?* Free Radical Biology and Medicine, 2013. **65**: p. 719-723.
186. Rivlin, J., et al., *Role of hydrogen peroxide in sperm capacitation and acrosome reaction.* Biology of Reproduction, 2004. **70**(2): p. 518-522.
187. Khadem, N., et al., *Sperm DNA fragmentation in couples with unexplained recurrent spontaneous abortions.* Andrologia, 2014. **46**(2): p. 126-130.
188. Barratt, C.L.R., et al., *Sperm DNA: organization, protection and vulnerability: from basic science to clinical applications-a position report.* Human Reproduction, 2010. **25**(4): p. 824-838.
189. Bjorndahl, L. and U. Kvist, *Human sperm chromatin stabilization: a proposed model including zinc bridges.* Molecular Human Reproduction, 2010. **16**(1): p. 23-29.
190. Martinie, R.J., et al., *Identifying proteins that can form tyrosine-cysteine crosslinks.* Metallomics, 2012. **4**(10): p. 1037-1042.
191. Rogers, M.S., et al., *Cross-link formation of the cysteine 228-tyrosine 272 catalytic cofactor of galactose oxidase does not require dioxygen.* Biochemistry, 2008. **47**(39): p. 10428-10439.
192. Bedford, J.M.B., M J ; Calvin, *Variations in the structural character and stability of the nuclear chromatin in morphologically normal human spermatozoa.* Journal of Reproduction and Fertility, 1973. **33**(1): p. 19-29.

VITA

Daniel Kirchhoff, MLS(ASCP)^{CM}

Education

Beaumont School of Medical Technology, Beaumont Hosp., Royal Oak, MI June 2011- Dec. 2011
B.S. Michigan State University, Medical Technology, East Lansing, MI 2006-2011
-Transferred from Central Michigan University 2004-2006

Professional Experience

Graduate Research Assistant, Dept. of Chemistry, University of Kentucky Dec. 2017- Present

Lead Teaching Assistant, Dept. of Chemistry, University of Kentucky Aug. 2015 – Dec 2016

Teaching Assistant, Dept. of Chemistry, University of Kentucky Aug. 2014 – May 2016

Senior Medical Technologist, Northwestern Memorial Hosp, Chicago, IL July 2013 – July 2014

Medical Technologist, Northwestern Memorial Hospital, Chicago, IL April 2012 – July 2013

Processing Clerk, Beaumont Hospital, Royal Oak, MI June 2011- Dec. 2011

Publications

DNA Protection In The Condensed State, Effect Of Packaging Density On Damage Susceptibility
Daniel Kirchhoff, Ehibai Oikeh, Cody Gay, Dr. Jason DeRouchey, *In Preparation*

Effect of Aberrant Protamine Ratios on DNA Integrity in Reconstituted DNA Condensates
Daniel Kirchhoff, Ehigbai Oikeh, Brady Ekman, Dr. Jason DeRouchey*, In Preparation*

Disulfide-Mediated Secondary Structure in Protamine is Critical for DNA Condensation in Mammalian Sperm Chromatin
Daniel Kirchhoff, Jackie Rhinehart, Christian Powell, Dr. Hunter Moseley, Dr. Jason DeRouchey, *In Preparation*

Awards and Honors

Kentucky Research Challenge Trust Fund Research Fellowship Spring 2016
Griffith Outstanding General Chemistry TA Award May 2015
ASCP Certification as a Medical Laboratory Scientist February 2012